



UNIVERSIDAD NACIONAL AUTÓNOMA DE MÉXICO  
PROGRAMA DE MAESTRÍA Y DOCTORADO EN INGENIERÍA  
ENERGÍA - FUENTES RENOVABLES

A THEORETICAL-EXPERIMENTAL STUDY TO IDENTIFY  
GEOCHEMICAL SIGNATURES FOR EXPLAINING  
COMPLEX HYDROTHERMAL ALTERATION AND SEALING  
PROCESSES IN HIDDEN GEOTHERMAL SYSTEMS

TESIS  
QUE PARA OPTAR POR EL GRADO DE:  
DOCTOR EN INGENIERÍA EN ENERGÍA

PRESENTA:  
GUSTAVO SANTOS RAGA

TUTOR PRINCIPAL  
DR. EDGAR ROLANDO SANTOYO GUTIÉRREZ  
INSTITUTO DE ENERGÍAS RENOVABLES  
COMITÉ TUTOR  
DR. JESÚS MARTÍNEZ FRÍAS, CSIC-UCM  
DR. PANDARINATH KAILASA, IER-UNAM  
DR. DANIEL PÉREZ ZÁRATE, IER-UNAM  
DR. FERNANDO J. GUERRERO MARTÍNEZ, IER-UNAM

TEMIXCO, MORELOS, JUNIO 2024



Universidad Nacional  
Autónoma de México

Dirección General de Bibliotecas de la UNAM

**Biblioteca Central**



**UNAM – Dirección General de Bibliotecas**  
**Tesis Digitales**  
**Restricciones de uso**

**DERECHOS RESERVADOS ©**  
**PROHIBIDA SU REPRODUCCIÓN TOTAL O PARCIAL**

Todo el material contenido en esta tesis esta protegido por la Ley Federal del Derecho de Autor (LFDA) de los Estados Unidos Mexicanos (México).

El uso de imágenes, fragmentos de videos, y demás material que sea objeto de protección de los derechos de autor, será exclusivamente para fines educativos e informativos y deberá citar la fuente donde la obtuvo mencionando el autor o autores. Cualquier uso distinto como el lucro, reproducción, edición o modificación, será perseguido y sancionado por el respectivo titular de los Derechos de Autor.

---

---

---

**PROTESTA UNIVERSITARIA DE INTEGRIDAD Y HONESTIDAD  
ACADÉMICA Y PROFESIONAL  
(Graduación con trabajo escrito)**

De conformidad con lo dispuesto en los artículos 87, fracción V, del Estatuto General, 68, primer párrafo, del Reglamento General de Estudios Universitarios y 26, fracción 1, y 35 del Reglamento General de Exámenes, me comprometo en todo tiempo a honrar a la Institución y a cumplir con los principios establecidos en el Código de Ética de la Universidad Nacional Autónoma de México, especialmente con los de integridad y honestidad académica.

De acuerdo con lo anterior, manifiesto que el trabajo escrito titulado **A Theoretical -Experimental Study To Identify Geochemical Signatures For Explaining Complex Hydrothermal Alteration And Sealing Processes In Hidden Geothermal Systems** que presenté para obtener el grado de Doctorado es original, de mi autoría y lo realicé con el rigor metodológico exigido por mi programa de posgrado, citando las fuentes de ideas, textos, imágenes, gráficos u otro tipo de obras empleadas para su desarrollo.

En consecuencia, acepto que la falta de cumplimiento de las disposiciones reglamentarias y normativas de la Universidad, en particular las ya referidas en el Código de Ética, llevará a la nulidad de los actos de carácter académico administrativo del proceso de graduación.

**Atentamente**



---

**Gustavo Santos Raga**  
**No. de cuenta UNAM 518004671**

*Al amor de mi vida, Daniela Juárez Bahena  
A mis padres, Eudosia Raga Silva y Arturo Santos  
Mis hermanos, Gabriela y Arturo Santos Raga  
Mis sobrinas, María Guadalupe y Nadia de Jesús Ramos Santos  
Por que mi familia es el motor y el tesoro más grande de mi vida,  
por su comprensión, apoyo y amor incondicional.  
En verdad, gracias.*

*“If you shut your door to all errors, the truth  
will be shut out”*

*Rabindraneth Tagore*

# Acknowledgements

---

A la Universidad Nacional Autónoma de México por la beca doctoral otorgada durante el primer año del posgrado (apoyo con número de cuenta: 518004671). Al CONAHCyT por el apoyo económico a otorgado durante los últimos 3 años a través de la beca de doctorado No. CVU 827548.

Por el apoyo financiero de los proyectos: (i) UNAM-DGAPA-PAPIIT, No. de proyecto IN 108322; (ii) CONAHCYT, No. de proyecto CF-2023-G-490.

A la Universidad Nacional Autónoma de México y al Instituto de Energías Renovables por haberme recibido como estudiante y por brindarme la formación en Energías Renovables.

A mi director de tesis, Dr. Edgar Rolando Santoyo Gutiérrez, por aceptar dirigir este proyecto, por su asesoría, enseñanza, dedicación e infinita paciencia.

A mis sinodales, el Dr. Pandarinath Kailasa, Dr. Daniel Pérez Zárate, Dr. Fernando Guerrero y al Dr. Jesús Martínez Frías, por sus acertados comentarios, sin duda ayudaron a mejorar de manera sustancial el presente trabajo de tesis.

A la M.C. Mirna Guevara García, por seguir brindándome el apoyo de siempre, por los consejos, correcciones y por su disponibilidad de siempre apoyarme.

A todas esas personas que me acompañaron durante esta maravillosa experiencia, amigas y amigos que llevaré siempre en el corazón: Sonny Díaz Calderón, Miguel Ángel Alvarado Morales, Ricardo Molina, Jorge Chavarría, Demian Uriel, Yarimeth Alarcón.

A mi compañero, amigo y asesor de vida, David Yáñez Dávila, gracias por tu apoyo y por siempre escuchar.

A mis hermanos de otra familia, que a pesar de la distancia siempre estuvieron conmigo, gracias Lalo, Josué (vaquero). Los quiero.



# Contents

---

<b>List of Figures</b> . . . . .	<b>VII</b>
<b>List of Tables</b> . . . . .	<b>XI</b>
<b>Resumen</b> . . . . .	<b>XIII</b>
<b>Abstract</b> . . . . .	<b>XV</b>
<b>Introduction</b> . . . . .	<b>1</b>
<b>Chapter 1 Worldwide status of geothermal exploration and development</b>	
<b>7</b>	
1.1 Geothermal Energy . . . . .	7
1.2 Current status of geothermal energy in the world . . . . .	8
1.2.1 Geothermal power generation . . . . .	8
1.2.2 Direct-uses of the geothermal energy . . . . .	11
1.3 Current outlook of geothermal energy in Mexico . . . . .	14
1.3.1 Geothermal power generation . . . . .	14
1.3.2 Direct-uses of the geothermal energy . . . . .	17
1.4 Remarks of Chapter 1 . . . . .	18
<b>Chapter 2 Updated understanding of the behaviour of rare earth</b>	
<b>elements (REE)in geothermal systems</b> . . . . .	<b>21</b>
2.1 Introduction . . . . .	22
2.2 Fundamentals and geochemical properties . . . . .	23
2.2.1 Thermodynamic conditions . . . . .	23
2.2.2 Physicochemical properties . . . . .	24
2.2.3 Geological setting and origin . . . . .	25
2.2.3.1 Abundances of the REE in rocks and standard nor-	
malization . . . . .	25
2.2.3.2 Fractional crystallization and mantle-melting pro-	
cesses . . . . .	30

2.2.3.3	Rare earth elements ore deposits . . . . .	31
2.3	Rare earth elements in geothermal systems: An updated bibliometric analysis . . . . .	32
2.3.1	Bibliometric analysis methodology . . . . .	33
2.3.1.1	Text data mining . . . . .	34
2.3.1.2	Intellectual Analysis (Stage 2: PeIA) . . . . .	36
2.3.2	Worldwide bibliometric database . . . . .	36
2.4	Results and discussions . . . . .	37
2.4.1	Analysis of bibliometric database . . . . .	37
2.4.1.1	Global scientific production . . . . .	37
2.4.1.2	Worldwide scientific distribution . . . . .	39
2.4.2	Chemical characterization of REE in rocks and fluid samples . . . . .	40
2.4.2.1	Chemical pretreatment . . . . .	41
2.4.2.2	Analytical techniques and limits of detection . . . . .	43
2.4.3	Worldwide geochemical databases (WGD) . . . . .	44
2.4.4	Mobility of rare earth elements in geothermal systems . . . . .	45
2.4.5	Experimental water-rock interactions studies . . . . .	49
2.5	REE applications and current and future challenges . . . . .	50
2.6	Remarks of Chapter 2 . . . . .	51

**Chapter 3 Geochemical signatures of REE in spring waters and outcropping rocks from the hidden geothermal system of Acoculco 53**

3.1	Introduction . . . . .	53
3.2	Geological setting of the study area . . . . .	57
3.3	Work methodology . . . . .	58
3.3.1	Geochemical field work . . . . .	60
3.3.2	Geochemometric analysis . . . . .	61
3.3.2.1	QA/QC of the chemical analyses . . . . .	61
3.3.2.2	Distribution of major and trace elements in water and rock samples . . . . .	62
3.3.3	Water-rock interaction . . . . .	62
3.3.3.1	Hydrogeochemistry . . . . .	63
3.3.3.2	Geochemical modelling of major and trace (REE) elements in waters . . . . .	63
3.3.3.3	Hydrothermal alteration . . . . .	64
3.3.3.4	Analysis of REE composition in rock samples . . . . .	64
3.4	Results . . . . .	65
3.4.1	Geochemometric analysis . . . . .	65
3.4.1.1	QA/QC for the chemical analyses of water . . . . .	65
3.4.1.2	Distribution of major and trace elements in water and rock samples . . . . .	67

---

3.4.2	Concentration patterns of REE and geochemical modelling	70
3.4.2.1	Chondrite-normalized REE patterns of waters . . .	70
3.4.2.2	Mineral saturation state and REE speciation . . .	71
3.4.3	Rock Geochemistry . . . . .	73
3.4.3.1	Hydrothermal alteration . . . . .	73
3.4.3.2	Composition of REE in rocks . . . . .	74
3.5	Discussion . . . . .	75
3.5.1	Concentration patterns of REE in water samples . . . . .	75
3.5.2	Geochemical modelling of REE . . . . .	76
3.5.2.1	Mineral saturation states . . . . .	76
3.5.2.2	Speciation of REE . . . . .	77
3.5.3	Concentration patterns of REE in outcropping rocks . . . . .	79
3.6	Remarks of Chapter 3 . . . . .	79
<b>Chapter 4 Fractionation of the rare earth elements: dissolution</b>		
<b>water-rock interaction experiments . . . . .</b>		<b>81</b>
4.1	Introduction . . . . .	82
4.2	Methodology . . . . .	82
4.2.1	Geochemometric treatment of experimental data . . . . .	83
4.2.2	Field work and collection of initial samples . . . . .	84
4.2.3	Sample preparation . . . . .	86
4.2.4	Experimental design . . . . .	88
4.2.4.1	Description of the experimental system . . . . .	88
4.2.4.2	Initial geochemical analysis . . . . .	90
4.2.5	Product sampling . . . . .	90
4.2.6	Analysis of physico-chemical parameters . . . . .	92
4.2.7	Geochemical analysis of products . . . . .	93
4.2.7.1	Rock geochemical analysis . . . . .	93
4.2.7.2	Water geochemical analysis . . . . .	93
4.2.8	Geochemical modelling . . . . .	94
4.3	Results and discussions . . . . .	94
4.3.1	Mass balance and water-rock ratio . . . . .	94
4.3.2	Physicochemical analysis and water classification . . . . .	95
4.3.3	Distribution of major and trace elements . . . . .	97
4.3.4	Concentration patterns of REE in rock samples . . . . .	99
4.3.5	Concentration patterns of REE in water samples . . . . .	101
4.3.6	Geochemical modelling . . . . .	103
4.4	Remarks of Chapter 4 . . . . .	106
<b>Chapter 5 Final conclusions . . . . .</b>		<b>109</b>

---

CONTENTS

---

**Bibliography . . . . . 113**

# List of Figures

---

1.1	Top 10 countries with the highest installed geothermal power capacity in the world . . . . .	10
1.2	Lindal diagram (Modified after Kaczmarczyk et al., 2020) . . . . .	12
1.3	Comparison of worldwide direct-use of geothermal energy in $TJ/y$ for the period 2000-2020. . . . .	13
1.4	Location of the main geothermal fields in Mexico and promissory areas. . . . .	16
2.1	Bibliometric methodology . . . . .	34
2.2	Worldwide production of REE scientific articles in geothermal systems. . . . .	38
2.3	Worldwide distribution of articles reported in peer-review journals and reviews on REE focussed on geothermal fractionation (1992–2024). . . . .	39
2.4	Histograms of the main chemical techniques used for the separation and determination of REE. . . . .	41
3.1	Base map of Mexican geothermal fields under exploitation, potential promissory sites, and simplified projections of the Acoculco Geothermal System. . . . .	56
3.2	Geological map of the Acoculco geothermal system. . . . .	59
3.3	Integrated work methodology developed for the study of the water-rock interaction processes of the AGS (Santos-Raga et al., 2021). . . . .	60
3.4	Results of the charge balance correction applied for sulphate-acid waters collected in the AGS. . . . .	66
3.5	Statistical descriptive plot showing the concentration patterns observed for major and trace elements measured in the hot and cold spring samples of the AGS . . . . .	68
3.6	Statistical descriptive plot showing the concentration patterns observed for major and trace elements determined in altered and less-altered rocks of the AGS. . . . .	69

## LIST OF FIGURES

---

3.7	Chondrite-normalized patterns of REE observed in spring waters of the AGS. . . . .	71
3.8	Saturation index of minerals for S and Al bearing minerals species versus the total sum of REE determined in spring water samples that emerge from the ZIC of the AGS (Santos-Raga et al., 2021). . . . .	72
3.9	Aqueous speciation of REE found in cold spring waters from the Alcaparrosa site of the AGS. . . . .	73
3.10	Classification of outcropping rocks of the AGS according to the degree of hydrothermal alteration. . . . .	74
3.11	Chondrite-normalized patterns of REE observed in rock (acid, intermediate, and basic) samples (Santos-Raga et al., 2021). . . . .	75
4.1	General methodology applied for the development of the experiments carried out at 150 °C. . . . .	83
4.2	Geological map of the Acoculco geothermal system (modified after Avellán et al., 2020). Surface geology, faults, and hydrothermal alteration zones are also shown, including the rocks sampling for water-rock interaction experiments. . . . .	85
4.3	Rock sample collection at the Caldera Complex Acoculco: a) rhyolitic rock, b) basaltic - trachyandesite rock, c) andesitic rock. . . . .	86
4.4	Sample preparation flow diagram. . . . .	87
4.5	Pre-treatment of rock samples: (a) crushed, (b) ultrasonic washing, and drying. . . . .	88
4.6	Conceptual model of the experimental system. . . . .	89
4.7	Experimental system: (a) teflon batch reactor, (b) Binder digital furnace, (c) metal support structure is employed to prevent steam leakage resulting from high temperature. . . . .	89
4.8	Experimental system: (a) Steam lake test, (b) steam leak test regression model. . . . .	90
4.9	Flow Diagram of product sampling process. . . . .	92
4.10	Time evolution of the physicochemical parameters of the experimental fluid collected at 150°C: (a) pH, (b) bicarbonate content and (c) electrical conductivity ( $\lambda$ ). . . . .	96
4.11	Piper diagram for the chemical classification of solutions produced by water-rock interaction experiments. . . . .	97
4.12	Statistical descriptive plot showing the main concentration patterns of major and trace elements in altered and less-altered rocks from water-rock interaction experiments. . . . .	98
4.13	Statistical descriptive plot showing the main concentration patterns of major and trace elements in waters. . . . .	99

4.14	REE concentrations patterns (in $\mu\text{g/g}$ ) of the experimental rocks as a function of time (months). . . . .	100
4.15	Chondrite-normalized patterns of REE. . . . .	101
4.16	REE concentrations patterns (in $\mu\text{g/L}$ ) of the experimental solutions measured using ICP-MS as a function of time (months). . . . .	102
4.17	Chondrite-normalized patterns of REE. . . . .	103
4.18	Mineral saturation indices from (a) andesite and, (b) basalt - trachyandesite . . . . .	104
4.19	Aqueous speciation of REE found in the WRI experiments: (a) Andesite and (b) trachyandesite. The abbreviation of Ln represents any of the fourteen elements of REE (La-Lu). . . . .	106



# List of Tables

---

1.1	Total installed capacity and geothermal power generation from 2015 to 2020, as well as expected installed capacity in 2025. . . . .	11
1.2	Effective capacity and annual production . . . . .	17
1.3	Summary table of geothermal direct heat uses . . . . .	18
2.1	Rare earth elements concentration of chondrite normalization standards in ppm. . . . .	27
2.2	Rare earth elements concentration of Upper Continental Crust, Post-Archean Australian Shale, North American Shale Composite and Primitive Mantle of normalization standards in ppm. . . . .	29
2.3	Summary of bibliometric indicators. . . . .	37
2.4	Detection limits commonly associated with the quantification of REE in spectrometric techniques. . . . .	44
2.5	Summary of a worldwide database of REE concentrations in rock samples collected from geothermal systems. . . . .	46
2.6	Summary of a worldwide database of REE concentrations in water samples collected from geothermal systems. . . . .	47
4.1	Water rock interaction experiments conditions . . . . .	83
4.2	Normative chemical and mineralogical composition of the initial rocks used in the water-rock experiments. The geochemical compositions are reported with their uncertainty, the units are reported in % (w/w). . . . .	86
4.3	Calculation of the mean, dispersion, uncertainty and w/r ratio of the weights measured during the preparation of the experimental systems. Calculations were performed after evaluating the data for outliers. . . . .	95



# Abstract

---

The PhD thesis work is based on three main stages: (i) a bibliometric and systematic analysis of the state-of-the-art literature on geochemical studies of REE applied to geothermal systems; (ii) the development of a new methodology for exploring and quantifying REE and other trace elements in spring samples and outcropping rocks from the hidden geothermal system of Acoculco (SGA); and (iii) the development of an experimental water-rock interaction work to study the processes related to geochemical signatures in the SGA.

The bibliometric analysis provided a better understanding of the kinetic processes governing the distribution of REE in geothermal rocks and fluids, highlighting the influence of temperature, pressure, pH, and water-rock interactions. It also underscored the key role of these elements as natural tracers of fluids and hydrothermal alteration processes, offering valuable information for characterizing unconventional geothermal deposits. This literature analysis laid the groundwork for the methodological development of subsequent stages.

Based on the mapping of REE concentrations in SGA samples, it was demonstrated that minerals containing  $\text{Al}^{3+}$ , Fe, and  $\text{F}^-$  are the main phases controlling their concentrations in acidic waters. Different degrees of REE complexation in waters within the Acoculco caldera clearly showed new signatures of geothermal activity.  $\text{LnSO}_4^+$  complexes and free  $\text{Ln}^{3+}$  ions were identified as the major species in acidic waters, while in less acidic waters,  $\text{LnF}^{2+}$  complexes showed an increase in their percentage of complexation. The concentration of REE in felsic and intermediate rocks shows chondrite-normalized patterns in the shape of a "seagull wing", characterized by an enrichment of LREE, a negative Eu anomaly, and a depletion of HREE with a flat trend. Geochemical signatures provide new evidence of deep temperatures between 200 °C and 300 °C.

Water-rock experiments were carried out to assess the kinetic behaviour of volcanic rock dissolution under medium-temperature geothermal conditions. Crushed basalt and andesite samples (500-1000  $\mu\text{m}$ ) were placed in batch reactors with acidified deionized water at a temperature of 150 °C using a W/R ratio of 10:1. In this study, the mobility of REE between volcanic rocks and acidic fluid under hydrothermal conditions was modelled for the first time in Mexico. These simulations indicate that temperature, salinity, and fluid compositions have a significant effect on the mobility and speciation of REE, which controls the different chondrite-normalized profiles observed in both volcanic rocks and fluids.

It was also observed that the fractionation and mobility of REE vary with dominant water-rock interaction processes. Integrated numerical models, experiments, and field observations are crucial to understanding the physicochemical conditions that explain the variability of REE concentrations in hidden geothermal systems.



# Resumen

---

El trabajo de tesis se basa en tres etapas principales: (i) un análisis bibliométrico y sistemático de la literatura en el estado del arte sobre los estudios geoquímicos de REE aplicados a sistemas geotérmicos; (ii) una metodología de exploración y cuantificación de REE y otros elementos traza en muestras de manantial y rocas del sistema geotérmico oculto de Acoculco; y (iii) el desarrollo de un protocolo experimental de interacción agua-roca para estudiar los procesos relacionados a las firmas geoquímicas en el SGA.

El análisis bibliométrico proporcionó un mejor entendimiento de los procesos de interacción agua-roca que gobiernan la distribución de REE en rocas y fluidos geotérmicos, destacando la influencia de la temperatura, la presión, el pH y las interacciones agua-roca. También resaltó el papel clave de estos elementos como trazadores naturales de fluidos y procesos de alteración hidrotermal, ofreciendo información valiosa para la caracterización de yacimientos geotérmicos no convencionales. Este análisis de la literatura planteó las bases del desarrollo metodológico de las etapas posteriores.

Con base en el mapeo de las concentraciones de REE en muestras del SGA, se demostró que los minerales que contienen  $\text{Al}^{3+}$ ,  $\text{Fe}$  y  $\text{F}^-$  son las principales fases que controlan sus concentraciones en aguas ácidas. Diferentes grados de complejación de REE en aguas ubicadas dentro de la caldera de Acoculco mostraron claramente nuevas firmas de actividad geotérmica. Complejos de  $\text{LnSO}_4^+$  e iones libres de  $\text{Ln}^{3+}$  fueron identificados como especies mayoritarias de las aguas ácidas, mientras que en aguas menos ácidas,  $\text{LnF}^{2+}$  muestran un aumento en sus porcentajes de complejación. La concentración de REE en rocas félsicas e intermedias muestran patrones normalizados de condritas en forma de “ala de gaviota”, caracterizados por un enriquecimiento de LREE, una anomalía negativa de Eu y un agotamiento de HREE con una tendencia plana. Firmas geoquímicas que proporcionan nueva evidencia de temperaturas profundas entre 200 °C y 300 °C.

Los experimentos agua-roca fueron realizados para evaluar el comportamiento cinético de la disolución de rocas volcánicas bajo condiciones geotérmicas de mediana temperatura. Muestras trituradas de basalto y andesita (500-1000  $\mu\text{m}$ ) fueron

colocadas en reactores batch con agua desionizada acidificada a una temperatura de 150 °C usando una relación W/R de 10:1. En este estudio, se modeló por primera vez en México la movilidad de REE entre rocas volcánicas y fluido ácido en condiciones hidrotermales. Estas simulaciones indican que la temperatura, la salinidad y la composición del fluido tienen un efecto significativo sobre la movilidad de los REE y su especiación, que controlan los diferentes perfiles normalizados de condritas observados tanto en las rocas volcánicas como en los fluidos.

El presente trabajo mostró que el fraccionamiento y la movilidad de REE varían respecto a los procesos de interacción agua-roca dominantes. Vincular modelos numéricos, experimentos y observaciones de campo es vital para comprender qué condiciones fisicoquímicas pueden conducir a estas concentraciones variables de REE en sistemas geotérmicos no convencionales.

# Introduction

---

Geothermal energy originates from the thermal energy produced by the Earth's core through fractional crystallization, residual heat from its formation, and nuclear fission processes occurring within the Earth (Marini, 2000; Yan et al., 2010; Gupta and Roy, 2007; DiPippo and Renner, 2014; Stober and Bucher, 2012). Based on the global average of the Earth's heat flux, it is estimated that the heat dissipated, which is transmitted from the Earth's interior to the surface each day, is equivalent to 2.5 times the average daily energy used by humans today (ling Wang et al., 2018). This energy can be classified into three main types of resources: shallow geothermal energy, hydrothermal geothermal resources, and Hot Dry Rock (HDR) geothermal resources. Concerning hydrothermal resources, hot springs, geysers, mud pots and fumaroles are dynamic surface features that represent interacting underground systems of water, heat and rock (Heasler and Jaworowski, 2009). Hydrothermal complexes associated with this volcanic activity are present in geothermal systems around the world (e.g. Yellowstone in the United States, Cerro Prieto in Mexico and Larderello in Italy, among others). Hutter (2021) mentions that power generation from deep hydrothermal resources is developing at an average growth rate of 5% per year, producing 95.0 TWh in 2020 in 30 countries. In this topic and compared to other renewable power plant technologies (hydro, biomass, solar PV, wind), geothermal lags far behind, both in installed capacity (GWe) and production (TWh: Rybach, 2022) in the world. The low productivity and growth rate of geothermal energy is because investments in solar PV and wind are significantly higher than in geothermal energy. The exploration and exploitation of HDR geothermal systems, based on deep petrothermal resources, could lead to significant favourable changes for the global geothermal industry (Rybach, 2022).

The main characteristic of these systems is that they have a heat source in shallow, permeable rocks within the Earth's crust, with no fluid available to store or transport the heat to the surface (Tenzer, 2001). Depending on the cause of the heat source, HDR can be classified as follows: (i) igneous-related, where heat is

transferred from magma or hot rocks surrounded by magmatic bodies, (ii) upper mantle-related, where heat is conducted into the Earth's crust through an unusually hot upper mantle, causing the thermal anomaly, and (iii) local, which refers to heat stored locally, either by a high concentration of radioactive minerals or by large-scale fault and/or fracture systems (Gupta and Roy, 2007). As this concept has evolved, HDR is also conventionally referred to as enhanced geothermal systems (EGS). However, it should be noted that there are important differences in their definition. An EGS is a geothermal system in which engineering activities such as hydraulic fracturing have been carried out to increase the permeability of the system. Although the geothermal system at the source need not necessarily be an HDR system, for example, a system where a significant volume of reservoir fluids is stored, but where the overlying rock column sealed by hydrothermal minerals prevents the process of natural recharge, it could be susceptible to becoming an EGS (Santos-Raga et al., 2021). Also, in recent years, the term Hidden Geothermal Systems (HGS) has been defined, which refers to geothermal systems that have no thermal surface manifestations (geysers, hot springs, etc.), a consequence of their impermeable lithology, which does not allow the ascent of fluids. This lack of surface expression makes it even more complex to locate and characterize the geothermal resource (Hanson et al., 2014).

Currently, Mexico ranks seventh worldwide in electricity production using hydrothermal geothermal systems, with an installed capacity >900 MW (Cariaga, 2024). This production is distributed among several geothermal fields, such as Cerro Prieto (570 MW), Las Tres Vírgenes in Baja California (10 MW), Los Azufres in Michoacán (275.1 MW), Humeros in Puebla (120.7 MW), and Domo de San Pedro in Nayarit (Palacios et al., 2024, 26.1 MW). The present study focuses on an unconventional area, the Acozulco Geothermal System (AGS), located in Puebla, within the eastern section of the Trans-Mexican Volcanic Belt (CVTM), 85 km from Puebla and 130 km northeast of Mexico City, near the boundary with the Sierra Madre Oriental (Viggiano-Guerra et al., 2009). The initial studies to assess the geothermal potential of the SGA were conducted in 1995 and 2008 (López-Hernández et al., 2009), with the drilling of exploratory wells EAC-1 and EAC-2, respectively (Viggiano-Guerra et al., 2009). These studies revealed temperatures exceeding 300°C and areas with intense fracturing at different depths, partially sealed by hydrothermal minerals such as pyrite, quartz, and calcite (Gammons et al., 2005; Pulido et al., 2011). Due to these characteristics, the AGS was classified as an HGS, implying the need for unconventional techniques for its study and exploitation (Pulido et al., 2011; Avellán et al., 2019; Sánchez-Córdova et al., 2020). From these promising exploration results, volcanological (e.g., García-Palomo et al., 2018; Sosa-Ceballos et al., 2018; Avellán et al., 2019, 2020; Pérez-Orozco et al., 2021; Liotta et al., 2023), and geophysical (e.g., López-

Hernández et al., 2009; Calcagno et al., 2018; Avellán et al., 2020; Deb et al., 2020; Guerrero-Martínez et al., 2020; Weydt et al., 2020; Kruszewski et al., 2021) studies have been conducted to evaluate in more detail some other structural features of the AGS. Concerning geochemical studies works such as those presented by Polak et al. (1982); Quinto et al. (1995); López Hernández (2009); Peiffer et al. (2014); Santoyo et al. (2020); Canet et al. (2010, 2015b,a); Pérez-Zárate et al. (2024); Santos-Raga et al. (2021), have described chemical characteristics of hydrothermal waters, gases and rocks.

On the other hand, the study of fluid-rock interaction processes, both theoretically and experimentally, is essential for elucidating the deep thermodynamic conditions of geothermal systems (Wood, 2006). In this regard, REE are a relatively immobile elemental group at low temperatures and often exhibit similar physicochemical properties, such as ionic radius and charge (Monecke et al., 2011). Their focused study in geothermal fluids has been investigated in previous works (for example, Yongliang and Yusheng, 1991; Lewis et al., 1998; Wood and Shannon, 2003; Peiffer et al., 2011; Fowler and Zierenberg, 2015; Chudaev et al., 2017), while their mobility has been selectively studied in some theoretical and water-rock experiments (for example, Migdisov and Williams-Jones, 2006; Migdisov et al., 2016; Woitischek et al., 2017; Rillard et al., 2019). The use of REE in Mexican geothermal systems has focused on the study of hydrothermal alteration in rocks (for example, Torres-Alvarado et al., 2007; Pandarinath et al., 2008; Verma et al., 2018; Pandarinath et al., 2020; Sanchez-Córdova et al., 2020), while in the case of fluids, a limited number of studies have been conducted in some hydrothermal volcanic structures in southern Mexico (for example, Taran et al., 2008; Peiffer et al., 2011).

Drawing from the aforementioned, undertaking a comprehensive geochemical study that models the fractionation of REE both theoretically and experimentally poses a significant methodological challenge, yet promises to yield a deeper understanding of the primary water-rock interaction processes within geothermal systems. Such an approach could prove pivotal for investigating unconventional systems like HGS, characterized by the absence of obvious thermal manifestations, thus necessitating the application of non-conventional geochemical methods.

## Objectives

To determine the geochemical behaviour of REE in anomalous hydrothermal alteration and self-sealing processes of hidden geothermal systems by using a theoretical geochemical modelling and selective water-rock experiments.

1. To design and develop a bibliometric methodology and a subsequent systematic analysis for creating a global database related to REE fractionation studies in geothermal systems (theoretical and experimental studies).
2. To evaluate the geochemical behaviour of REE in geothermal fluids and lithological units for different mineralogical compositions of hidden geothermal systems;
3. To carry out new water-rock interaction experiments under medium-high temperature conditions to elucidate and study the main mechanisms of REE element fractionation in geothermal systems.
4. To apply geochemical models to assess the kinetics of major and trace element reactions (mainly REE) under controlled experiments.
5. To evaluate the role of REE in hydrothermal alteration and self sealing processes of hidden geothermal systems, mineral saturation, scaling and weathering processes.

## Overview

Chapter 1 presents both a global and national perspective on the current state of geothermal energy, encompassing both geothermal power generation and its direct uses. It provides a comprehensive overview of active geothermal fields and the progress made in evaluating the country's geothermal capacity.

Chapter 2 examines the state of the art in previous studies on theoretical and experimental investigations of REE geochemistry under geothermal conditions. This review encompasses mobility studies conducted under high temperature and pressure conditions, chemical equilibrium modelling for aqueous species calculation, mobility, and water-rock interaction experiments. Furthermore, it offers a detailed summary of the application of REEs in various industrial contexts, primarily in the geothermal industry. This review culminated with the development of a methodology for evaluating water-rock interaction processes in the Acoculco Geothermal System (SGA), along with a geochemometric approach for conducting water-rock interaction experiments with extended reaction times.

Chapter 3 presents the results obtained from the geochemical mapping of REE and other trace elements in water and rock samples from the hidden geothermal system of Acoculco. This chapter describes a study of water-rock interaction that contributed to the identification of new geochemical signatures and the estimation of deep formation temperatures based on REE analysis, thus becoming an effective tool for discovering compelling anomalies in hidden geothermal systems.

Chapter 4 describes the experimental methodology applied to perform interaction experiments between volcanic rocks and deionised water at 150 °C, with a maximum reaction time of 6 months. The field methodology for selecting and obtaining rock samples with minimal hydrothermal alteration, the rock sample pre-treatment process, the acidification of the reaction fluid, the design of the batch reactors and the product sampling process are described. A key aspect of the methodology was the application of advanced statistical tools (geochemometrics) to optimise the experimental data and improve the interpretation of the results.

In Chapter 5, the main conclusions of this doctoral project are presented based on the successfully achieved results. Additionally, recommendations for future work are provided to correlate the main geochemical properties of REE with the exploration of unconventional geothermal systems. Furthermore, the utilization of geochemical studies of water-rock interaction to address challenges encountered in the geothermal industry is discussed.



# Worldwide status of geothermal exploration and development

---

## 1.1 Geothermal Energy

Geothermal energy is the energy contained in the form of heat inside the Earth, associated with various physical-chemical and tectonic processes inherent in the complex dynamics of our planet. Geoscientists quantify the energy and temperature on Earth in terms of heat flow and temperature gradient (DiPippo and Renner, 2014). Since the Earth's interior is much hotter than its surface, energy flows continuously from the deep, hot interior up to the surface. This is known as terrestrial heat flow gradient (Toth et al., 2017). Nonetheless, the complete extraction of the heat in the Earth's crust remains unattainable due to the absence of technology capable of fully exploiting all geothermal resources (Gallup, 2009). This thermal energy originates inside Earth's crust and is derived from three main components: (i) the heat generated during the formation of Earth, (ii) the heat constantly generated by the decay of radioactive isotopes, mainly those with a long half-life, such as  $^{40}K$ ,  $^{238}U$ ,  $^{235}U$ , and  $^{232}Th$ , and (iii) the differential movement existing between the different tectonic plates. Tectonic dynamics give rise to geothermal systems (Gupta and Roy, 2007) within different geological environments.

The utilization of this heat energy spans a wide array of applications due to its recognition as an economically viable, environmentally friendly, adaptable,

dependable, and abundant resource (Lund et al., 2011). Common applications include (i) electricity generation; (ii) residential conditioning via geothermal heat pumps (for heating and cooling); (iii) recreational tourism and balneology; (iv) agricultural greenhouse cultivation; (v) fish farming; and (vi) industrial and manufacturing processes (Tomarov and Shipkov, 2023; Stober and Bucher, 2012).

The comprehensive geological, geophysical and geochemical carried out for the analysis of hydrothermal systems has facilitated the exploitation of geothermal energy for electricity generation. Essentially, a geothermal system consists of (i) a heat source, typically a cooling magmatic chamber or from radioactive decay; (ii) an aquifer where fluid-rock interaction processes occur; (iii) a seal layer comprised of low permeability rocks, preventing fluid seepage towards the surface; and (iv) a recharge zone (DiPippo and Renner, 2014; Gupta and Roy, 2007). Geothermal fluids predominantly comprise water along with varying proportions of gases and dissolved salts resulting from interactions between the fluid and rock within the aquifer, which produce geothermal brine. The exploitation of these hydrothermal geothermal systems for the production of electricity involves extracting energy in the form of heat transported by the geothermal brine in the vapour phase, from depths to high temperatures (Brown et al., 1966; Lü et al., 2009). The fluid is then routed through vapour pipelines to a geothermoelectric power plant, where conventional electricity generation occurs. Geothermal energy is highly attractive in this industry because it is not intermittent, meaning a geothermal power plant could be operational almost 24 hours a day and 7 days a week, producing continuously.

Due to this process that proposes the use of heat produced naturally in the Earth's crust, geothermal energy is considered a clean energy alternative for electricity generation, or through its direct use for any other industrial application (process heat for food drying, etc.), agricultural, or domestic (DiPippo, 2012).

## 1.2 Current status of geothermal energy in the world

### 1.2.1 Geothermal power generation

The utilization of geothermal resources for electricity generation began in 1904 in Larderello (Italy), with the construction of the first device to produce electricity from a geothermal well (Pérez-Zárata, 2014). Ten years later, in 1914, the first commercial geothermal plant was connected to the public grid, using a 250 kW

turbo-alternator (Chamorro et al., 2012). Since then, several countries, including Mexico, have established geothermal plants to harness natural high-temperature hydrothermal systems. Currently, Yolcan (2023) mentioned that the electricity generation through renewable energies has shown a significant increase, with wind, solar, and geothermal energy standing out. Regarding geothermal energy, based on the latest report published by Cariaga (2024) with updated information until July 2019, there was an installed capacity of 16,355 MW worldwide. The United States was the leading electricity producer through geothermal resource utilization, with an installed capacity of 3,900 MW. On the other hand, Tomarov and Shipkov (2023) reports that for the first time, electricity generation was started at geothermal power plants in Belgium (0.8 MW), Chile (48.0 MW), Croatia (16.5 MW), Honduras (35.0 MW), and Hungary (3.0 MW). During this period, the world witnessed the drilling of 1159 geothermal wells, with over \$10 billion invested in new projects aimed at constructing these power plants. The consistent trend of capacity growth in geothermal power plants is attributed to the comparatively low cost of electricity, the highest rates of installed capacity utilization among renewable energy sources, and their environmentally friendly nature. The top 10 countries with the highest installed capacity are shown in Figure 1.1, according to Cariaga (2024).

## 1. Worldwide status of geothermal exploration and development

---

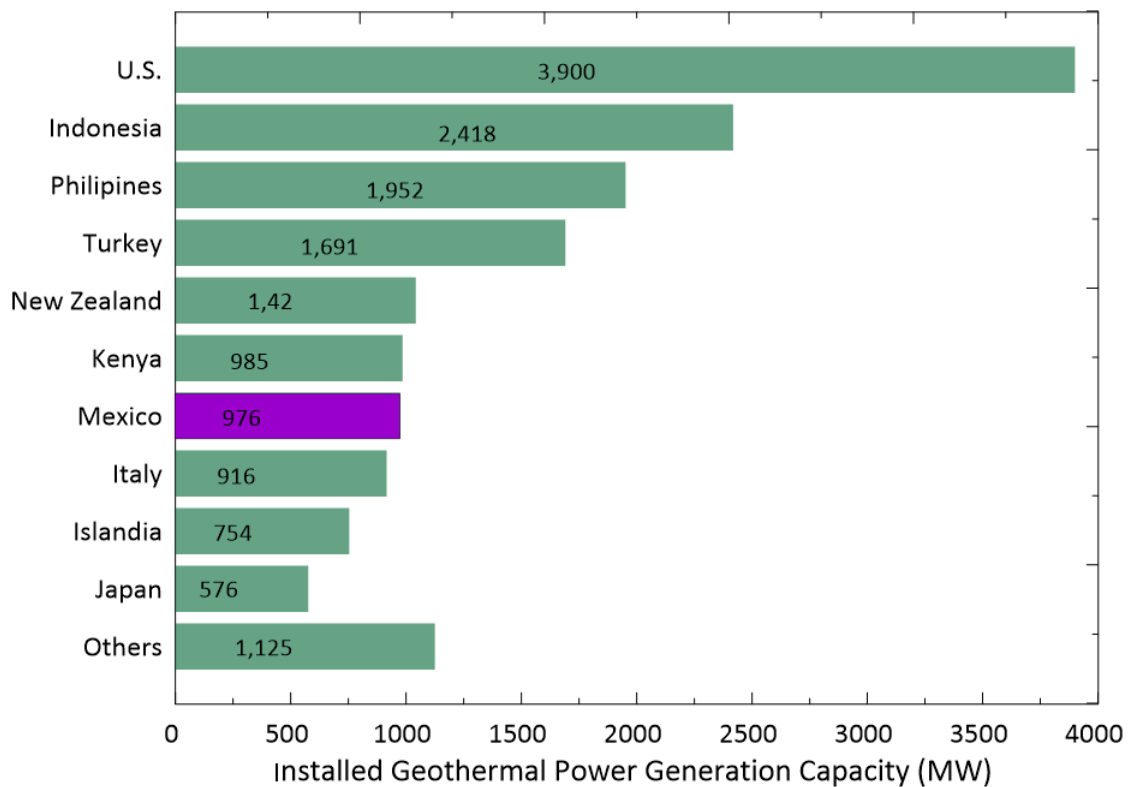


**Figure 1.1:** Top 10 countries with the highest installed geothermal power capacity in the world (Data compiled from: Cariaga, 2024)

Another reliable source of information reporting the evolution of geothermal energy, including installed capacity, geothermal energy produced, and the use of geothermal heat for direct uses worldwide, is provided by the World Geothermal Congress (WGC) in five-year periods. The report for the 2015-2020 period published by Tomarov and Shipkov (2023) outlines that the installed capacity of geothermal plants worldwide up to 2015 was 15,950 MW, and the energy produced was 95,098 GWh/year. Below, Table 1.1 displays the total installed capacity and total energy production for the period from 2015 to 2020 reported by Tomarov and Shipkov (2023), as well as the projection for production in 2025 IEA (2023).

**Table 1.1:** Total installed capacity and geothermal power generation from 2015 to 2020, as well as expected installed capacity in 2025 (Modified after: Tomarov and Shipkov, 2023).

Continent	2015		2020		2025
	Installed capacity (MW)	Electricity production (GWh/year)	Installed capacity (MW)	Electricity production (GWh/year)	Installed capacity (MW)
Europe	2659	18254	2849	20364	2064
Africa	601	2858	1200	9988	631
America	1639	9753	1766	9802	2126
Asia	3716	22965	5873	33994	9234
Oceania	1055	7432	1075	7825	250

## 1.2.2 Direct-uses of the geothermal energy

The earliest forms of harnessing geothermal resources worldwide were through direct uses, which refer to the immediate use of thermal energy instead of converting it to electrical energy (Chandra, 2019). Among the main forms of direct utilization are balneology, swimming, food dehydration, wood drying and space heating.

Líndal (1992) proposed a diagram classifying different uses of geothermal energy based on the temperature and pressure of the fluid, known as the Lindal cascade diagram (Figure 1.2). Analyzing this diagram, it can be observed that aquaculture and agriculture require low temperatures (25 to 90°C), while wood and meat drying require temperatures above 160 °C. This implies that when talking about **cascade** use, it means efficiently utilizing energy, first at higher temperatures and then passing the fluid to other processes that require lower temperatures.

## 1. Worldwide status of geothermal exploration and development

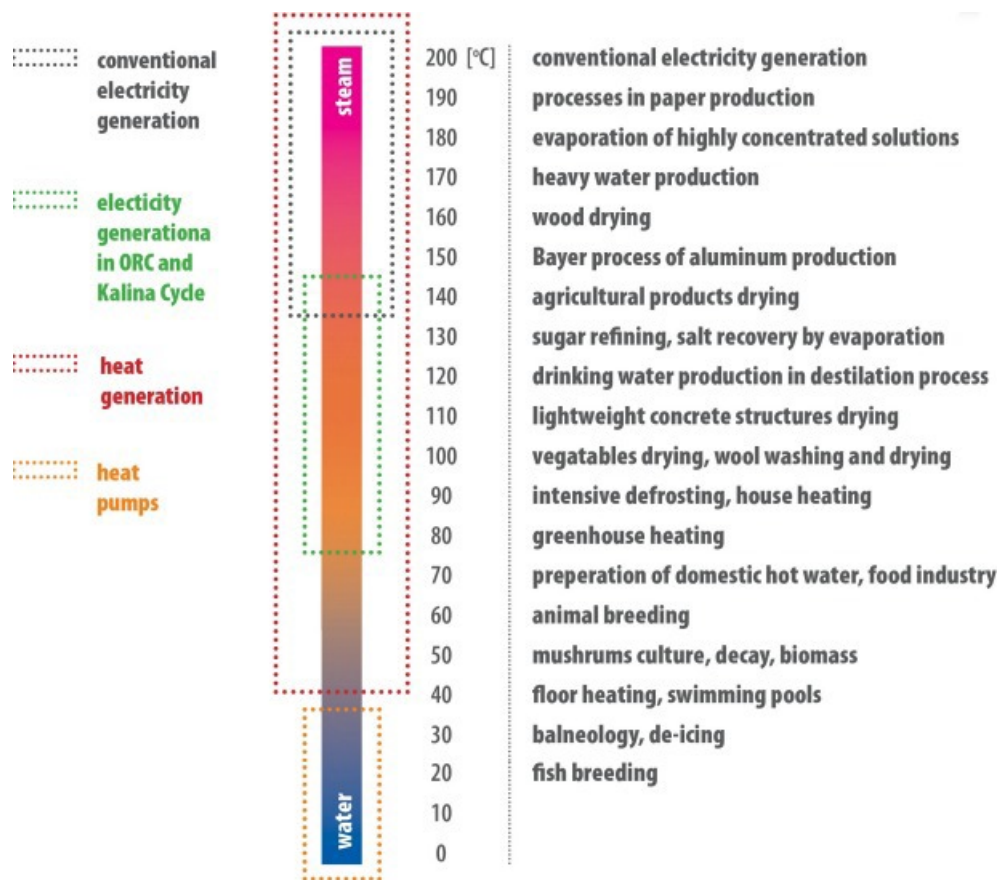


**Figure 1.2:** Lindal diagram (Modified after Kaczmarczyk et al., 2020)

Based on this information, it is evident that for several years now, the world has placed greater emphasis on the direct use of geothermal energy, as well as the technological and research challenges it represents. Global installed capacity has increased from 70,885 to 107,727 MWt over 5 years, representing a 52% increase in percentage terms. Total energy use saw a 72.3% increase from 2015 to 2020, reaching 1,020887 TJ (Lund, 2020: 283,580 GWh).

On the other hand, it has been observed that the use and installed capacity of technologies that directly take advantage of geothermal energy has had great growth worldwide, but some uses have been more popular than others, due to various socio-economic factors and the different needs of each region. According to Lund and Boyd (2016), direct uses can be divided into the following categories: (i) geothermal heat pumps, (ii) space heating, (iii) greenhouse heating, (iv) aquaculture, (v) agricultural drying, (vi) industrial use, (vii) balneology, (viii) cooling and (ix) others. Below, in Figure 1.3, the annual utilization of the main direct uses worldwide is depicted. It can be observed that the popularity of heat pumps

has had the most significant impact, growing by 83% from 2015 to 2020 in annual energy use. This is mainly attributed to the increase in the number of countries with heat pump installations, rising from 82 in 2015 to 88 in 2020, with North America, Europe, and China having the highest number of installations (Lund, 2020). In contrast, the use of geothermal energy for cooling/snow melting shows very little significant progress over the last 20 years, with only 5 countries, including Iceland, Japan, Argentina, United States, and Slovenia, reporting the use of geothermal energy for this application.

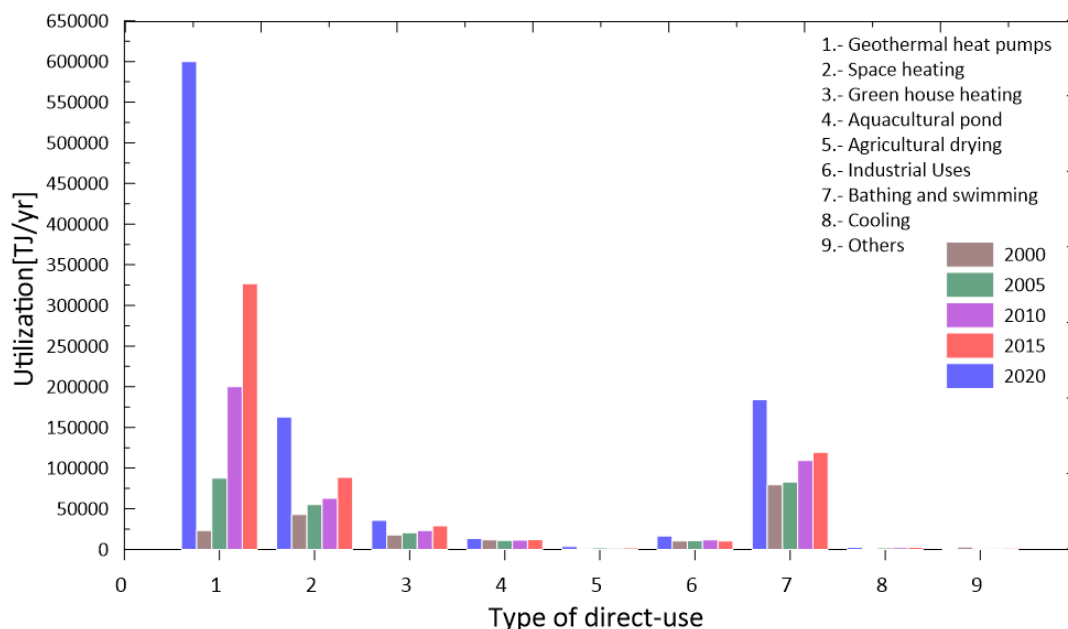


**Figure 1.3:** Comparison of worldwide direct-use of geothermal energy in  $TJ/y$  for the period 2000-2020.

Countries like China, Japan, Iceland, the United States, and Germany currently stand out as leaders in the use of direct geothermal technologies. However, there is still a long way to go, as fossil fuels remain significant competitors, along with the high initial investment costs of geothermal projects. Through research and technological innovation, these projects are becoming increasingly competitive in today's energy market.

## 1.3 Current outlook of geothermal energy in Mexico

### 1.3.1 Geothermal power generation

Mexico ranks seventh in using geothermal energy to produce electrical energy worldwide with an installed capacity of 976 MW (Cariaga, 2024). Over 400 areas with favourable indications for geothermal exploration have been identified, making Mexico a privileged area in the world due to its high geothermal potential. Regarding heat flow, estimated values range from 4 to 1,263  $MW/m^2$  (Espinoza-Ojeda et al., 2017).

According to several studies aimed at evaluating the country's thermal resources (Pan et al., 2016; Gutiérrez-Negrin, 2019), Mexico has been divided into two main regions. The first is the Mexicali region, where the Cerro Prieto geothermal field is located, which is the largest geothermal field in the country and one of the largest in the world. In addition, the geothermal power plant of the Las Tres Vírgenes geothermal field is located. This region has a very high potential due to the phenomenon of plate separation that has formed along the entire secondary fault system of the San Andreas Fault, creating zones of weakness where the magma approaches the surface, considerably increasing the geothermal gradient. The second region is the Trans-Mexican Volcanic Belt (Ferrari et al., 2012, : TMVB), which has a larger territorial area than the previous one. Its formation is attributed to the subduction of the Cocos Plate under the North American Plate, giving rise to several volcanic events from Jalisco to Veracruz. As mentioned previously, this area presents the structural geological conditions necessary for the formation of areas with anomalous geothermal gradients. Some of the geothermal fields located in this area that are currently in exploitation are Los Azufres, Los Humeros and Domo de San Pedro. The Cerritos Colorados field, with a potential of 75 MWe confirmed by several deep wells drilled in the eighties, is still in standby with good probabilities to be developed in the future (Gutiérrez-Negrin et al., 2021).

#### Cerro Prieto

Cerro Prieto is the oldest and operational geothermal field in the country. It is located in the northern part of the state of Baja California Norte, about 30 km southeast of Mexicali, situated on a pull-apart basin formed by the active fault system Cerro-Prieto-Imperial, which is part of the San Andrés fault system. This

field covers an approximate area of  $20 \text{ km}^2$ , with an additional  $18 \text{ km}^2$  associated with vapour emissions. Over the last 50 years, approximately 429 geothermal wells have been drilled, with an average depth of 2430 m and a maximum depth of 4400 m. It has an installed capacity of 570 MW and generates 3,554 GWh of electricity (Gutiérrez-Negrín, 2019).

### **Las Tres Vírgenes**

The Las Tres Vírgenes geothermal field is small operating fields in the country, located in the central part of the Baja California Sur peninsula, within a complex of three Quaternary-age volcanoes with a north-south trending location. Geothermal fluids in the area are stored in intrusive volcanic rocks (granodiorites), which do not outcrop on the surface but have been intersected by all geothermal wells at an approximate depth of 1,000 m (Verma et al., 2006). The heat source of this system is associated with the magma chamber of the most recent volcano, La Virgen. Currently, it has an installed capacity of 10 MWe distributed in two condensation units of 5 MW each and annually generates 47 MWh of electricity (Gutiérrez-Negrín et al., 2021).

### **Los Azufres**

Los Azufres geothermal field is located in the central part of the country, 250 km west of Mexico City in the state of Michoacán, within the physiographic province of the Trans-Mexican Volcanic Belt, which is an area with active volcanism and great geothermal potential. Geologically, the origin of this geothermal field is defined by a period of volcanic activity in the Neogene, with basaltic and andesitic lava flows (Torres-Alvarado, 2002). Volcanic fluids in the area are stored in andesitic rocks with secondary permeability, caused by three fault systems, the most important of which has an E-W trend and dominates the movement of subcortical fluids. Currently, it has an installed capacity of 247.5 MW and generates annually 1,441 GWh of electricity (Gutiérrez-Negrín et al., 2021).

### **Los Humeros**

The Los Humeros geothermal field is located within a Quaternary volcanic caldera (Los Humeros Caldera) at the eastern end of the Trans-Mexican Volcanic Belt, just on the borders of the states of Puebla and Veracruz. The geology of this field is typified by andesitic rocks overlying a basement of metamorphic, sedimentary, and intrusive igneous rocks. The fluids present in this geothermal field are mainly high-enthalpy vapour with low water volume, forming a mixture of sodium-

## 1. Worldwide status of geothermal exploration and development

---

chloride and sulfate-bicarbonate types, with high content of boron, ammonia, and arsenic (Izquierdo et al., 2012). The installed capacity of Los Humeros is 119.8 MWe, with two flash units of 26.7 MWe each, and eight backpressure turbogenerators of 5 MWe each. However, five of these units are kept inactive to be used only when the flash units are out of service, leaving an operational capacity of 68.4 MW and an annual electricity production of 501.5 GWh (Gutiérrez-Negrín et al., 2021).

### Domo de San Pedro

This geothermal field is in the western part of the country, in the southwest of Nayarit. The San Pedro Dome geothermal plant is the first plant created with private investment (Grupo Dragón), according to Gutiérrez-Negrín et al. (2021), it has an installed capacity of 35.5 MW and generates 126.6 GWh of electricity. Fig. 1.4 shows the geothermal power plants currently being exploited and promising areas.

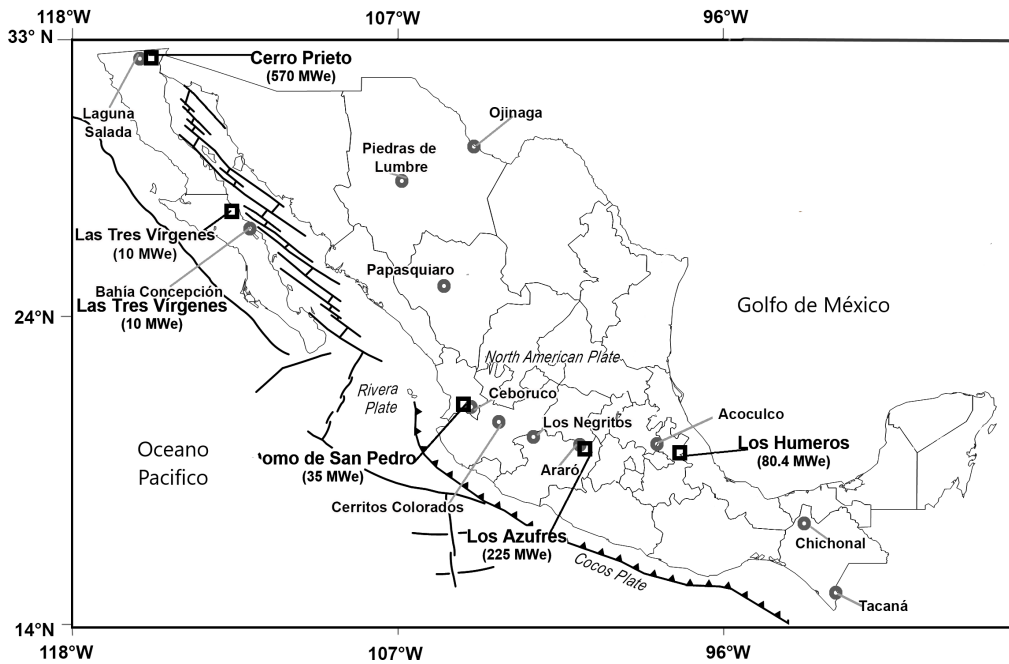


**Figure 1.4:** Location of the main geothermal fields in Mexico and promissory areas.

According to the national energy balance reported by the Ministry of Energy (SENER), Mexico had an effective capacity of 876.3 MWe and an annual electrical production of 127.4 PJ (see Table 1.2), distributed in five geothermal fields described above.

**Table 1.2:** Effective capacity and annual production reported by the National Energy Balance (SENER, 2022).

Year	Effective capacity (MW)	Annual production (PJ)
2015	873.6	134.5
2016	873.6	132.5
2017	873.6	127.4
2018	873.6	113.2
2019	873.6	112.9
2020	950.7	112.2
2021	975.6	92.2
2022	975.6	98.2

### 1.3.2 Direct-uses of the geothermal energy

The use and exploitation of geothermal resources directly have progressed very slowly in Mexico, mainly because most efforts are directed towards electricity generation. According to (Gutiérrez-Negrín et al., 2021), direct uses of geothermal energy in Mexico are restricted practically to bathing and swimming facilities with recreational and/or therapeutic purposes, despite the great number of thermal manifestations identified on the surface.

Below, in Table 1.3, the classification of direct uses and their installed capacity in Mexico is shown, based on information gathered until June 2019 (Gutiérrez-Negrín et al., 2021).

**Table 1.3:** Summary table of geothermal direct heat uses (Modified from Gutiérrez-Negrín et al., 2021).

Use	Installed capacity (MWt)	Annual energy use (TJ/año)	Capacity factor
Individual Space Heating <sup>1</sup>	0.16	3.63	1.00
District Heating	ND <sup>1</sup>	ND	ND
Air Conditioning	ND	ND	ND
Greenhouse Heating	0.004	0.028	0.210
Fish Farming	ND	ND	ND
Animal Farming	ND	ND	ND
Agricultural Drying	0.52	13.23	0.81
Industrial Process Heat	0.028	ND	ND
Snow Melting	ND	ND	ND
Bathing and Swimming	155.35	4166.51	0.85
Geothermal Heat Pumps	0.13		ND
Other uses	ND	ND	ND
<b>Total</b>	0.067	4174.004	0.849

Similarly, in Table 1.3, it can be seen that there are some projects other than balneology and swimming which, although they have a much smaller capacity, represent important advances in this area. The projects are related to space heating, greenhouse heating, and agricultural drying; they were developed by the CFE in the Los Azufres geothermal field.

## 1.4 Remarks of Chapter 1

Currently, geothermal energy is considered an economically exploitable, clean, reliable, and abundant resource, potentially useful in various applications. Among the most common uses of geothermal energy are electricity generation, space heating through geothermal heat pumps, and recreation (balneology and tourism). Among all renewable resources, geothermal energy presents the greatest potential contribution to future energy systems worldwide.

Regarding electricity generation, geothermal power plants have demonstrated significant growth worldwide, and several countries have made substantial investments to expand their geothermal capabilities. The constant increase in installed capacity reflects the attractiveness of geothermal energy as a source of electricity. The total installed generation capacity worldwide exceeds 15,000 MW. The five

countries with the highest installed capacity of geothermal resources in 2023 are the United States, Indonesia, the Philippines, Turkey, and New Zealand.

Mexico, ranking seventh worldwide, stands out as a notable competitor in the geothermal field (with an installed capacity  $> 900$  MW), with a wide range of geothermal fields such as Cerro Prieto, Tres Vírgenes, Los Azufres, Humeros, and the first geothermal field of private industry, Domo de San Pedro. The country's vast geothermal potential, particularly in regions such as the Mexicali area and the Trans-Mexican Volcanic Belt, positions it as a key contributor to the global geothermal energy landscape. In addition, recent efforts have focused on the exploration and exploitation of unconventional geothermal systems. These promising areas are inherently more abundant than hydrothermal systems.

In conclusion, geothermal energy shows a promising future, with continuous advances positioning this energy as a sustainable energy solution. With ongoing research, investment, and strategic planning, geothermal energy has the potential to play an important role in meeting the world's growing energy needs while mitigating the impacts of climate change.



# Updated understanding of the behaviour of REE in geothermal systems

---

2.1	Introduction . . . . .	22
2.2	Fundamentals and geochemical properties . . . . .	23
2.2.1	Thermodynamic conditions . . . . .	23
2.2.2	Physicochemical properties . . . . .	24
2.2.3	Geological setting and origin . . . . .	25
2.3	Rare earth elements in geothermal systems: An updated bibliometric analysis . . . . .	32
2.3.1	Bibliometric analysis methodology . . . . .	33
2.3.2	Worldwide bibliometric database . . . . .	36
2.4	Results and discussions . . . . .	37
2.4.1	Analysis of bibliometric database . . . . .	37
2.4.2	Chemical characterization of REE in rocks and fluid samples . . . . .	40
2.4.3	Worldwide geochemical databases (WGD) . . . . .	44
2.4.4	Mobility of rare earth elements in geothermal systems . . . . .	45
2.4.5	Experimental water-rock interactions studies . . . . .	49
2.5	REE applications and current and future challenges . . . . .	50
2.6	Remarks of Chapter 2 . . . . .	51

## 2.1 Introduction

The REE are strictly composed of 15 lanthanide elements, yttrium, and scandium (IUPAC). Considering that scandium behaves rather differently to the other REE, and that the promethium is a radioactive element, these REE are frequently referred as a physicochemical coherent group, which is also referred as REY (Balaram, 1996; Wall, 2021). The physicochemical properties of some REE (e.g., Ce, Dy, and Nd) make that these elements to be essential components for cutting-edge technologies (including batteries, catalysts, and magnets), which provide a fundamental position in ensuring energy security, promoting economic growth, and promoting environmental sustainability (Dushyantha et al., 2020; Opare et al., 2021). Concerning to geological exploration studies, Yongliang and Yusheng (1991) reported that the REE may be considered as mobile elements at high-temperature conditions ( $>350$  °C). However, Sanyal (2005) pointed out that REE may also coexist from medium-to-high temperatures in some geothermal systems. This author reports that the REE may exhibit a different behaviour of mobility depending on the distribution or partition processes among the chemical composition of fluids and rocks. These geochemical features usually provide a valuable information of the water-rock interaction (WRI) processes taking place in a geothermal system (Wood and Shannon, 2003). These studies provide significant evidence for inferring paleo-thermal conditions, geochemical processes (e.g., Cao et al., 2023; Chudaev et al., 2017; Fowler et al., 2019a; Hannigan, 2005; Hatipo et al., 2020; Möller et al., 2008; Pappaterra et al., 2022; Wei et al., 2022a,b; Wood, 2006; Xiao et al., 2013; Zhang et al., 2023). The dissolution, transport, and precipitation of major and trace elements (REE) through WRI could provide additional geochemical signatures in waters and rocks (primary minerals), which may reflect the main physicochemical conditions of a geothermal system (Göb et al., 2013; Inostroza et al., 2022; Marín-Camacho et al., 2022; Sánchez-Córdova et al., 2020; Shoedarto et al., 2022; Wang et al., 2023).

For the analysis of rock samples, the analysis of REE have been mainly focused on the study of hydrothermal alteration (e.g., Pandarinath et al., 2020, 2008; Sánchez-Córdova et al., 2020; Torres-Alvarado et al., 2007; Verma et al., 2018); whereas for water samples, the study of REE has been less exploited. In general, the scarce application of REE studies in geothermal fluids in the past has been due to the lack of sensitive analytical techniques for their determination at trace levels of concentration (Santoyo et al., 2007; Verma et al., 2002). This analytical barrier was totally overcome with the emergence of new highly sensitive analytical techniques with lower detection limits, and high precision and accuracy (e.g., ICP-MS, ICP-OES, ICP-AES, among others: Fisher and Kara, 2016; Liang et al., 2005; Santoyo et al., 2007). With these important advances in analytical

geochemistry, the possibility to study the REE in geothermal fluids as natural tracers in a wide variety of geothermal systems has been revitalized. Respect to mineral formation, Atwood (2012) noted that, aside from scandium, only sodium and calcium exhibit similar sizes to the REE among the principal cations involved in mineral formation in the Earth's crust and mantle. Based on this, the International Mineralogical Association (2023), there are over 250 minerals containing REE within their chemical structure including various phosphates, carbonates, oxides, and silicates. Among these REE minerals are monazite and bastnaesite with high grades of Light-REE (LREE) and xenotime which contains higher grades of High-REE (HREE: Zeng et al., 2013).

This chapter aims to provide a comprehensive summary of the behaviour of REE in geothermal systems, by covering both rocks and fluids. An analysis of field observations, experimental methodologies, and theoretical evaluations are used seek to an understanding of the intricate dynamics governing REE mobility in these systems. Furthermore, the present chapter addresses some of the main challenges currently facing the study of REE in the geothermal context and highlights specific areas that require further attention and research.

## 2.2 Fundamentals and geochemical properties

### 2.2.1 Thermodynamic conditions

Temperature (T), pressure (P), entropy ( $\Delta S^\circ$ ) Gibbs energy and enthalpy ( $\Delta H$ ) are thermodynamic properties that provide relevant information such as the amount of energy released per mole, and if these reactions are exothermic or endothermic (Haas et al., 1995; Pereira et al., 2019). Several theoretical investigations (e.g., Cetiner and Xiong, 2008; Fowler et al., 2019a; Haas et al., 1995; Lewis et al., 1998; Michard, 1989; Navrotsky et al., 2015; Nesbitt, 1979; Shock et al., 1997; Xiong, 2011) and experimental studies (e.g., Allen and Seyfried Jr, 2005; Drüppel et al., 2020; Firsching and Brune, 1992; Kikawada et al., 2001; Migdisov et al., 2009; Perry and Gysi, 2020; Terakado et al., 1993) have evaluated these thermodynamic properties and their implications on REE fractionation.

The stability of aqueous REE species in complexation processes, among other properties (e.g., composition and fluid redox and pH), depend on the pressure and temperature conditions (Migdisov et al., 2016, 2009). Haas et al. (1995) reported some theoretical works related to REE complexes at high pressures and temperatures, where they pointed out that the formation of REE complexes increases at higher temperatures as the values of the dielectric constant for H<sub>2</sub>O decrease.

Smith et al. (2000) suggests that high CO<sub>2</sub> mole fractions in the hydrothermal fluids also enhance or affect the REE fractionation. In this context, Haas et al. (1995) concluded that although REE tends to form complexes in aqueous solutions over a wide range of temperatures and pressures, only at low temperatures and in dilute solutions exist a significant fraction of free REE cations. Concerning the standard enthalpy, it is considered a significant and fundamental property characteristic of matter's energy content. It is directly associated to the Gibbs energy, equilibrium constant (K), entropy change, and temperature (Pereira et al., 2019). Wood (1990a) reported that most of the complexation reactions of the REE-trivalent oxidation state are considered hard (acid)- hard (base) reactions. These hard-acid with hard-base reactions show a negative dissociation between enthalpy and entropy (?). On the other hand, Gschneidner (1990) proposed that the variation in the enthalpy of formation is correlated reactions with the lanthanide contraction in compound series relative to the contraction in pure metals. Based on this, this correlation can predict unknown enthalpy values if at least one enthalpy of formation value is known in the considered series of compounds (Colinet, 1995; Navrotsky et al., 2015). In a general context, Navrotsky et al. (2015) pointed out that although the study of new optimized materials based on REE-oxides has increased in the last two decades, the thermodynamic database for REE-minerals is still incomplete.

### 2.2.2 Physicochemical properties

The REE are relatively immobile at low temperatures and exhibit similar physicochemical properties such as ionic radius and charge (Bau, 1991; Lewis et al., 1997; Monecke et al., 2011). The trivalent oxidation state (except for Eu and Ce) and the small but steady decrease in ionic radius with an increase in atomic number (lanthanide contraction: diameter of 10.45 nm for La to 8.61 nm for Lu), are some of the main properties of the lanthanide series (Verma and Santoyo, 2007). The decrease in ionic radii with higher atomic number is well-known to be the increase in effective nuclear charge related to the filling of  $4f$  orbitals in their electronic configuration (Seitz et al., 2007). The electrons in this orbital do not shield the other electrons from the positive attraction of the nucleus, and therefore as the atomic number (and thus the number of protons in the nucleus) increases, the electrons move closer together to the core (Wall, 2021). Henderson (1984) mentioned that the electrons  $4f$  orbital are well shielded by the sub-shells ( $5s^2$  and  $5p^6$ ) so that they are not significantly involved in chemical interactions. The differences in the number of electrons in the  $4f$  orbital do not produce significant differences in chemical behaviour. The REE, therefore, tend to appear naturally as a group rather than individually or as a combination of some of them. Zepf (2013) noted

that due to lanthanide contraction, the trivalent ionic radii of most REE resemble the radii of  $\text{Ca}^{2+}$ ,  $\text{Th}^{4+}$ , and  $\text{U}^{4+}$ , and  $\text{Eu}^{2+}$  shares a similar radius with  $\text{Sr}^{2+}$  as a product of lanthanide contraction. This physicochemical feature is important for understanding rock-forming mechanisms because REE often substitute elements with comparable ionic radii (Migaszewski and Gałuszka, 2015b). Consequently, REE may be found in rocks containing Ca, Th, U, and Sr.

Van Gosen et al. (2017), also indicated that the systematic decrease in ionic radii may have two possible implications: (i) the effects on the REE fractionation, which allows their separation in geological environments, and (ii) the increase to unique magnetic and optical properties.

Regarding magnetism, some REE, such as Gd, Dy, Er, Nd and Sm, exhibit complex potentials used in the production of magnets (Zepf, 2013). Jensen and Mackintosh (1991) stated that the magnetism of rare earth elements originates from the angular momentum of the electrons in the  $4f$  suborbital of the atoms. Furthermore, McGuire (1972) noted that, unlike the  $3d$  transition series, the REE- $4f$  electrons generally remain localized in the solid and form magnetic electrons (except Yb, Eu, and Ce). In a broader context, Wall (2021) mentioned that most REE exhibit paramagnetic behaviour, and that the strong magnetism that results from their combination with transition metals (e.g., Fe and Co) is the most important feature. On the other hand, some REE provide sharply defined energy states which can be efficiently used in lighting and laser applications (Zepf, 2013). In terms of optical characteristics, Moeller (1962) observed that ions such as Sc, Y, La, and Lu do not display absorption bands within the wavelength span of 2000–10,000 Å, as anticipated based on their electronic configurations ( $3^+$ ). In contrast, all other Ln ions exhibit distinctive absorption bands within the wavelength region. Specifically, Ce, Eu, Gd, and Tb ions absorb entirely or predominantly in the ultraviolet region, resulting in a colourless appearance. The Yb ion is absorbed exclusively in the near-infrared region, which is why it also acquires colourless properties. The remaining ions are noticeably absorbed in the visible region, providing various colours as observed in ions such as Pr, Nd and Er.

## 2.2.3 Geological setting and origin

### 2.2.3.1 Abundances of the REE in rocks and standard normalization

The REE distributions in meteorites and their mineralogical-lithological components provide fundamental information about the origin and history of the solar system (McLennan and Taylor, 2012). Based on this information REE enrichment or depletion processes gives valuable information for interpreting local hydrothermal processes. These meteorites are characterized by metals, silicates, and sul-

phides, and the abundances of non-volatile elements in nearly solar proportions (Boynton, 1984). According to Van Schmus and Wood (1967) and Wasson and Chou (1974), chondrite meteorites can be classified in chemical groups: (i) carbonaceous, (ii) ordinary, and (iii) enstatite. The carbonaceous group is subdivided into meteorites with high carbon content and nearly solar composition (CI); well-defined chondrules and high carbon content (CM); small chondrules and Al/Si ratios  $<0.11$  (CO), and large chondrules and Al/Si ratios  $>0.11$  (CV). The ordinary group is characterized by chondrites with low total Fe and low content of metals (LL), low total Fe (L), and high total Fe (H). Finally, the enstatite chondrites (E) are typified by highly reduced silicates with nearly no oxidisation (McLennan and Taylor, 2012). Some chondrite normalization values typically utilized in geosciences are reported in the literature by Anders and Grevesse (1989); Boynton (1984); Evensen et al. (1978); Haskin et al. (1968); McDonough and Sun (1995); Palme et al. (1981); Sun et al. (1989); Wakita et al. (1971): see Table 2.1.

**Table 2.1:** Rare earth elements concentration of chondrite normalization standards in ppm.

Element	$Z$	<sup>1</sup> CI	<sup>2</sup> CI	<sup>3</sup> CI	<sup>4</sup> CI	<sup>5</sup> CI	<sup>6</sup> CI	<sup>7</sup> CI	<sup>8</sup> CI
La	57	0.33	0.34	0.25	0.25	0.31	0.24	0.24	0.24
Ce	58	0.88	0.91	0.64	0.64	0.81	0.60	0.61	0.61
Pr	59	0.11	0.12	0.096	0.10	0.12	0.09	0.10	0.09
Nd	60	0.60	0.64	0.47	0.47	0.60	0.45	0.47	0.46
Sm	62	0.18	0.20	0.15	0.15	0.20	0.15	0.15	0.15
Eu	63	0.07	0.07	0.06	0.06	0.07	0.06	0.06	0.06
Gd	64	0.25	0.26	0.20	0.20	0.26	0.20	0.21	0.20
Tb	65	0.05	0.05	0.38	0.04	0.05	0.04	0.04	0.04
Dy	66		0.30	0.25	0.25	0.32	0.24	0.25	0.25
Ho	67	0.07	0.08	0.06	0.06	0.07	0.06	0.06	0.06
Er	68	0.20	0.20	0.17	0.17	0.21	0.16	0.17	0.16
Tm	69	0.03	0.03	0.03	0.03	0.03	0.02	0.03	0.03
Yb	70	0.20	0.22	0.17	0.17	0.21	0.16	0.17	0.16
Lu	71	0.03	0.03	0.03	0.03	0.03	0.02	0.03	0.03
$\Sigma$ REE	—	3.00	3.45	2.94	2.60	3.29	2.48	2.56	2.51
$\Sigma$ LREE	—	2.17	2.28	1.67	1.67	2.11	1.58	1.62	1.60
$\Sigma$ HREE	—	0.83	1.17	1.27	0.93	1.18	0.90	0.94	0.91
Ratio $\Sigma$ LREE/ $\Sigma$ HREE	—	2.62	1.95	1.31	1.78	1.78	1.76	1.73	1.77
Chemical technique	—	Tit.	INAA	INAA	INAA	IDMS	IDMS	IDMS	IDMS

<sup>1</sup>Haskin et al. (1968), <sup>2</sup>Wakita et al. (1971), <sup>3</sup>Evensen et al. (1978), <sup>4</sup>Palme et al. (1981), <sup>5</sup>Boynton (1984), <sup>6</sup>Anders and Grevesse (1989), <sup>7</sup>Sun et al. (1989), <sup>8</sup>McDonough and Sun (1995). The REE compositions are analysed by: Titration (Tit.); Instrumental Neutron Activation Analysis (INAA), and Isotope Dilution Mass Spectrometry (IDMS).

On the other hand, the Upper Continental Crust (UCC), being the most accessible part of our planet, has long been the target of geochemical investigations. There are two basic methods used to determine the composition of the upper

## 2. Updated understanding of the behaviour of rare earth elements (REE) in geothermal systems

---

crust: (i) weighted averages of the compositions of rocks exposed at the surface and (ii) averages of the composition of insoluble elements in fine-grained clastic sedimentary rocks or glacial deposits and using these to infer upper-crust composition (Rudnick and Gao, 2003). REE-UCC patterns are equivalent to granodiorite, plutonic igneous rocks (Taylor et al., 1981). Some UCC normalization values reported in the literature include Rudnick and Gao (2003); Taylor et al. (1981); Taylor and McLennan (1995); Wedepohl (1995). Another normalization standard value commonly utilized is the North American Shale Composite (NASC: Gromet et al., 1984; Taylor and McLennan, 1985). This geological normalization standard was measured to determine the represented average relative abundance of REE in the Earth's crust (Taylor and McLennan, 1985). Gromet et al. (1984) noted that the NASC showed a relative enrichment of LREE based on the REE-chondrite values, probably attributed to differentiation processes that formed the Earth's crust. Finally Post-Archean Australian Shale (PAAS: Taylor and McLennan, 1995; Pourmand et al., 2012) and Primitive Mantle (PM: McDonough and Sun, 1995; Sun et al., 1989; Taylor et al., 1981) are usually used for some geochemical studies (2.2).

**Table 2.2:** Rare earth elements concentration of Upper Continental Crust, Post-Archean Australian Shale, North American Shale Composite and Primitive Mantle of normalization standards in ppm.

Element	Z	<sup>3</sup> UCC	<sup>4</sup> PAAS	<sup>5</sup> PAAS	<sup>6</sup> PAAS	<sup>7</sup> NASC	<sup>8</sup> NASC	<sup>9</sup> PM
La	57	31.000	44.56	38.00	38.20	32.00	31.10	0.65
Ce	58	63.000	88.25	80.00	79.60	73.00	66.00	1.68
Pr	59	7.100	10.15	8.90	8.83	7.90		0.25
Nd	60	27.000	37.32	32.00	33.90	33.00	27.40	1.25
Sm	62	4.700	6.88	5.60	5.55	5.70	5.59	0.47
Eu	63	1.000	1.22	1.10	1.08	1.240	1.18	0.15
Gd	64	4.000	6.04	4.70	4.66	5.20		0.54
Tb	65	0.700	0.89	0.77	0.77	0.85	0.85	0.10
Dy	66	3.900	5.33	4.40	4.68	5.80		0.67
Ho	67	0.83	1.05	1.00	0.99	1.04		0.15
Er	68	2.30	3.08	2.90	2.85	3.40		0.16
Tm	69	0.30	0.45	0.40	0.46	0.50		0.03
Yb	70	2.00	3.01	2.80	2.82	3.10	3.06	0.16
Lu	71	0.31	0.44	0.43	0.43	0.48	0.45	0.03
ΣREE	—	148.14	208.67	183.0	184.77	173.21	135.63	6.22
ΣLREE	—	133.80	188.38	165.60	167.16	152.84	131.27	4.39
ΣHREE	—	14.34	20.29	17.40	17.61	20.37	4.37	1.84
Ratio ΣLREE/ ΣHREE	—	9.33	9.29	9.58	9.49	7.50	30.066	2.39
Chemical tech- nique	—	INAA	MC- ICP- MS	INAA	INAA	INAA	INAA	INAA

<sup>1,5,7</sup>Taylor and McLennan (1985), <sup>2</sup>Wedepohl (1995), <sup>3</sup>Rudnick and Gao (2003), <sup>4</sup>Pourmand et al. (2012), <sup>6</sup>McLenan (1989), <sup>8,9</sup>Gromet et al. (1984). The REE compositions are analysed by: Instrumental Neutron Activation Analysis (INAA), and Isotope Dilution Mass Spectrometry (IDMS).

### 2.2.3.2 Fractional crystallization and mantle-melting processes

Igneous processes such as fractional crystallization, assimilation of material from the Earth's crust, partial melting and melt immiscibility are crucial in the development of a rock matrix with a high concentration of REE (Perry and Gysi, 2020; Vasyukova and Williams-Jones, 2020; wan Wei et al., 2023). These processes determine the concentration and distribution of REE in some mineral phases and rocks. In addition, can explain the tetrad effect patterns found in igneous rocks (Monecke et al., 2000; Veksler et al., 2005).

Van Gosen et al. (2017) mentioned that during the crystallization of silicate minerals such as amphiboles, feldspars, and olivine, most of the REE tends to be retained in the coexisting melt. In contrast,  $\text{Eu}^{2+}$  is frequently removed from magmas and integrated into feldspar crystals due to its valence state. In addition to this europium anomaly, Atwood (2012) suggested that the presence of heavy rare earth element (HREE) depletion often points to the involvement of garnet fractionation in the evolution of its precursor magmas. On the other hand, wan Wei et al. (2023), concluded that calcite crystallization from carbonate magmas with high Si activity produces further HREE enrichment in the residual melt. As a result, the lanthanides typically accumulate in magmatic fluids that form later in the process and in mineral phases that crystallize during the later stages (McLennan, 1989; Voncken, 2016). Concerning to the magmatic assimilation and the partial melting, Vasyukova and Williams-Jones (2020) show that the effect of lower crustal assimilation is very modest. However, in assimilation occurring in the upper crust, the effect is quite substantial due to the higher high field strength elements (HFSE) content of the upper crust. On the other hand, McLennan and Taylor (2012) explain that plagioclase is only stable at high pressure and depth, so the anomalous behaviour of REE elements such as europium in igneous rocks is a clear sign of a relatively igneous partial melting process.

When the concentration of a specific mineral reaches saturation at a temperature above the mineral's melting point (melt immiscibility), a secondary magma drops precipitates instead of forming a solid mineral grain. These liquids with contrasting compositions, are a common phenomenon in alkaline igneous systems composition and can result in the formation of valuable ore deposits (Skinner, 2022). Some studies conducted in the field and through experiments have verified that liquid immiscibility is a notable mechanism playing a crucial role in creating diversity in the composition of igneous rocks (Treiman and Essene, 1985; Trofanenko et al., 2016; Vasyukova and Williams-Jones, 2020, 2014; Veksler et al., 2005; wan Wei et al., 2023). Regarding REE, wan Wei et al. (2023) mentioned that the liquid immiscibility between silicate and carbonate melts results in LREE enrichment relative to HREE. This observation is supported by Vasyukova and Williams-Jones (2014), who concluded that this process, specifically the immisci-

bility of the silicate-fluoride melt, significantly contributes to concentrating REE at potential economic levels. Finally, it is worth mentioning that these processes can be varied with respect to the geological settings, for example, Brophy (2008) proposed a model for determining the fractionation or amphibolite melting origin for felsic magmas in intra-oceanic arc environments. Vasyukova and Williams-Jones (2020) developed a series of magmatic steps for nephelite magma which culminate in the enrichment of the LREE and Y. However, most researchers agree that a combination of flow melting degrees in the mantle source and a prolonged subsequent differentiation history is not sufficient to explain the unusual enrichment of halogens, HFSE, REE, and other rare and incompatible elements mainly in peralkaline rocks (Marks and Markl, 2017).

### 2.2.3.3 Rare earth elements ore deposits

REE are typically found in geological formations such as carbonatites (Cangelosi et al., 2020; Hari et al., 2018; Öztürk et al., 2019; Ramasamy et al., 2013; Sarapaa et al., 2013; Trofanenko et al., 2016; Verplanck et al., 2016; wan Wei et al., 2023), alkaline/peralkaline igneous rocks (Horiuchi et al., 2014; Petrosino et al., 2013; Sallet et al., 2005; Sarapaa et al., 2013; Vasyukova and Williams-Jones, 2020), Ion Adsorption clay (Sanematsu and Watanabe, 2019), placer-type (Sengupta and Gosen, 2019) and phosphorite-type Emsbo et al. (2016). The primary focus of this section is carbonatite and alkaline/peralkaline deposits because their geology is more related to the geothermal environment.

Currently, the most important REE (especially LREE, that includes La, Ce, Pr, and Nd) deposits in the world are closely related to carbonatites Voncken (2016). These intrusive igneous rocks (with more than 50% carbonate minerals) are associated with volcanic activity in intracontinental rift zones and hot-spot areas, enriched with phosphate minerals like apatite and monazite as well as bastnaesite and other minerals (Voncken, 2016). REE concentration in carbonatites is related to apatite (commonly higher than 1 wt% total REE) and burbankite Cangelosi et al. (2020). There are still many controversies about the genesis of the mineral and the mechanisms of REE enrichment in carbonatite deposits; wan Wei et al. (2023) propose that it is related to the melting of carbonate peridotite or eclogite, liquid immiscibility between the alkali silicate melt and the carbonate melt, and the fractionation of crystals from the carbonate silicate melt. On the other hand, Verplanck et al. (2016) mentioned that to understand the enrichment of critical elements in carbonatite deposits there is the notion that the formation of initial carbonatite melts or highly alkaline silica-rich melts in the Earth's mantle requires a source of the mantle rich in lithophilic elements, along with the presence of water and carbon dioxide. These constituents are essential not only for

the origin of melt carbonatites but also contribute significantly to the concentration of REE, which leads to the development of an ore deposit. Finally, Wang et al. (2020) proposes that REE enrichment is not a product of immiscibility or fractional crystallization of the parental carbonate-silicate magma, but rather occurs after the formation of carbonatite magma during the gradual evolution of this magma through fractional crystallization of carbonate minerals and immiscibility of melt and hydrothermal fluid. These REE deposits can be classified by origin: primary magmatic (e.g., Mountain Pass, USA), ii) hydrothermal (e.g., Bayan Obo, China) and iii) carbonatite weathering-crust (e.g., Mount Weld, Australia); or based on wt.% ratios of the major elements: i) magnesiocarbonatites, ii) ferrocyanatites and iii) calciocyanatites (Wang et al., 2020). Understanding the geochemistry and genesis of carbonatites is crucial for identifying potential sources of these critical elements and for exploring sustainable methods for their extraction. Concerning Alkaline/peralkaline deposits, these are made up of rocks from undersaturated silica (nepheline syenites) to supersaturated silica (granites), and occur in intraplate tectonic environments, mainly in continental environments and are typically associated with rifting, faulting and/or crustal extension (Dostal, 2016). Concerning their overall volume, alkaline igneous rocks constitute less than one per cent of the igneous rocks (Voncken, 2016). These deposits represent one of the most economically important resources of HREE, including Y (Dostal, 2016; Dushyantha et al., 2020; Verplanck et al., 2016). On the other hand, Wang et al. (2013) mentioned that the Igneous rocks characterized by elevated concentrations of REE, such as carbonatites or alkaline igneous complexes, serve as excellent origins for hydrothermal fluids enriched with REE. This process results in deposits containing both primary igneous and hydrothermal mineralization of REE. Based on this, geothermal systems can be considered promising REE deposits, due to water-rock interaction associated with high temperatures, pressures, and chemical conditions inherent to these thermal systems.

## 2.3 Rare earth elements in geothermal systems:

### An updated bibliometric analysis

Bibliometric analysis (BA) is a qualitative and quantitative method based on mathematical and statistical tools applied (e.g., text mining) to obtain a better understanding of research patterns about used authors, networking groups, institutions, journals, and countries (Echchakoui, 2020; Yáñez-Dávila et al., 2023). The present BA aimed to identify key research aspects of rare earth elements concentration in fluids and rocks in geothermal systems and their application as a

geochemical exploration tool.

### **2.3.1 Bibliometric analysis methodology**

This integral bibliometric methodology is divided into two evaluation stages; Text Mining (TeM) and Performance-Intellectual Analysis (PeIA) which minimize bias and error in the mapping of accumulative scientific studies (2.1). TeM stage is used to find out the most representative patterns of scientific productivity and involves three sub-stages: (1) the data retrieval that defines the search criteria; (2) the data collection from the indexed citation database; and (3) the semantic metadata that adjustment and refinement of the searching criteria. PeIA stage is used to find the patterns of the scientific productivity and involves two sub-stages: (4) the data analysis and visualisation of the TeM and PeIA through mapping and envisioning the temporal evolution of the research subject; and (5) the conclusion and outlook for future research (Yáñez-Dávila et al., 2023).

## 2. Updated understanding of the behaviour of rare earth elements (REE) in geothermal systems

---

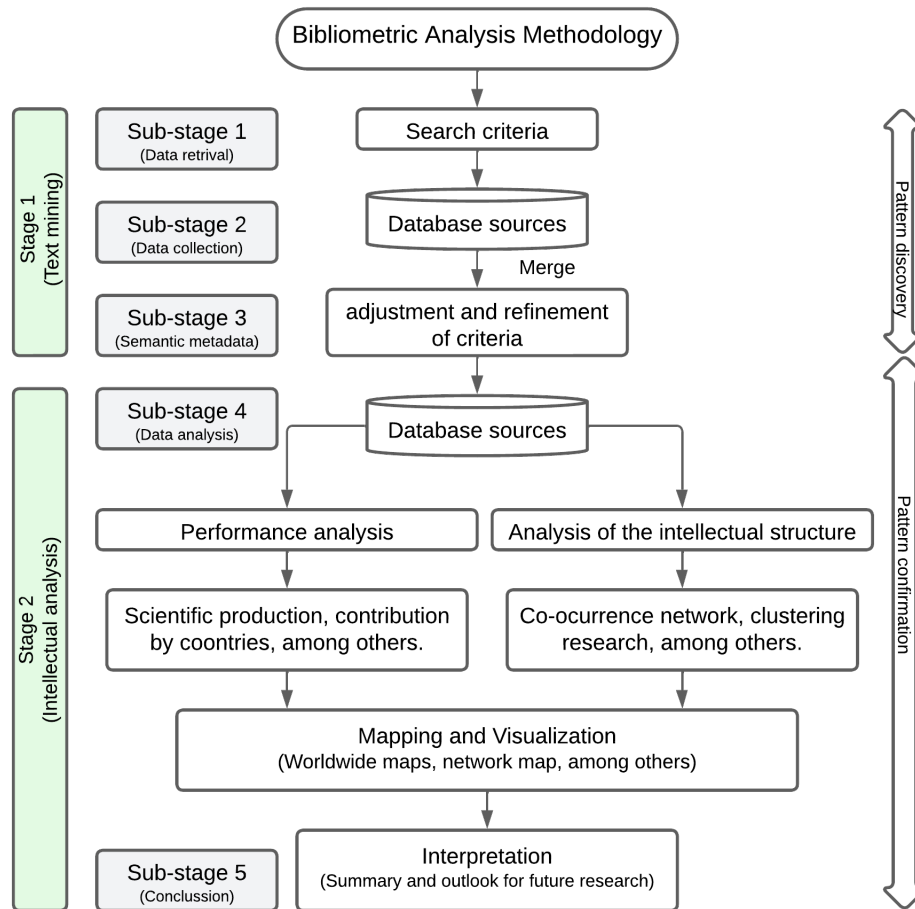


**Figure 2.1:** Flow diagram showing the methodology implemented for the bibliometric analysis (modified after Yáñez-Dávila et al., 2023).

### 2.3.1.1 Text data mining (Stage 1: TeM)

TeM techniques are used to transform unstructured text into normalized and structured data Yáñez-Dávila et al. (2023). This stage allows new information to be excluded from previous bibliometric database.

#### *Data retrieval (sub-stage 1)*

In this sub-stage, the suitable supervised keywords to describe the knowledge on the research subject under evaluation were defined: (i) rare earth elements, (ii) hydrothermal waters, (iii) geothermal energy, (iv) water-rock interaction ex-

periments, (v) geochemical modelling, among others. These supervised keywords will allow representative scientific publications to be identified and complied with. On the other hand, the following inclusion/exclusion criteria were also defined: Language: English; Document type: article and reviews; Period: undefined to December 2023; and Specific condition: geothermal system.

#### *Bibliometric data collection (sub-stage 2)*

Considering the advantages and singularities reported in several BA for Web of Science<sup>©</sup> (WoS) and Scopus<sup>©</sup> (Goodman, 2007; Vera-Baceta et al., 2019), these citation databases were selected as searching tools. Both databases have advantages or singularities and are considered viable alternatives when selecting databases of peer-reviewed scientific literature (Vera-Baceta et al., 2019). WoS shows extensive coverage across years, whereas Scopus offers higher journal selection (Goodman, 2007), in part because the addition to articles contains other documents such, as conference proceedings and books. The suitable Boolean strings (keywords and syntax variants) were defined according to the nomenclature of these databases. This process was carried out on December 7<sup>th</sup>, 2023, by two technical researchers to mitigate bias.

The syntaxes described provide readers with the criteria used to reproduce the WoS and Scopus searching results. The primary statistical sample was 510 published articles (PA) from which Scopus and WoS reported 375 and 135 PA, respectively. To avoid duplicated publications the primary bibliographic samples were filtered using a merge method suggested by Echchakoui (2020). The merging process was carried out using *R* open-source programming code that involved several algorithm steps: (i) the conversion of both bibliography files (Scopus and WoS) to bibtex files; (ii) the formatting of WoS.bib and Scopus.bib files to have the same tag fields; (iii) the merging of two databases for removing duplicates and converting the WoS and Scopus bib files to Excel file. After applying the merging process, a secondary statistical sample of 281 PA was obtained.

#### *Semantic metadata (sub-stage 3)*

In the secondary statistical sample of 281 PA was implemented a final manual refinement. This refinement was also carried out for data normalization and spelling errors to satisfy the strict conditions of geothermal systems. As a result of this refinement, a ternary statistical sample of 144 PA was obtained from peer-reviewed journals. This tertiary statistical sample was defined as the final working database for carrying out this BA (M.xlsx file). All final working databases have been listed in Table 1S of the supplementary material, which may be used for

addressing past and latest studies on the mobility of Rare Earth Elements in geothermal systems.

### **2.3.1.2 Intellectual Analysis (Stage 2: PeIA)**

#### *Data analysis and visualization (sub-stage 4)*

This stage includes performance analysis and an analysis of the intellectual structure through clustering and multicriteria analysis based on the bibliometric database. For this process, it is necessary to collect data on scientific production, notable authors, preferred peer-reviewed journals, global institutions, highly referenced articles and significant contributions from various countries. Zupic and Čater (2015) mentioned that an intellectual framework analysis involves using search results related to the research topic to identify: (i) the domain of scientific knowledge; (ii) key fields of interdisciplinary research; (iii) predominant research themes; and (iv) the schematic pattern of interrelationships between research topics. Each analysis used Bibliometrix, an R-tool for science mapping analysis. This software allows the construction, exploration, and graphic representation of easy-to-interpret two-dimensional maps of bibliometric networks, such as author co-occurrence maps, author co-citation, and country collaboration maps, among others.

### **2.3.2 Worldwide bibliometric database**

With the application of this bibliometric methodology, a complete analysis of the study of rare earth elements in geothermal systems from 1963 to 2022 was carried out. This analysis allowed obtaining the most representative bibliometric indicators on the research topic. Published articles, preferred publication journals, research leaders (authors, network groups, institutions and countries) and future research trends were also compiled from a comprehensive search of global databases. Table 2.3 shows the general statistical information inherent in the bibliometric database created based on the methodology described in this section.

**Table 2.3:** Summary of bibliometric indicators found in Scopus and Web of Science databases on the research subject of REE in geothermal systems (time period 1992-2024).

Main information about data	
Time period	1992-2024
Articles sources	58
Articles	144
Average years from publication	8.43
Average citations per articles	25.16
<b>Article content</b>	
Keywords Plus	1468
Author's Keywords	483
<b>Authors information</b>	
Number of authors	588
Authors of single-authored documents	6
Authors of multi-authored documents	582
<b>Authors collaboration</b>	
Articles per author	0.25
Authors per articles	4.08
Co-Authors per Documents	5.01
Collaboration Index	4.25

## 2.4 Results and discussions

### 2.4.1 Analysis of bibliometric database

#### 2.4.1.1 Global scientific production

The analysis of the advanced search by data mining with keywords resulted in a total of 144 documents produced from 1992 to 2024. A graphical representation of the cumulative frequency of these PA is presented in Fig. 2.2a, with the intersecting green dashed line denoting the most crucial inflexion point of the exponential function (Andreo-Martínez et al., 2020; Carrión-Mero et al., 2020; Sinclair, 1974). This exponential function ( $F(t) = ae^{bt}$ : Price, 1963) describes the growth in the study of REE in geothermal systems over time. The current tendency of the number of articles related to the study of REE composition in geothermal systems as a natural tracer of water-rock interaction shows that it is a research field in the phase of exponential growth.

## 2. Updated understanding of the behaviour of rare earth elements (REE) in geothermal systems

---

The variability of the number of PA over time is represented in Fig. 2.2b using the well-known Price's Law phases (Price, 1963). Price's phase 1 is defined as the "forerunners" zone, and phase 2 is the "growth" zone (Yáñez-Dávila et al., 2023). The green dashed line in Fig. 2b represents the time boundary between these two phases, estimated from the inflection point of the cumulative frequency plot (Fig. 2.2a). Price's phase 1 describes the period between 1992 and 2014, during which 43 articles were published. These PA represent  $\approx 30\%$  of the total number of articles ( $n = 144$ ) published during the entire period (1992 to 2024). On the other hand, Price's Phase 2 identified the period between 2014 and 2024, during which scientific production exhibited an exponential increase, with 101 PA representing  $\approx 70\%$  of the total number of publications.

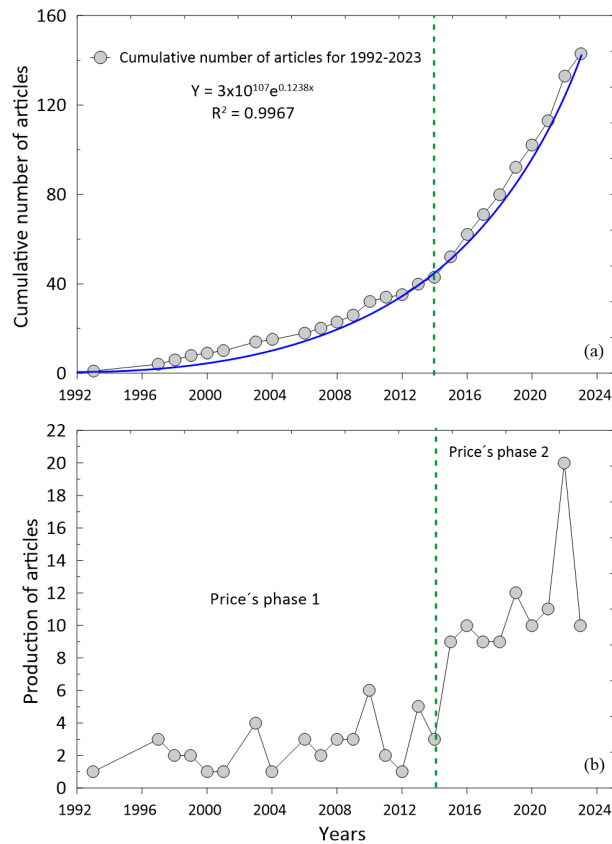


**Figure 2.2:** Plots of the scientific output documented on REE in geothermal systems: (a) exponential growth patterns describing the correlation among the number of articles per year; (b) The scientific productivity of REE in geothermal systems articles associated with geothermal applications, where Price's Phase 1 is classified as the "forerunners zone" in research, and Price's phase 2 is identified as the "growth zone" which began significantly in 2014.

### 2.4.1.2 Worldwide scientific distribution

A global distribution of articles published in peer-reviewed journals is shown in Fig. 2.3. After reviewing the information on author affiliations and countries of origin, the contribution of PA by country was quantified for the global period (1992-2024). The percentage of collaboration between researchers and institutions from different countries was also inferred, with the strongest collaborative ties achieved between the United States and the United Kingdom (12%). Lower collaborative ties were observed for other country pairs (up 6%). It was also found that the research topic under evaluation has been studied in only 20 countries.

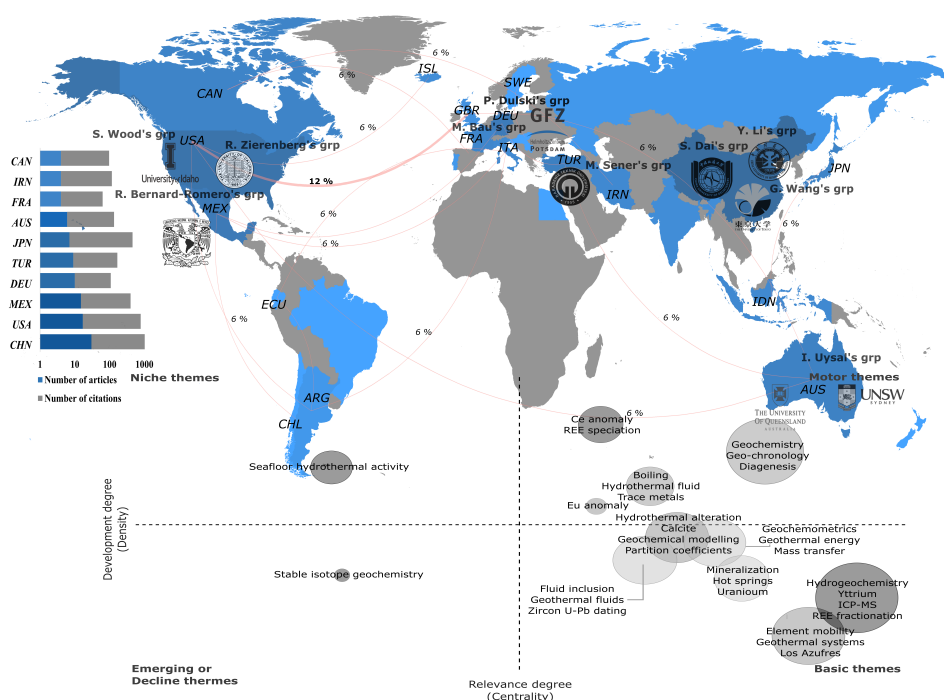


**Figure 2.3:** Worldwide distribution of articles reported in peer-review journals and reviews on REE focussed on geothermal fractionation (1992–2024). The thickness of the red line indicates the high percentage of collaboration. The name of the countries is abbreviated using the international convention suggested by ISO-3166 international standard. The logarithmic scale of the number of citations ranges from 1 to 1000, and it is overlapped with the number of published articles.

On the other hand, the top ten countries leading in article publication and their citation records are attributed as follows: (i) China, ranked with a total publication of 30 articles from 144 PA, representing approximately a 21% contribution and 608 citations; (ii) the USA with 17 PA ( $\approx 12\%$ ) and 904 citations; (iii) Mexico with 15 PA ( $\approx 10\%$ ) and 182 citations; (iv) Germany with 10 PA ( $\approx 7\%$ ) and 325 citations;

(v) Turkey with 9 PA (6%) and 164 citations; (vi) Japan with 7 PA ( $\approx 5\%$ ) and 126 citations; (vii) Australia with 6 PAs ( $\approx 4\%$ ) and 250 citations; and (viii, ix, and x) France, Iran, and Canada with 4 PA ( $\approx 3\%$ ) each, along with 118, 84, and 55 citations respectively. Other countries, such as Iceland, India, Indonesia, Korea, Chile, New Zealand, Russia, Croatia, Egypt, Poland, Serbia, Sweden, and Tanzania, exhibited lower productivity with an integrated contribution of almost  $\approx 26\%$ .

The percentage of collaboration among researchers and institutions from different countries was also inferred, where the stronger links of collaboration were achieved for the pairs USA-Great Britain (12%). A lower collaboration links were observed for other country pairs (6%).

This brief bibliometric analysis reveals that REE as a tool for geothermal exploration research has gradually emerged as a prominent topic among geochemist researchers engaged in geothermal prospecting and exploitation studies.

## 2.4.2 Chemical characterization of REE in rocks and fluid samples

Golloch (2022) mentioned that the REE technological applications research and their quantification based on chemical analytical techniques have grown hugely since World War II. The first analytical techniques utilized by REE quantification were gravimetric, radiochemical, and titrimetric methods, spectrophotometry and X-ray absorption and emission spectrometry (Golloch, 2022, and references therein). Subsequently, X-ray fluorescence (Chen et al., 1993; Roelandts, 1981; Schramm, 2016), Neutron activation analysis (Oddone et al., 1984), mass spectrometry (Balaram, 1996) and isotope dilution (Greaves et al., 1989) were developed. For geothermal systems, over the past two decades, the determination and evaluation of REE behaviour in rocks and fluids as a new and powerful geothermal exploration tool have increasingly, primarily due to the use of sensitive analytical methods capable of detecting these elements at low concentrations ranging from micrograms per litre ( $\mu\text{g/L}$ ) to nanograms per litre ( $\text{ng/L}$ ), respectively (Pourmand et al., 2012; Santos-Raga et al., 2021). Additionally, the scarcity of reference standards for calibrating instruments and analysing water and rock samples posed a significant challenge (Verma et al., 2002). These difficulties were overcome as highly sensitive analytical techniques like Inductively Coupled Plasma Mass Spectrometry (ICP-MS), Laser Ablation-ICP-MS (LA-ICP-MS), Quadrupole-ICP-MS (Q-ICP-MS), High Resolution-ICP-MS (HR-ICP-MS), Multicollector-ICP-MS (MC-ICP-MS), ICP-Atomic Emission Spectroscopy (ICP-AES), Fusion-ICP (FUS-ICP), ICP-Optical Emission (ICP-OES) (Baker et al.,

2002; Fisher and Kara, 2016; Golloch, 2022; Migaszewski and Gałuszka, 2015a; Santoyo et al., 2007). These advancements in analytical geochemistry facilitated a renewed interest in investigating REE in geothermal rocks and fluids, leveraging them as natural tracers, across a diverse array of geothermal systems (Santos-Raga et al., 2021). Figure 2.4 shows histograms to illustrate the main chemical techniques used for REE quantification based on the bibliometric database (unpublished compilation).

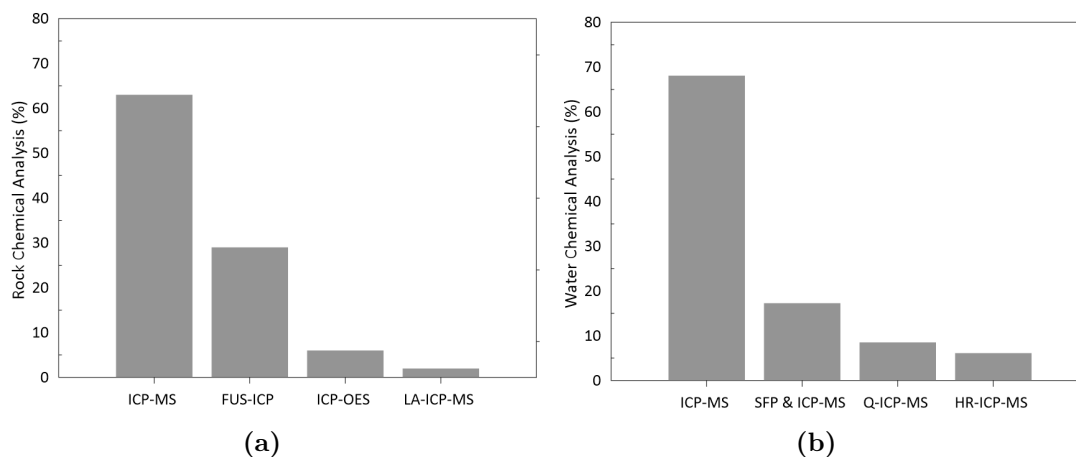


**Figure 2.4:** Histograms of the main chemical techniques used for the separation and determination of REE in rock and water samples from geothermal systems (%).

Based on Figure 2.4, it is observed that the most commonly used technique for quantifying REE in geothermal systems is ICP-MS, which is utilized for 62% of rocks and 68% of fluid samples. The remaining percentage is divided among other ICP-based techniques, such as FUS-ICP (30%), ICP-OES (6%), LA-ICP-MS (2%) for rocks, and SFP & ICP-MS (16%), Q-ICP-MS (10%), and HR-ICP-MS (6%) for fluids.

#### 2.4.2.1 Chemical pretreatment

In some samples (e.g., water samples), the amounts of REE are negligible, and the dissolution leads to a significant reduction in sample concentration, hindering precise quantification. Therefore, separation/preconcentration group techniques are usually required as sample pretreatment (Pinto et al., 2012; Santos et al., 2010). The most usual techniques for this process are precipitation/coprecipitation, liquid-liquid extraction, liquid-phase microextraction, solid-phase extraction and solid-phase microextraction (Golloch, 2022). In many studies, it was difficult

to obtain a clear-cut picture of the type of group separation used to evaluate and calibrate the system in quantification of REE, because only some studies from the database report the pretreatment method. Some studies that report this pretreatment, was outlined below.

Schmidt et al. (2007b) mentioned that rare earth elements and yttrium (REY) were determined by matrix separation and preconcentration following the protocol of Schmidt et al. (2010), and measured with a PerkinElmer Elan 5000 quadrupole ICP-MS in Bremen. The reported matrix separation methodology consists of diluting 10-20 ml of the sample to 1 L with deionized water, acidifying with ultrapure HCl (MERCK suprapure, pH = 2), and adding 1 ml of 250 ppb Tm. The Tm concentration was then quantified as a reference, and the sample was passed through an ion exchange column (Sep-Pak C18 cartridges, BioRad) loaded with a mixture of ethyl-hexyl-phosphates. Based on this methodology, they were able to remove the main alkaline and alkaline earth elements, allowing them to achieve a quantification accuracy of 2% RSD (relative standard deviation) for all REE except Eu (<3% RSD) and Y (<5% RSD). The author concluded that the good agreement of results obtained with two independent methods (matrix separation and preconcentration) reduces the possibility of systematic errors in their chemical data. Other methodology is reported by Kaczor-kurzawa et al. (2022) in pre-treatment stage, consisted of using two chromatographic columns integrated with a mixture of chelating resins with ethyl-enediaminetetraacetic acid and iminodiacetic acid functional groups. Achieving a 10-fold enrichment factor and chemical matrix removal prior to ICP-MS measurements. The applied methodology allowed both an efficient removal of major ions such as  $\text{Na}^+$ ,  $\text{Mg}^{2+}$ ,  $\text{Ca}^{2+}$ ,  $\text{Sr}^{2+}$ ,  $\text{Ba}^{2+}$  and  $\text{Cl}^-$  (>99.9%) and the elimination of spectral interferences that affect some REE results. Finally, Marín-Camacho et al. (2022) applied the  $\text{Fe}(\text{OH})_3$  co-precipitation and interchanged cationic column packed with a Dowex AG50WX8 resin (100–200 mesh) for the separation of the REE from matrix elements.

In the case of rock chemical analysis, the sample preparation for REE quantification through ICP techniques mainly requires wet solution methods (e.g., acid digestion or alkaline fusion), followed by dissolution (Pinto et al., 2012). The acid digestion process consists of crushing and then grinding to a fine powder. Then, a sample volume of dry powder is digested by acid attack ( $\text{HF}$ ,  $\text{HClO}_4$ ,  $\text{HNO}_3$ ). Works that describe this processes are Lewis et al. (1997), Zhang et al. (2012) Feng et al. (2014), Verma et al. (2018) and Santos-Raga et al. (2021). On the other hand, studies like Shoedarto et al. (2022) and Sosa-Ceballos et al. (2018) indicate that apart from employing acid digestion, they utilize matrix separation through exchange columns (such as BioRad AG50W-x8) and RE-Spec resin, respectively. Additionally, Sosa-Ceballos et al. (2018) perform Nd separations using glass columns filled with hydrogen di-ethyl-hexyl-phosphate resin.

### 2.4.2.2 Analytical techniques and limits of detection

Based on Verma (2020) the limit of detection (LOD), is defined as the lowest concentration of the target element that can be identified using an analytical technique. In this context, the very effective methods are the ICP analyses, which show the lowest LOD by quantifying elements by ionizing them in an inductively coupled Argon plasma and measuring their mass-charge ratios (ICP-MS) or emission spectra (ICP-OES). The ICP-OES, developed in 1980, is frequently applied in analysing REE due to its ability to swiftly detect multiple elements in water and rock samples, over a wide concentration range. Nevertheless, the REE concentration in samples is generally well below the technique's LODs, and matrix effects can occur due to significant components like organic compounds and inorganic salts (Zawisza et al., 2011). On the other hand, the ICP-MS technique was developed around 1990, has great acceptance due to its high efficiency. The principle of operation of this technique is the formation of positively charged ions, a result of the ionization process in Argon plasma, and subsequently extracted and transferred to a mass analyser for elemental quantification. The other ICP-MS-based methods combine pretreatments with chemical element quantification methodology (e.g., FUS-ICP, LA-ICP-MS, and others), preserving low matrix effects compared to other conventional analytical techniques and very low detection limits values (Table 2.4). However, certain inquiries have revealed that the sensitivities and limits of detection for various chemical elements differ significantly, even when employing the same method (Verma et al., 2002; Santoyo and Verma, 2003). Santoyo et al. (2007) mentioned that the LOD from REE show a systematic zigzag pattern, where the odd atomic number elements have lower LOD than the even atomic number neighbouring elements (e.g.,  $^{57}\text{La}$ - $^{58}\text{Ce}$ ;  $^{63}\text{Eu}$ - $^{64}\text{Gd}$ ;  $^{70}\text{Yb}$ - $^{71}\text{Lu}$ , etc.). Based on this the estimation of individual LOD of lanthanides should also be recognized as a fundamental task to describe the analytical performance of the technique, especially at trace concentrations (Santoyo and Verma, 2003; Santoyo et al., 2007; Tian et al., 2019; Zhang et al., 2016b; Shoedarto et al., 2022; Li et al., 2022). Sensitivity data for quantifying REE have seldom been provided. Only a few of the papers documented in this paper report these values individually: Santos-Raga et al. (2021), Shimada et al. (2010), Fukuyama and Chen (2021). Still others estimate and report a single detection limit for the whole group of elements (e.g., Lewis et al., 1997; Gammons et al., 2005; Kaczor-kurzawa et al., 2022). This methodology does not take into account the odd-even effect inherent to the concentration of REE.

2. Updated understanding of the behaviour of rare earth elements (REE) in geothermal systems

---

**Table 2.4:** Detection limits commonly associated with the quantification of REE in spectrometric techniques.

Analytical technique	Sample	LODs ( $\eta\text{g/L}$ )	Ref
	Water		
ICP-MS	Rock	<0.01-0.08	1
	Gas		
LA-ICP-MS	Rocks	<100	2
	Water		
Q-ICP-MS		<0.2-0.4	3
	Rocks		
	Water		
HR-ICP-MS		<0.001-0.01	4
	Rocks		
	Water		
MC-ICP-MS		<0.01-0.1	5
	Rocks		
	Water		
ICP-AES		<0.1-10	6
	Rocks		
	Water		
ICP-OES		<10-100	7
	Rocks		

<sup>1</sup>Zawisza et al. (2011), <sup>2</sup>Jarvis and Williams (1993), <sup>3</sup>Stead et al. (2017), <sup>4</sup>Liu et al. (2020), <sup>5</sup>Pourmand et al. (2012), <sup>6</sup>Ramanaiah (1998), <sup>7</sup>Yang et al. (2018).

### 2.4.3 Worldwide geochemical databases (WGD)

A worldwide geochemical database of rocks (WGD-R: Table 2.5) containing a total of 372 samples and a worldwide geochemical database of water (WGD-W: Table 2.6) with 374 samples were compiled from geochemical studies applied to REE behaviour analysis from geothermal systems. Both tables share common columns (columns 1, 2, 3, and 5). The first column indicates the countries of various geothermal fields, the second column provides information about the number of reported samples, the third specifies the geothermal field, and column 5 reports the analytical technique used for quantifying the REE.

Furthermore, the tetrad effect was calculated and documented in the WGD-R, with the calculation carried out based on the method proposed by Monecke et al. (2002). This natural phenomenon indicates a separation of chondrite-normalized REE patterns into four rounded segments referred to as tetrads (first tetrad, La-Ce-Pr-Nd; second tetrad, Pm-Sm-Eu-Gd; third tetrad, Gd-Tb-Dy-Ho; fourth tetrad, Er-Tm-Yb-Lu). These rounded segments can be either convex or concave, leading to M-shaped and W-shaped lanthanide distribution patterns, respectively (Masuda, 1987). Monecke et al. (2002) noted that significant tetrad effects (T) should have values exceeding 0.2, while the  $t_i$  (tetrad effect in the  $i$  segment:  $i = 1 \dots 4$ ) values must be below 0.8 for concave and higher than 1.2 for significant convex tetrad effects. The occurrence of a convex tetrad effect is common in whole-rock samples derived from magmatic and hydrothermal sources.

#### **2.4.4 Mobility of rare earth elements in geothermal systems**

The geochemical fractionation of REE under geothermal conditions is the product of the interaction of hydrothermal fluid and host rock. The circulation of these hydrothermal solutions produces physicochemical changes (hydrothermal alteration) and a set of chemical reactions, which tend to approach equilibrium and, through processes of dissolution and precipitation development of new mineral assemblages and REE aqueous complexes in fluids (Lintjewas and Setiawan, 2018; Migdisov et al., 2016; Pirajno, 2009; Yongliang and Yusheng, 1991).

In geothermal water, it has been demonstrated that anion ligands govern the mobility of REE, forming complexes with fluorides (e.g., Chambefort et al., 2017; Gammons et al., 2005; Haas et al., 1995; Lewis et al., 1998, 1994; Marín-Camacho et al., 2022; Michard and Albarède, 1986; Middleton et al., 2013; Mourad Mahdy et al., 2013; Pinto et al., 2012), chlorides (e.g., Bao et al., 2008; Cole et al., 2014; Fowler et al., 2019a; Lewis et al., 1997; Libbey and Williams-Jones, 2016; Migdisov et al., 2016; Möller, 2002; Schmidt et al., 2007a), phosphates (e.g., Gieré, 1993; Louvel et al., 2015; Thair and Sarapaa, 2014), sulphates (Gammons et al., 2005; Gieré, 1993; Migdisov et al., 2016; Santos-Raga et al., 2021; Wood and Shannon, 2003), carbonates (e.g., Cetiner and Xiong, 2008; Kaczor-kurzawa et al., 2022; Leybourne et al., 2000; Ohannesson et al., 1999; Ramasamy et al., 2013; Shoedarto et al., 2022; Wang et al., 2020; Wei et al., 2022a; Wood and Williams-Jones, 1994), hydroxides (e.g., Fowler et al., 2019a; Li et al., 2022) and CO<sub>2</sub>-rich (e.g., Gilbert and Williams-Jones, 2008; Michard, 1989; Möller et al., 2009; Rillard et al., 2019; Smith et al., 2000) solutions. Although several studies based on field observations and experimental results differ about the dominant anion ligand.

## 2. Updated understanding of the behaviour of rare earth elements (REE) in geothermal systems

**Table 2.5:** Summary of a worldwide database of REE concentrations in rock samples collected from geothermal systems.

Country	No. Samples	Geothermal Field	Type of rock	Chemical analysis	Average		Ref.
					Ratio $\Sigma\text{LREE}/\Sigma\text{HREE}$	Tetrad effect	
Turkey	2	Ayder and Ikizdere	Granite	ICP-MS	6.75	1.43	1
	2		Altered granite		11.1	1.4	
	1		Basalt		5.21	1.44	
	2	Pasinler	Rhyolite	ICP-MS	8.93	1.37	2
	2		Basalt		6.99	1.32	
1		Rhyolitic tuff		10.01	1.42		
USA	5	Yellowstone	Rhyolite	ICP-MS	8.93	8.93	3
	6		Breccia		7.69	1.41	
	14		Tuff		10.64	10.64	
Iran	6	Taftan	Andesitic-dacitic	ICP-MS	10.75	1.39	4
	2	Los Azufres	Subalkaline basalt	ICP-MS	5.66	1.37	5
	2		Rhyolite		4.37	1.54	
	15		Rhyolitic rocks		7.23	1.49	
16		Rhyolite	ICP-OES	7.33	1.51	7	
Mexico	16		Dome		7.59	1.5	8
	3		Enclave		6.64	1.44	
	3		Ignimbrite		8.38	1.52	
	14	Acoculco	Lava	FUS-ICP	6.43	1.47	9
	1		Scoria		0.3	1.47	
	2		Basalt		7.25	ND	
	2		Basalt-trachyandesite		11.28	ND	
	3		Andesite		8.97	ND	
	1		Rhyolite		12.23	ND	
	32	Acid rock	41.56	ND			
	20	Intermediate rock	51.14	ND	10		
	13	Basic rock	39.87	ND			
	China	11	Tengchong	Basalt	ICP-MS	10.58	1.4
10		Trachyandesite		14.4		1.39	
3		Dacite		14.2		1.4	
1		Trachybasalt		10.02		1.38	
18		Granites		11.95		1.47	
15		Metamorphic rock	9.58	1.46	12		
10		Volcanic rock	9.37	1.37			
4		Rehai	Volcanic rock	8.58	1.45	13	
3			Sandstone	8.39	1.38	14	
4		Gezha area	Slate	9.46	1.38		
27			Granite	7.65	1.46	15	
11	Tibetan Plateau	Sinter	4.08	1.41	16		
5	Wayang Windu	Fresh lavas	ICP-OES	4.56	1.4	17	
Italy	18		Rhyolite		14.82	1.41	18
	21		Latite-trachytes	ICP-MS	24.34	1.48	
	1		Trachyte		55.01	ND	
1		Latite		59.43	ND		
Namibia	2	Okorusu carbonatite complex	Mafic dike	LA-ICP-MS	34.67	ND	19
	2		Dioside-bearing carbonatite		48.48	1.6	
	3		Pegmatite carbonatite		85.01	ND	
1		Altered carbonatite		16.8	ND		
France	4	Soultz-sous-Forets	Monzonite	ICP-MS	18.26	1.43	20
	8		Basalt		2.83	1.46	
Iceland	2	Reykjanes	Dolerite	ICP-MS	2.11	1.41	21
	1		Marine sediments		2.61	1.57	

<sup>1</sup>Hatipoğlu Temizel et al. (2020), <sup>2</sup>Temizel and Gültekin (2018), <sup>3</sup>Lewis et al. (1997), <sup>4</sup>Shakeri et al. (2015), <sup>5</sup>Torres-Alvarado et al. (2007), <sup>6</sup>Pandarínath et al. (2008), <sup>7</sup>Verma et al. (2018), <sup>8</sup>Sosa-Ceballos et al. (2018), <sup>9</sup>Verma (2001), <sup>10</sup>Santos-Raga et al. (2021), <sup>11</sup>Zhang et al. (2012), <sup>12</sup>Wang et al. (2020), <sup>13</sup>Li et al. (2022), <sup>14</sup>Wei et al. (2022b), <sup>15</sup>He et al. (2013), <sup>16</sup>Feng et al. (2014), <sup>17</sup>Bogie and Mackenzie (1998), <sup>18</sup>Fulignati et al. (1999), <sup>19</sup>Cangelosi et al. (2020), <sup>20</sup>Middleton et al. (2013), <sup>21</sup>Ottolini et al. (2012). The tetrad effect was calculated by methodology propose by Monecke et al. (2002).

**Table 2.6:** Summary of a worldwide database of REE concentrations in water samples collected from geothermal systems.

Country	No. Sample	Geothermal Field	Geological environment	Chemical analysis	Average				Ref.
					Temperature (°C)	pH	Eh (mV)	Ratio $\Sigma$ LREE/ $\Sigma$ HREE	
USA	18	Yellowstone	Caldera	ICP-MS	82.71	3.24	ND	5.39	1
Argentina	20	Rio agrio	Crater lake	ICP-MS	19.95	4.63	602.67	5.77	2
Colombia	16	Azufra	Caldera	Q-ICP-MS	13.04	2.46	209.44	5.05	3
	4	Puracé volcano	Volcanic chain	IC-MS	64.55	2.48	208.5	3.71	4
Russia	7	Mutnovsky volcano	volcanic belt	HR-ICP-MS	53.34	5.52	ND	338.46	5
Turkey	6	Kirsehir	Fault system		48.83	6.61		6.16	6
	12	Kozakli	Crystalline complex	ICP-MS	53.6	6.8	ND	8.03	7
	10	İkizdere			41.3	8.01		5.12	8
	16	Lake Van	Karst		31.8	7.7	0.08	3.24	9
Mexico	78	Acoculco	Caldera	ICP-MS	23.54	4.7	ND	33.5	10
	14	Queretaro graben	Volcanic belt	Q-ICP-MS	77.4	8.5	374.93	5.85	11
	16	Yunnan	Arc	HR-ICP-MS	71.3	7.74	ND	7.22	12
	10	Simao	Basin	ICP-MS	37.6	5.99	118.33	9.16	13
China	8		Basin		77.75	8.86		3.86	14
	11	Cuopu		ICP-MS					
	16	Rehai	Volcanic belt		83.78	7.17	ND	8.43	15
	16	Xifeng	Craton	ICP-MS	76.03	6.57		4.79	16
	25	Kahui and Gezha	Orogenic belt	Q-ICP-MS	32	8.04		11.56	17
Indonesia	31	Windu	Crater	ICP-MS	64.92	7.99	62.67	9.94	18
Vanuatu Island	5	Ninfonea vent	Caldera	ICP-MS	31.11	6.49	ND	3.98	19
Polish	35	Several fields	Plataform	ICP-MS	267	3.67	ND	8.63	20
					23.24	6.99	167.42	2.6	21

<sup>1</sup>Lewis et al. (1997), <sup>2</sup>Gammons et al. (2005), <sup>3</sup>Inguaggiato et al. (2017), <sup>4</sup>Inguaggiato et al. (2020), <sup>5</sup>Chudaev et al. (2017), <sup>6</sup>SENER (2019), <sup>7</sup>SENER (2019), <sup>8</sup>Hatipoğlu Temizel et al. (2020), <sup>9</sup>Sasmaz et al. (2021), <sup>10</sup>Santos-Raga et al. (2021), <sup>11</sup>Marín-Camacho et al. (2022), <sup>12</sup>Zhang et al. (2016a), <sup>13</sup>Zhang et al. (2020), <sup>14</sup>Tian et al. (2019), <sup>15</sup>Wang et al. (2020), <sup>16</sup>Li et al. (2022), <sup>17</sup>Li et al. (2021), <sup>18</sup>Wei et al. (2022b), <sup>19</sup>Shoedarto et al. (2022), <sup>20</sup>Schmidt et al. (2017), <sup>21</sup>Kaczor-kurzawa et al. (2022).

Lewis et al. (1998) suggested based on equilibrium speciation calculation, that at 100°C the fluoride complexes ( $\text{LnF}_3$ ,  $\text{LnF}_2^+$ ,  $\text{LnF}^{2+}$ ) dominate the mid pH range; whereas for hydrothermal fluids with low and high pH values, the carbonate and chlorides are the main complexes formed, respectively (Haas et al., 1995). Theoretical studies carried out by Wood (1990a,b), who studied speciation in hydrothermal solutions at 350 °C at saturation water vapour pressures, determined that REE-fluoride ( $\text{LnF}_3$ ,  $\text{LnF}_2^+$ ) complexes become increasingly stable at higher temperatures, therefore, fluorides must predominate over other REE-complexes over a wide range of pH values. Gimeno-Serrano et al. (2000) mentioned that acid water elements such as aluminium are more susceptible to complexation with fluorides than REE, mainly through the formation of  $\text{AlF}^{2+}$  and  $\text{AlF}^+$  complexes. Furthermore, for fluid with pH <2, the H<sup>+</sup> ion is another factor that competes for dissolved fluoride (Santos-Raga et al., 2021; Shakeri et al., 2015; Wood, 1990b).

On the other hand, the evidence obtained by Migdisov et al. (2016), through the study of fractionation of the REE, suggests that in hydrothermal solutions, the main REE transporting ligands are chloride and sulphate, whereas fluoride, carbonate, and phosphate are considered mainly as depositional ligands. This hypothesis agrees with the study of REE in boiled fluids performed by (Fowler et al., 2019b), which concludes that: (i) the REE are incorporated into well scale by fluorapatite precipitated from lower pH fluids with a seawater component; (ii) the chloride is effective at transporting REE because the stability of REE-chloride species exceeds that of HCl. Cole et al. (2014), who studied the behaviour of REE as indicators of hydrothermal processes within the subduction zone, suggested that the REE normalized pattern (characteristic of their system) described in terms of differential leaching and stabilization of the REE as chloride complexes.

The distribution and speciation of REE in acid-sulphate waters have been widely studied in water-rock interaction processes associated with geothermal sites, mainly because the acidic sulphate waters show the highest contents of REE up to  $\approx 5$  order of magnitude higher compared to other water types (Gammons et al., 2005). Gieré (1993), demonstrated that REE can be transported in hydrothermal fluids containing large amounts of reduced sulphur species, this migration in H<sub>2</sub>S-rich fluids may occur in a wide range of geological environments. Shakeri et al. (2015), mentioned that the absence of the chloride species in acid waters probably indicates temperatures <200°C. Craddock et al. (2010), predicts based on thermodynamic calculations that REE-chloride complexes at temperatures >200°C are the main compounds contributing to REE speciation in acid-sulphate waters. The bibliography compiled is indicative of the mobility of REE in solutions rich in F, Cl, SO<sub>4</sub>, P, and in a wide range of physiochemical conditions (T, P, pH, among others).

### 2.4.5 Experimental water-rock interactions studies

Some of the water-rock interaction processes experiments discussed in this section agree with the theoretical studies. Migdisov and Williams-Jones (2006) demonstrated that although the stability of chloride complexes is probably about four orders of magnitude weaker than that of REE complexes with  $F^-$ , the concentration of chlorine in REE-bearing hydrothermal solutions is commonly on the order of tens of wt%, whereas that of fluorine is on the order of hundreds of ppm. Thus, the chloride complexation may be as important for the genesis of hydrothermal REE deposits as REE-fluoride complexation. Later, Migdisov et al. (2009) performed an experimental study of the solubility and speciation of REE in fluoride and chloride-bearing aqueous solutions at up to 300 °C, suggesting that at elevated temperatures LREEF species are more stable than HREEF species. On the other hand, Terakado et al. (1993) mentions that during rhyolite-hydrothermal water interactions, the behaviour of REE is largely dependent on the HCl concentration in the solution. Experiments carried out by Sanada et al. (2006) agree that the acidity of the fluid is very important in the REE fractionation, concluding that their concentration in acid-hot spring waters can be very useful tools for revealing changes in the processes that give rise to geothermal systems. The experimental study carried out by Köhler et al. (2005) to understand the behaviour of the REE during low-temperature water-rock interaction concluded that: (i) the apatite dissolution from pH 2 to 7 is strongly influenced by rhabdophane (mineral of phosphate), and (ii) the dissolution and precipitation of rhabdophane in the presence of apatite are sufficiently rapid such that this process controls the REE concentration. This study highlights the relevance of phosphate-bearing minerals in the control of REE in water springs. Yongliang and Yusheng (1991) concluded that to know the exact behaviour of REE in aqueous solutions, the following systematic experimental work is required: (i) experimental investigations of REE mobilization and fractionation as a function of fluid chemistry, e. g. the activities of  $F^-$ ,  $Cl^-$ ,  $HCO_3^-$ ,  $CO_3^{2-}$ ,  $HPO_4^{2-}$ ,  $PO_4^{3-}$ ,  $HS^-$ ,  $S_2^{2-}$ ,  $SO_4^{2-}$ , etc; (ii) experimental determination of REE mobility and fractionation as a function of T, P, pH (and Eh), and water/rock ratio; (iii) systematic studies of REE partitioning between hydrothermal minerals and solutions, and (iv) experimental determination of REE chemical evolution of the parent fluid. Finally Migdisov et al. (2016) mentioned that the experimental data on the distribution of REE in carbonate-solution are lacking. Limited information is available about the endurance of hydroxyl complexes of REE at high temperatures, the stability of pure forms of REE fluorocarbonates such as bastnäsite, and the resilience of various other REE minerals that could be of significance.

## 2.5 REE applications and current and future challenges

Rare earth elements are crucial in various industries, from cutting-edge technology (e.g., computer memory, batteries, mobile phones), renewable energy production (solar panels, super magnets for wind turbines, batteries), transportation (autocatalytic converters), among others (Balaram, 2019; Opare et al., 2021). However, the extraction and application of these elements present significant challenges that require attention to ensure their availability. Current challenges in this area of research, including supply dependency and environmental impacts of extraction, have been highlighted in studies such as that of Balaram (2019). Supply disruptions, whether caused by geopolitical issues or environmental problems, can have global repercussions across various industries. China, Russia, Brazil, Vietnam, and India have the largest mining production of these elements, producing more than 200,000 of the 300,000 tons worldwide and holding reserves of more than 130 million tons (U.S. Geological Survey, 2023). On the other hand, rare earth (such as any minerals) mining often entails significant environmental impacts. The mining and processing of these elements can generate toxic waste and contribute to environmental degradation (Barakos et al., 2015). Zapp et al. (2022), agree that the main problems are the large quantities of chemicals needed to process REE and the large quantities of tailings generated during beneficiation, extraction and separation that contain the naturally occurring radionuclides  $^{232}\text{Th}$  and  $^{238}\text{U}$  and their decay products. Considering these existing challenges, it is very important to diversify REE recovery by exploring new deposits characterized by high REE content and the lowest possible amount of associated radioactive elements. Additionally, these new sources of REE must be globally accessible, making alternative production routes outside of China essential to ensure a stable supply and meet current and future demands (Opare et al., 2021; Zapp et al., 2022). Based on this, the recovery of REE from geothermal fluids (e.g., geothermal brine) emerges as a potentially significant source of valuable minerals and metals. The co-recovery of these elements alongside geothermal energy production presents an attractive and sustainable system (Brewer et al., 2019; Neupane and Wendt, 2017; Smith et al., 2017; Stringfellow and Dobson, 2020; Zierenberg et al., 2013; Fowler et al., 2018).

## 2.6 Remarks of Chapter 2

This bibliometric methodology presents a clear framework of the evolution of rare earth element studies and their application in the geochemical exploration of geothermal systems. According to Price's law phases, the productivity evolution and latest developments of these research studies were typified by two main periods (before and after 2014), during which 101 publications were compiled in the present bibliometric study. Before 2014, the productivity of these publications was characterized by the 'forerunners' phase, whereas for the period 2014-2024, the number of publications depicted a rapid and substantial increase typified by an exponential growth phase. During this growth phase, research on REE in geothermal systems has gradually become a hot topic for Earth science researchers involved in geothermal prospecting and exploitation studies. Within this context, researchers from the China, USA, Mexico, Germany and Turkey are leading the publication of articles on REE in geothermal systems in peer-reviewed journals.

Based on the systematic analysis of the literature, it was observed that the quantification of REE concentration in fluid and rock samples is mainly performed by spectrometric techniques such as ICP-MS. These techniques demonstrate high sensitivity and low detection limits (ppm to ppb). Many of the studies compiled in this research agree that pre-treatment of the samples by pre-concentration and/or group separation allows for reduction of sources of errors associated with elemental chemical analysis of REE in these techniques. Furthermore, we consider that the LOD should be reported individually and not as groups of elements, as is common in several studies referenced in this work.

Regarding REE fractionation, we have summarised that anionic ligands, such as fluorides, chlorides, sulphates, carbonates, phosphates and hydroxides, play a crucial role in governing the mobility of REE in geothermal waters. The dominant anionic ligand varies depending on factors such as temperature, pH and fluid composition. While fluoride complexes prevail at moderate pH and temperature, chloride and sulphate complexes are significant in high temperature solutions. The experimental studies corroborate the theoretical findings on the behaviour of REE in the water-rock interaction process, such as:

(i) fluid acidity is very important in REE fractionation, its concentration in acidic thermal waters can be a very useful tool to reveal changes in the processes that give rise to geothermal systems.

(ii) Chloride complexation may be as important for the genesis of REE hydrothermal reservoirs as REE-fluorine complexation.

In conclusion, the combined findings of the theoretical and experimental studies provide valuable information for understanding the mobility and behaviour of REE in geothermal systems, which is crucial for practical applications in resource ex-

## 2. Updated understanding of the behaviour of rare earth elements (REE) in geothermal systems

---

ploration. Further studies and experimental investigations are needed to improve our understanding of the geochemistry of REE in geothermal environments.

# Geochemical signatures of REE in spring waters and outcropping rocks from the hidden geothermal system of Acoculco

---

### 3.1 Introduction

The study of water-rock interaction in geothermal systems provides useful signatures for inferring geochemical processes and paleo-thermal conditions. The dissolution, transport and precipitation of major and trace elements (REE) provide key geochemical signatures in waters and rocks, which help to elucidate deep thermodynamic conditions of geothermal systems (Wood, 2006). REE are relatively immobile at low temperatures, where used to exhibit similar physicochemical properties such as ionic radius and charge (Monecke et al., 2011). In geothermal systems ( $>190^{\circ}\text{C}$ ), the REE show different mobilities that depends on their individual fractionation between fluids and rocks (Sanyal, 2005).

The first studies related to the REE concentrations in submarine and continental hydrothermal fluids were attributed to Michard and Roekens (1983), Michard and Albarède (1986), Michard (1989). These authors pointed out that: (i) the concentration of REE in hydrothermal fluids is generally lower than in parental rocks, and (ii) the increase of REE concentrations is generally associated with a decrease in the pH of the fluids. The concentration of REE in geothermal fluids has

been investigated in previous works (e.g., Yongliang and Yusheng, 1991; Wood and Shannon, 2003; Peiffer et al., 2011; Fowler and Zierenberg, 2015; Chudaev et al., 2017); whereas their mobility has been selectively studied in some theoretical and water-rock experiments (e.g., Migdisov and Williams-Jones, 2006; Migdisov et al., 2016; Woitischek et al., 2017; Rillard et al., 2019). The distribution and speciation of REE in acid-sulphate waters have been studied in water-rock interaction processes of geothermal systems (e.g., Lewis et al., 1998; Sanada et al., 2006; Wood, 2006; Shakeri et al., 2015). The use of REE in geothermal systems of Mexico has been focused to the study of hydrothermal alteration in rocks (e.g., Torres-Alvarado et al., 2007; Pandarinath et al., 2008; Verma et al., 2018; Pandarinath et al., 2020; Sánchez-Córdova et al., 2020); whereas for fluids, a limited number of studies have been conducted in some hydrothermal volcanic centres of the South of Mexico (e.g., Taran et al., 2008; Peiffer et al., 2011).

Between 1980's and 2000's, the limited application of REE in geothermal fluids was attributed to the lack of sensitive analytical techniques for their determination at low concentrations ( $\mu\text{g/L}$  to  $\text{ng/L}$ ), and the scarce of geochemical reference standards for the instrumental calibration and analysis of water and rock matrices (Verma et al., 2002). These analytical barriers were overcome with the emerging of highly-sensitive analytical techniques (e.g., ICP-MS, ICP-AES, CE, among others: Santoyo et al., 2007; Fisher and Kara, 2016), and with the use of water reference standards that appeared for a better calibration of such techniques (e.g., Verplanck et al., 2001). With these advances in analytical geochemistry, the possibility to study the REE in geothermal fluids (as natural tracers) in a wide variety of geothermal systems has resurged with more strength. With a prospection approach, a new study of the REE and trace elements in spring waters and outcropping rocks from the hidden geothermal system of Acoculco caldera is proposed in the present investigation work.

The Acoculco geothermal system (AGS) is a hidden geothermal system located in the Mexican Volcanic Belt (MVB: Fig. 3.2) which has been characterized by argillic hydrothermal alteration, cold springs with acid fluids, cold-gas emissions (also referred as Kaipohans), and surface temperatures between 10 and 26 °C (López Hernández, 2009). An early exploration program carried out by the "Comisión Federal de Electricidad" (CFE) of Mexico based on the drilling of exploratory wells (EAC-1 and EAC-2), and bottom-hole temperatures around 300 °C at 2 km depth, indicated an anomalous geothermal gradient of  $\approx 150$  °C/km (Lorenzo-Pulido et al., 2010). From these promising exploration results, vulcanological (García-Palomo et al., 2018; Sosa-Ceballos et al., 2018; Avellán et al., 2020; Pérez-Orozco et al., 2021), and geophysical (López-Hernández et al., 2009; Calcagno et al., 2018; García-Palomo et al., 2018; Avellán et al., 2020; Deb et al., 2020; Guerrero-Martínez et al., 2020; Weydt et al., 2020; Kruszewski et al., 2021)

studies have been conducted to evaluate in more detail some other features of the AGS. In relation to previous geochemical studies, Polak et al. (1982) carried out regional surveys in the Eastern portion of the MVB where the chemical and isotopic composition of noble gases were studied in the AGS.

High isotopic ratios of  $^3\text{He}/^4\text{He}$  ( $R/R_{\text{air}} = 6.3$ ) were associated with a deep magmatic origin. In other exploration studies, the spring discharges were characterised by acid-sulphate and calcium-bicarbonate waters with a preferential flow pattern from Southeast to Northeast (Hernández, 1997). The composition of gas emissions was preliminary characterised by major ( $\text{CO}_2$  and  $\text{H}_2\text{S}$ ) and trace gases ( $\text{H}_2$ ,  $\text{N}_2$ , and  $\text{CH}_4$ ), which were used to predict temperatures around  $173^\circ\text{C}$ . Quinto et al. (1995), López Hernández (2009), and Peiffer et al. (2011) carried out short-time sampling campaigns of water and soil-gas measurements to evaluate the origin of these fluids. The first two works were conducted to confirm the hydrogeochemistry classification of some water sources: (i) acid-sulphate waters (formed by oxidation of  $\text{H}_2\text{S}$ ) for the cold springs; (ii) sodium-bicarbonate waters for the caldera structure periphery; and (iii) calcium-bicarbonate waters for some hot springs located in the South of the AGS. Peiffer et al. (2014) performed short-term measurements of soil-gas fluxes and gas-phase compositions in some emission sites of Alcaparrosa and Los Azufres where a magmatic origin was confirmed. Subsurface temperatures close to  $200^\circ\text{C}$  were determined by gas geothermometry. Santoyo et al. (2020) and Santos-Raga et al. (2020) carried out an exhaustive field work in the AGS based on continuous sampling and monitoring campaigns of fluids (between 2014 and 2019) to determine their spatial and temporal variability (inside and outside of the calderic structure), from where the present research work is derived.

In relation to hydrothermal alteration studies, the presence of secondary minerals of quartz, calcite, pyrite, clays (illite, smectite, and kaolinite), and iron oxides were identified in the lithological columns of two exploratory wells (López Hernández, 2009). A later study based on short-wave infrared spectral measurements were conducted by Canet et al. (2010) where two major alteration zones were identified: (i) a shallow zone between 500 and 600 m, characterized by argillic alteration (ammonium illite); and (ii) a deeper zone between 600 and 1500 m associated to a propylitic alteration of epidote-calcite-chlorite.

Canet et al. (2015b) proposed a conceptual model of hydrothermal alteration based on the appearance of six SWIR-active minerals found in outcropping altered rocks (opal, kaolinite, alunite, ammoniojarosite, buddingtonite, and interstratified illite-smectite). By integrating hydrothermal alteration, numerical modelling of temperatures, and radiocarbon dating studies, Canet et al. (2015a) proposed the evidence of earlier hydrothermal explosions product from the paleo self-sealing processes occurred in the AGS. Sánchez-Córdova et al. (2020) reported mineral

3. Geochemical signatures of REE in spring waters and outcropping rocks from the hidden geothermal system of Acozulco

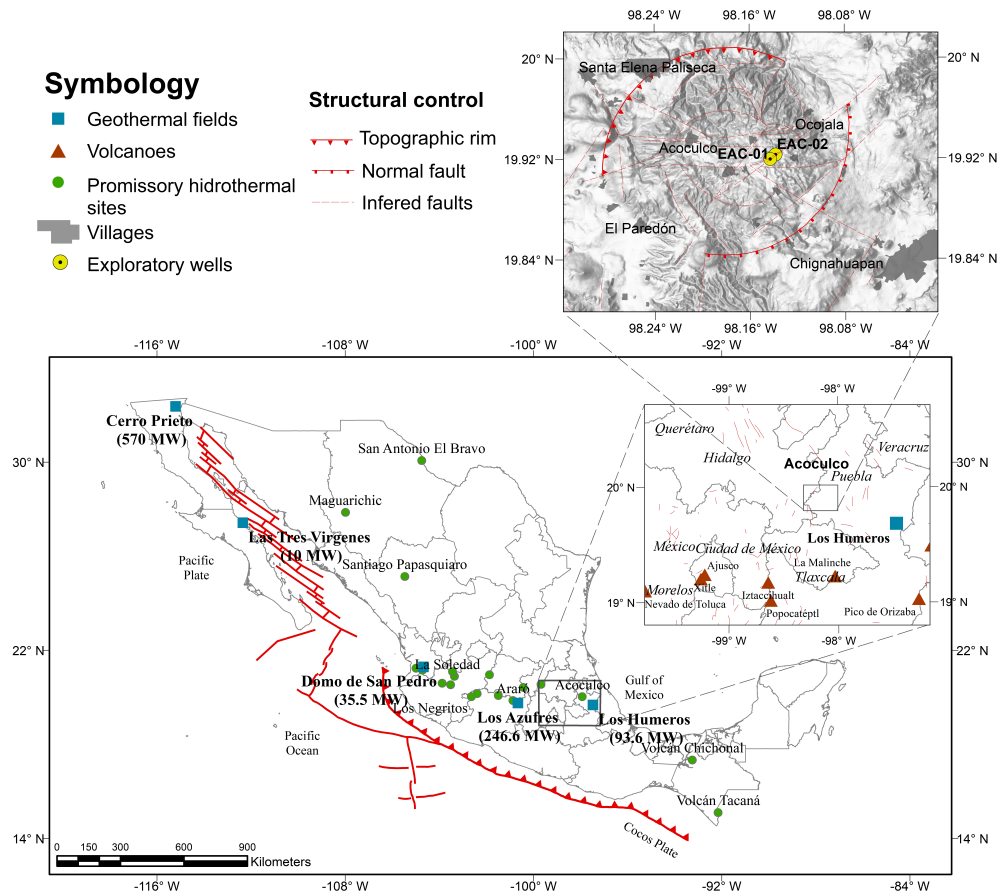


**Figure 3.1:** Base map of Mexican geothermal fields under exploitation, potential promissory sites, and simplified projections of the Acozulco Geothermal System (a). The main volcanic centres (triangle symbols) located in the MVB are shown in projection (b), including the location of the Los Humeros geothermal field (Puebla), as geographical reference (square symbol). The geological caldera of Acozulco (modified after Avellán et al., 2020; García-Palomo et al., 2018), and the exploratory wells (EAC-01 and EAC-02) are shown in projection (c).

assemblages in outcropping rocks that are in full agreement with an upward fluid flow of moderate temperatures ( $\approx 100$  °C), and fluid pH changes from acid to neutral. Pandarinath et al. (2020) recently evaluated mineralogical and geochemical changes due to hydrothermal alteration in some AGS volcanic rocks, where the mobility of major oxides and trace elements, and the mass changes (gain or loss) were analysed. High mobility in most of the major and trace elements (including HREE) was observed, whereas the LREE and MREE (except Dy and Ho) behaved as immobile elements.

By considering the geological and geophysical maps created for the AGS, the geothermal prospection sites for collecting spring waters and outcropping rocks were roughly defined in two major zones: inside-caldera (which includes Los Azufres, AZ; Alcaparrosa, AP; San Francisco Terrerillos, SFT; and Cruz Colorado, CC sampling sites); and outside-caldera (which was composed by Jicolopa, JI; Quetzalapa, QTZ; and Chignahuapan, CHIG sites). The location of these sampling sites is shown in Fig. 2. The zone of inside-caldera (ZIC) which is characterized by bubbling springs with low temperatures (close to ambient), cold soil-gas emissions, and an intense hydrothermal alteration in the outcropping rocks. The zone of outside-caldera (ZOC) is typified by hot hydrothermal springs with temperatures up to 49°C, and high emissions of gas (mainly CO<sub>2</sub>). Based on these two extensive zones (ZIC and ZOC) of the AGS, a new geothermal prospection work was carried out in this research work.

The geochemical prospection study of this promising geothermal system of Mexico represented a methodological challenge that was programmed with the following goals: (i) to study, for the first time, the geochemical behaviour of REE and trace elements in spring waters and outcropping rocks; (ii) to track new geochemical signatures based on a comprehensive chemical and isotopic characterisation of the same spring waters and outcropping rocks; (iii) to study the water-rock interaction processes that dominate in the AGS; and (iv) to propose new evidences that explain the geochemical signatures found in the analysis of fluid and rock samples, and their relationships with bottomhole temperatures measured in two exploratory wells, hidden geological structures, and fluid flow paths existing in the AGS. Details of this geochemical prospection are outlined.

## 3.2 Geological setting of the study area

The AGS is located about 130 km Northeast of Mexico City and between the states of Puebla and Hidalgo on the East portion of the MVB (Fig. 1.4). The MVB is a calc-alkaline magmatic arc that extends from Nayarit to Veracruz, whose geological origin is associated to the subduction of the Cocos and Rivera plates

beneath the North American plate (Ferrari et al., 2012). The Eastern portion of MVB is characterized by normal faults, aligned with the NW-SE direction, and by volcanic structures (dikes and domes) associated to an extensional regime (Pardo and Suárez, 1995). The AGS complex is structurally characterized for impermeable layers, and sealed faults by either calcite or silica that have restricted the upflow transport of fluids and gases from deep-seated sources towards the surface (Canet et al., 2010). The AGS is hosted by a caldera related to Pliocene to Quaternary volcanic activity, with a surface geology composed by andesite-rhyolite volcanic rocks, and rhyolite-dacite ash-flow tuffs (López Hernández, 2009). These authors reported the existence of a volcanic complex composed of two calderic structures. The oldest structure is the Tulancingo Caldera (TC) with a Pliocene age (3-2.7 Ma) and a diameter of 32 km, and a second structure named Acoculco Caldera with a small diameter of 18 km, and a more recent volcanic activity (1.7-0.24 Ma).

On the other hand, Avellán et al. (2019) carried out stratigraphy and geochronology studies ( $^{40}\text{Ar}/^{39}\text{Ar}$ ) within the AGS, where the existence of TC is rejected, and the volcanic activity of the Acoculco Caldera is associated to the Pliocene ( $2.73 \pm 0.184$  Ma). Avellán et al. (2020) recently proposed a simplified geological map based on geochronology studies, where the existence of four major eruptive phases of the Acoculco Caldera is described: syn-caldera (2.7 Ma), early post-caldera (2.6-2.1 Ma), late post-caldera ( $2.0 < 0.01$  Ma), and extra-caldera (2.4- 0.19 Ma): Fig. 3.2.

### 3.3 Work methodology

To achieve the proposed investigation goals, an integrated work methodology consisting in four major sections was developed (Fig. 3.3). The methodology includes a comprehensive geochemical field work that integrates sampling campaigns of spring waters and outcropping rocks, chemical characterisation of major and trace elements, application of geochemometric techniques for the quality assurance of the chemical analyses, and the study of the water-rock interaction based on hydro-geochemistry, the mobility preferences of trace elements (REE and others) between waters and rocks, and a geochemical modelling of the probable fractionation processes (more detail in Santos-Raga et al., 2021).

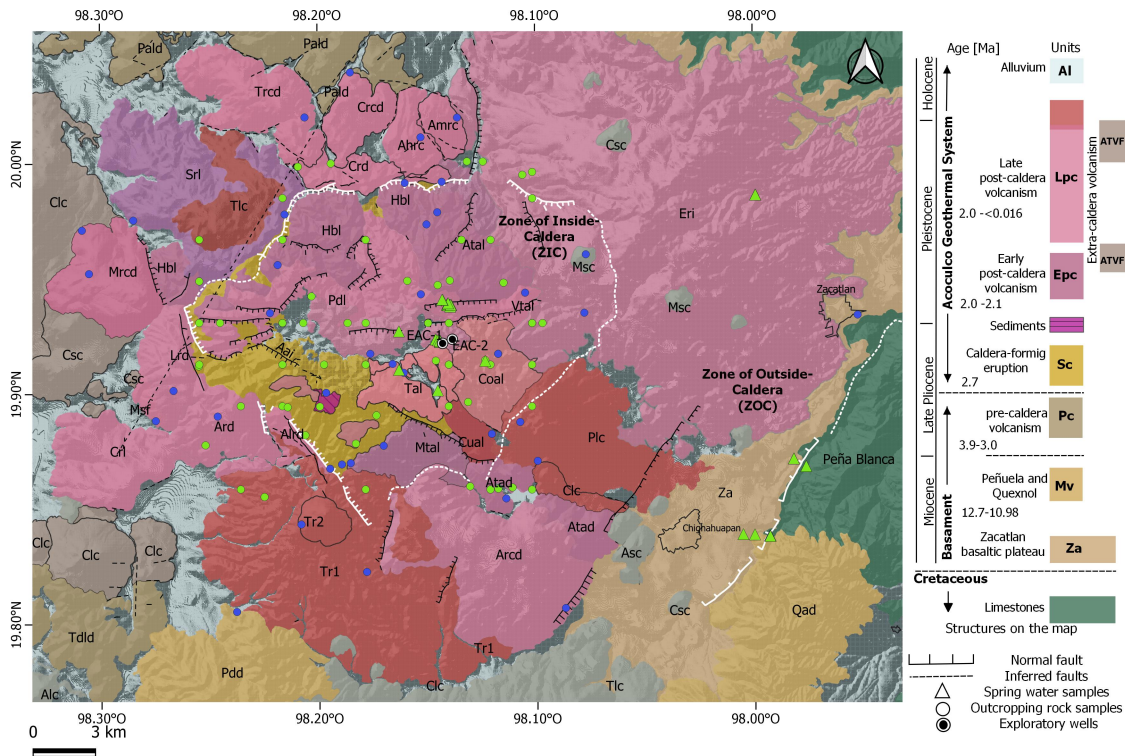


**Figure 3.2:** Geological map of the Aocolulco geothermal system (modified after Avellán et al., 2020). Surface geology, faults, and hydrothermal alteration zones are also shown, including the sampling sites of the spring waters (triangle symbols) and outcropping rocks (green circles). (For interpretation of the references to colour in this figure legend, the reader is referred to the web version of this article.)

### 3. Geochemical signatures of REE in spring waters and outcropping rocks from the hidden geothermal system of Acoculco

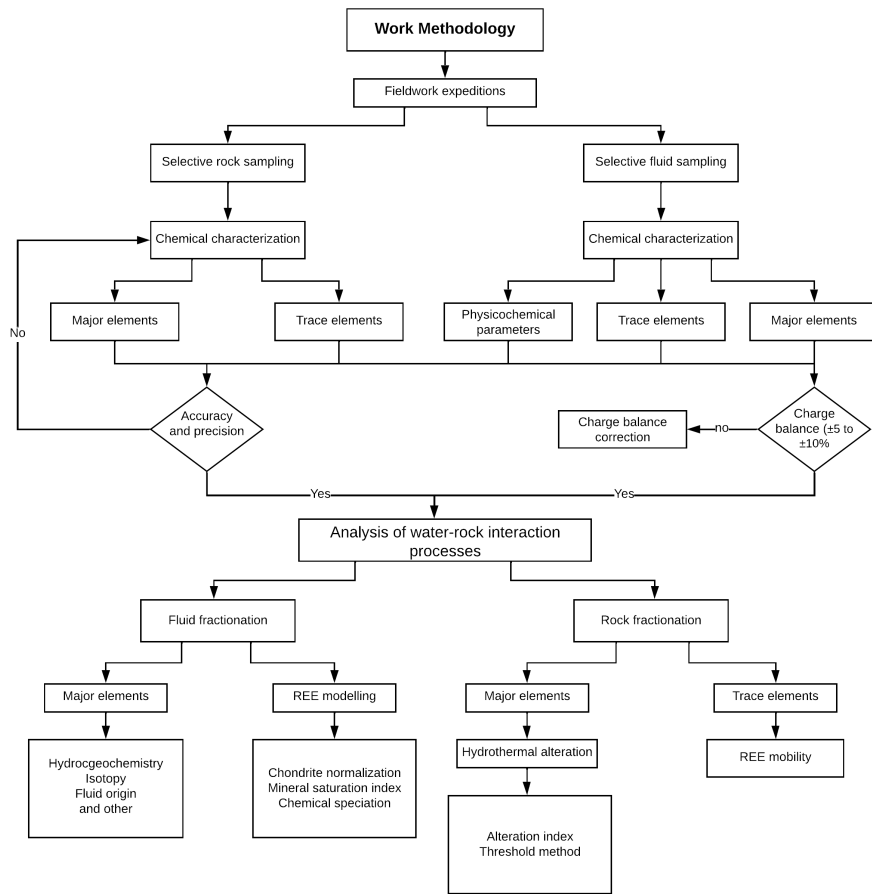


**Figure 3.3:** Integrated work methodology developed for the study of the water-rock interaction processes of the AGS (Santos-Raga et al., 2021).

#### 3.3.1 Geochemical field work: Collection of water and rock samples

The collection program of water and rock samples was carried out as a part of the research project P09 of the Mexican Centre for Innovation in Geothermal Energy, CeMIEGeo (Romo-Jones., 2017). This campaign aimed to apply unconventional geochemical methods of fluids and rocks (hydrothermal alteration) for a new geothermal prospection of the AGS (Santoyo et al., 2019). The water samples were collected in cold and hydrothermal springs located in the ZIC and ZOC using a standardised sampling methodology (Almirudis et al., 2018). Total alkalinity ( $\text{HCO}_3^-$  and  $\text{CO}_3^{2-}$ ) and physicochemical parameters (temperature, pH, and

electrical conductivity) were measured in situ.

For the measurement of temperature and pH, a calibrated portable WTW potentiometer was used, whereas for the conductivity, a HACH multimeter was utilized. Total alkalinity was determined by triplicate using a micro-burette titration proposed by Nicholson (1993). Ten replicates of these measurements were performed in each sample. The maximum measurement errors of pH were less than 1.4%; whereas for the temperature and conductivity were less than 2.1%, and 2.0%, respectively.

By considering the most representative outcropping lithologies reported in previous geological studies (Fig. 3.2), altered and relative fresh (or less altered) rocks were collected using conventional sampling methods (e.g., Silva-Romo and Mendoza-Rosales, 2011). In summary, fifty-three water samples were collected for the chemical analysis of major (cations, anions, and some other components) and trace elements (conservative, REE, and others), and stable isotopes ( $^{18}\text{O}/^{16}\text{O}$ , and D/H); whereas sixty-five rock samples (altered and less-altered) were collected for major and trace analyses (see Table 1 in: Santos-Raga et al., 2021).

### 3.3.2 Geochemometric analysis

Considering the definition of “Geochemometrics” as a science that results from the integration of geochemistry with statistics, mathematics, and computation (Verma, 2020), in the present prospection study, several geochemometric techniques were applied: (i) the quality assurance and quality control (QA/QC) of the chemical analyses; (ii) the calculation of the distribution, and the statistical variability of major and trace elements in spring waters and rocks; (iii) the calculation of mineral saturation states of REE in spring waters (complexation and speciation); and (iv) the evaluation of hydrothermal alteration indicators for a better discrimination of less-altered and altered rocks. Geochemometric tasks (i) and (ii) are outlined in this section, whereas (iii) and (iv) will be described in the water-rock interaction section.

#### 3.3.2.1 QA/QC of the chemical analyses

The quality of the water chemical analyses was evaluated using the standardised method of charge- balance between anions and cations. The charge-balance calculation is defined as the most straightforward parameter of QA/QC for evaluating the reliability of water chemical analyses (Nordstrom et al., 2009). According to Nicholson (1993), the charge-balance should be between  $\pm 5\%$  and  $\pm 10\%$ , if the sampling and chemical analyses are carefully carried out in the field and laboratory, respectively. Other authors have specified that values less than  $\pm 20\%$  may

still be acceptable (e.g., Nordstrom et al., 2009). It is also possible that some water samples may exceed such quality boundaries ( $\pm 10\%$  or  $\pm 20\%$ ) due to acidity problems. For these cases, a chemical equilibrium correction based on a recalculation of pH must be applied for either reducing or minimising the charge unbalances, and with this, to recover the analysis of these water samples. To correct this problem, the calculation of the  $H^+$  acidity in acidic water samples (pH < 3.5) is recommended. Nordstrom et al. (2009) suggest the use of a chemical speciation model for correcting the  $H^+$  acidity through the simplified Eq. 3.1 (in molality units):

$$Acidity_{h^+} = Acidity_{Total} - Acidity_{Fe} - Acidity_{Al} - Acidity_{SO_4} - Acidity_{As} - Acidity_F \quad (3.1)$$

where the  $Acidity_{h^+}$  is the recalculated acidity (AH+), and the  $Acidity_{Total}$  represents the titration-acidity (AT) that includes the strong and weak acidity produced by the dissolved chemical species (Barringer and Johnsson, 1996). Other parameters of Eq. 3.1 represent the  $H^+$  ions produced by hydrolysis of the  $Fe^{3+}$  and  $Al^{3+}$  ions, and the dissociation of  $HSO_4^-$ ,  $H_3AsO_4^0$ , and  $HF^0$ . In this speciation model, the recalculated pH for an acidic-water sample requires the calculation of the AT by computing the negative logarithm of the  $H^+$  ion activity, as a product of the activity coefficient (which is calculated using the PHREEQC code: Parkhurst and Appelo, 2013) and AH molality.

### 3.3.2.2 Distribution of major and trace elements in water and rock samples

The compositional analysis of geochemical data was performed using robust statistical methods for a better representation of the distribution of major and trace elements in water samples. Central tendency (median) and dispersion (interquartile range) statistical parameters were calculated. An extended statistical version of the *Schoeller diagram* was used to represent the concentration patterns identified in the spring waters collected from the ZIC and ZOC of the AGS. A similar diagram was plotted for the rock samples, which were grouped by considering the composition type of magmas (i.e., acid, intermediate, and basic).

### 3.3.3 Water-rock interaction

A comprehensive study of water-rock interaction was suggested as a suitable method to identify new geochemical signatures of the paleo-thermal conditions

occurred in the AGS. With these purposes, the hydrogeochemistry of major elements and stable isotopes, the geochemical modelling of major and trace elements in waters, the mobility or preferential fractionation of trace elements (REE and others) between water and rock samples, the hydrothermal alteration of outcropping rocks, and the analysis of REE were broadly studied.

### **3.3.3.1 Hydrogeochemistry**

For the classification of spring waters, the concentration of major ionic elements was recalculated to 100%, and plotted on the well-known diagram of Piper. A ternary diagram of conservative elements (Li-Cs-Rb) was also used both to study the mineral precipitation kinetics, and to elucidate the mixing or interaction sources that control the concentrations of alkali metals in spring waters, and their relationships deep formation temperatures. The low mobility of alkali metals was used to evaluate the main mechanisms that control their chemical distribution (Giggenbach, 1991). Stable isotope ratios of hydrogen (D/H) and oxygen ( $^{18}\text{O}/^{16}\text{O}$ ) were also used to determine the origin of the spring waters, and the recharge sources. Stable isotopes of hydrogen and oxygen were reported as  $\sigma\text{D}$  and  $^{18}\text{O}$  where  $\sigma$  represents the variation of samples with respect to the Standard Mean Ocean Water (SMOW). All the isotopic data measured in spring water samples were plotted together with the Global Meteoric Water Line, GMWL ( $\delta\text{D}=8\delta^{18}\text{O}+10$ ), which was used as a geochemical reference (Craig, 1961).

### **3.3.3.2 Geochemical modelling of major and trace (REE) elements in waters**

The concentrations of REE detected in spring waters were normalized with respect to chondrites (McDonough and Sun, 1995), and plotted on a bivariate diagram for determining the fractionation processes (dissolution or precipitation), the influence of physicochemical parameters, and the identification of major geochemical signatures. Mineral saturation indexes and aqueous speciation of REE were calculated using the software Geochemist's Workbench in combination with the geochemical database thermo\_minteq.dat (Bethke, 1996). This database considers the main aqueous species for REE complexes (carbonate, sulphate, fluoride and hydroxide ligands), and thermodynamic data of ionic strength and temperature with values up to  $<0.1$  and  $100^\circ\text{C}$ , respectively (Haase et al., 2013). The equilibrium speciation for REE is controlled by temperature, pH, salinity, and abundances of ligands (Lewis et al., 1997, 1998). For the present study, the equilibrium speciation and the mineral saturation index of twenty-seven waters were calculated at three different temperatures ( $25^\circ\text{C}$ ,  $50^\circ\text{C}$  and  $100^\circ\text{C}$ ) using the pH values measured in-situ

(or those data corrected by effect of a strong acidity) as main input data for the geochemical modelling calculations.

### 3.3.3.3 Hydrothermal alteration

Hydrothermal alteration is a complex water-rock interaction process that involves changes in texture, mineralogy, and fractionation of major and trace elements (Verma et al., 2005; Pirajno, 2009). In geothermal systems, this process results from the interaction between paleo-thermal fluids and rocks (surface and sub-surface). To determine the relative hydrothermal alteration observed in outcropping rock samples, chemical index of alteration (CIA) and statistical threshold methods were applied. (Nesbitt, 1979) propose the use of the CIA to study the chemical weathering of feldspar minerals in altered rocks. The CIA was calculated using the following equation:

$$CIA = \frac{Al_2O_3}{Al_2O_3 + Na_2O + K_2O + CaO^*} \quad (3.2)$$

where  $CaO^*$  represents the content of calcium incorporated into the silicate fraction, with the corresponding correction for volcanic rocks. This correction was proposed by McLennan (1993), which considers the presence of Ca in carbonates (calcite, dolomite) and phosphates (apatite). To define the boundaries of less-altered rocks, the intervals of CIA values reported by Nesbitt (1979) were used for acid (45-55) and basic (30-45) rock compositions. For intermediate rocks, the less-altered boundaries were defined with respect to a standard CIA value of 46.5, which is suggested for an andesite geochemical reference material. For the statistical discrimination of threshold LOI values of relatively less-altered and altered rocks, the graphical method proposed by Sinclair (1974) was used through a cumulative probability plot.

### 3.3.3.4 Analysis of REE composition in rock samples

To study the REE concentration patterns, the analysed rock samples were classified by type of magma (acid, intermediate, and basic) by considering the geological map of the AGS proposed by Avellán et al. (2020). The concentrations of REE were also normalized to chondrite (McDonough and Sun, 1995), and used to analyse the REE concentration patterns of altered rocks in comparison to relative fresh rocks (or less-altered). This information was used both for evaluating the degree of hydrothermal alteration, and to elucidate the most probable water-rock interaction processes that support the mobility of REE into the surrounding waters.

## 3.4 Results

### 3.4.1 Geochemometric analysis

#### 3.4.1.1 QA/QC for the chemical analyses of water

Conventional charge balances were calculated from the chemical analysis of water samples using the major composition of anions and cations in meq/L ((see Table 2 from Santos-Raga et al., 2021)). A total of 31 out of 78 water samples ( $\approx 40\%$ ) are in full agreement with a strict confidence interval of  $\pm 10\%$  recommended by Nicholson (1993), whereas 7 out of 78 ( $\approx 9\%$ ) were in a less strict criterion but still acceptable ( $\pm 20\%$ ). Most of these samples were characterised by pH's ranging from 6.9 to 9.1 (neutral to slight alkaline), and mostly correspond to hot spring waters located in the ZOC. From the 51% of remaining samples (40 out of 78), 30 cold spring waters exhibited  $\text{pH} \leq 3.5$ . These samples exhibited large charge balances ( $> \pm 30\%$ ), whereas the remaining samples with a  $\text{pH} > 3.5$  (ranging from 5.5 to 8.5) were equally distributed in two groups of charge balances ( $\pm 25\%$  and  $\pm 61\%$ ). Most of these water samples present acidic pH's values, and emerged from cold springs located in the ZIC (AP and AZ sampling sites).

### 3. Geochemical signatures of REE in spring waters and outcropping rocks from the hidden geothermal system of Acoculco

---

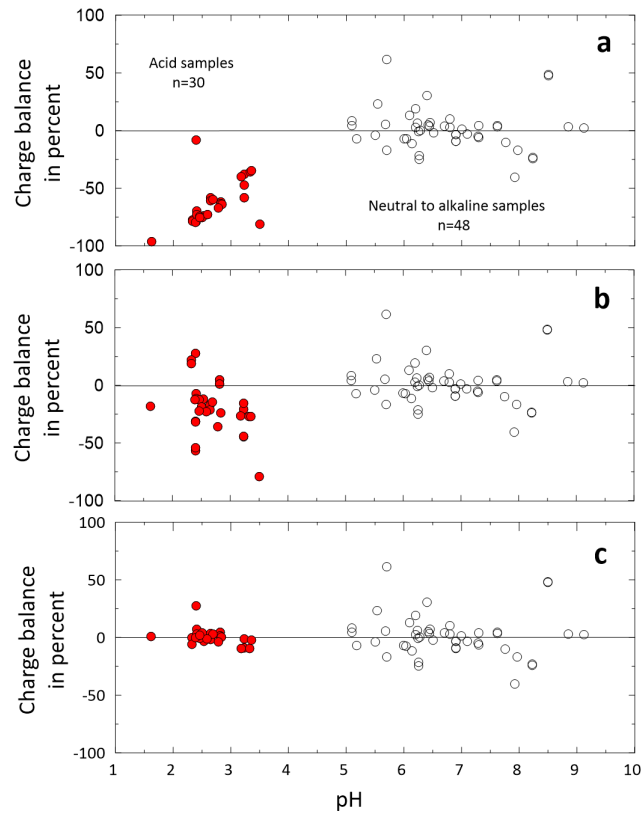


**Figure 3.4:** Results of the charge balance correction applied for sulphate-acid waters collected in the AGS. (a) Charge balance calculated without the  $H^+$  correction; (b) Charge balance calculated with  $H^+$  but without speciation; and (c) Charge balance calculated after  $H^+$  and speciation corrections (Santos-Raga et al., 2021).

The acidic geochemical nature of these cold spring waters from ZIC (and mainly coming from the AP) has caused a historical analytical problem due to anomalous charge imbalances that has been neglected in most of the previous studies conducted at the AGS (Tello-Hinojosa, 1994; Quinto et al., 1995; López Hernández, 2009; Peiffer et al., 2014). From the exploration point of view, this problem may affect the reliability of the chemical analyses used for the early interpretation of the water/rock interaction processes reported in the AGS. Charge balances greater than  $\pm 20\%$  may come from error sources related to the neglect of the  $H^+$  concentration and the acidity speciation (e.g.,  $SO_4$ , Fe, Al, As and F). To correct this problem, a calculation of the  $H^+$  acidity was performed in all the acidic waters ( $pH < 3.5$ ) using the chemical speciation model proposed by Nordstrom et al. (2009) (which is schematically described in Fig. 2S from Santos-Raga et al., 2021) under the following convergence criteria: (i) the recalculated pH must be equal to the in-situ pH measurement (as a key input parameter); and (ii) the corrected charge

balance of these acidic-water samples must be  $\pm 10\%$ . A total of thirty acid-water samples were processed by applying this correction method. An effectiveness of 77% was roughly corrected and recovered Figs 3.4. As an initial calculation step, the charge balances and pH data were plotted in Fig. 3.4 (a), where two groups of waters were clearly identified: water samples with pH's  $> 3.5$  (shown as unfilled circles) which were only plotted as a reference; and acidic waters with pH's  $< 3.5$  (represented as filled circles) which required the acidity correction. As a second calculation step, the acid water samples corrected by the effect of the  $H^+$  ion activity were plotted in Fig. 3.4 (b). After applying the speciation model, the resulting correction due to the effects of water acidity (Eq. 3.1) was achieved. A total of 23 out of 30 acidic-water samples were effectively corrected, resulting in new and acceptable charge balances which range from -9.4 to  $\pm 7.2\%$ : Fig. 3.4(c). Water samples with uncorrected charge balances were not considered for the calculation of mineral saturation indices and the REE speciation.

### 3.4.1.2 Distribution of major and trace elements in water and rock samples

Extended statistical versions of the Schoeller diagram showing the concentration distributions of major and trace elements for the spring waters of the ZIC and ZOC were plotted in Figs. 3.5 (a-c) and 3.6 (d-f), respectively. Six major groups of elements represented as median values, and the 25-75% percentiles were plotted (i.e., anions, alkali metals, alkaline earth metals, metalloids, transition metals and metals, and some radioactive elements). From the anion group, it was observed in the ZIC and ZOC water samples that the  $SO_4^{2-}$  and  $HCO_3^-$  were the dominant anionic species, respectively, whereas the Na-K and Ca-Mg were similarly the major cationic species. A zig-zag pattern in the Li-Cs-Rb alkali metals is also observed for all spring waters of ZIC and ZOC, together with a systematic negative anomaly or depletion due to Sb and Ga: see Figs. 3.5 (a-f). A strong enrichment of Al was also observed for the ZIC waters, whereas for the ZOC, a less pronounced enrichment of this element was found. The geochemical signature of Al enrichment and the pH changes play an important role in the behaviour of the REE exhibited in spring waters.

Concerning to other trace elements, a depletion signature in Ga and Tl was almost systematically observed in hot spring waters (ZOC) respect to the cold spring waters (ZIC), whereas an opposite enrichment of Zn was nearly found in the same water samples, except for the hydrothermal waters from Jicolapa (JI). A positive correlation between Ga and high temperature systems was reported by Elmi et al. (2010), including a strong correlation with Sb (Krupp and Seward, 1987). For the radioactive trace elements, Th shows a consistent depletion in cold

### 3. Geochemical signatures of REE in spring waters and outcropping rocks from the hidden geothermal system of Aocolulco

spring waters of the ZIC, whereas a reverse process of enrichment was observed for the hot spring waters of the ZOC. Regarding this signature, (Fall et al., 2020) mentioned that the radioactive elements (K, Th, and U) presents high mobility due to hydrothermal alteration or weathering, which may be attributed to magmatic, intense fluid-rock interaction, and mineralization processes.

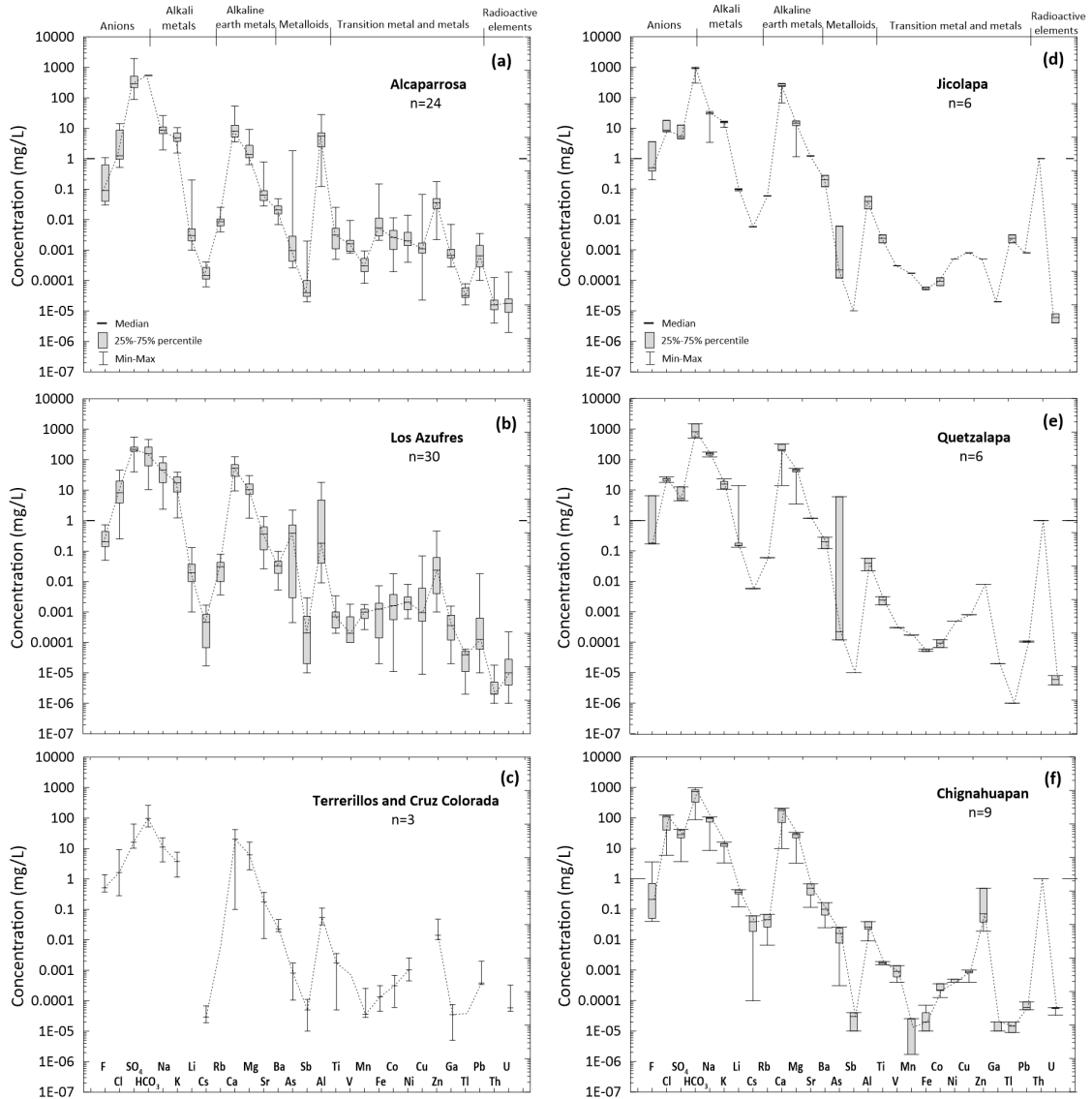


**Figure 3.5:** Statistical descriptive plot showing the concentration patterns observed for major and trace elements measured in the hot and cold spring samples of the Aocolulco Geothermal System. (Santos-Raga et al., 2021).

In relation to the rock samples, similar concentration patterns for major oxides are systematically observed: Figs. 3.6 (a-c), which are characterised by a depletion in  $\text{TiO}_2$ ,  $\text{MnO}$ , and  $\text{P}_2\text{O}_5$ . A typical more pronounced enrichment of  $\text{Na}_2\text{O}$  and  $\text{K}_2\text{O}$  was observed for acid rocks. Concerning to trace elements, lower concentrations of Ni, Co, Cu, and Ta were found in presence of higher enrichments of Ba (only in acid rocks), Zn, Zr, and Rb: Figs. 3.6 (d-f).

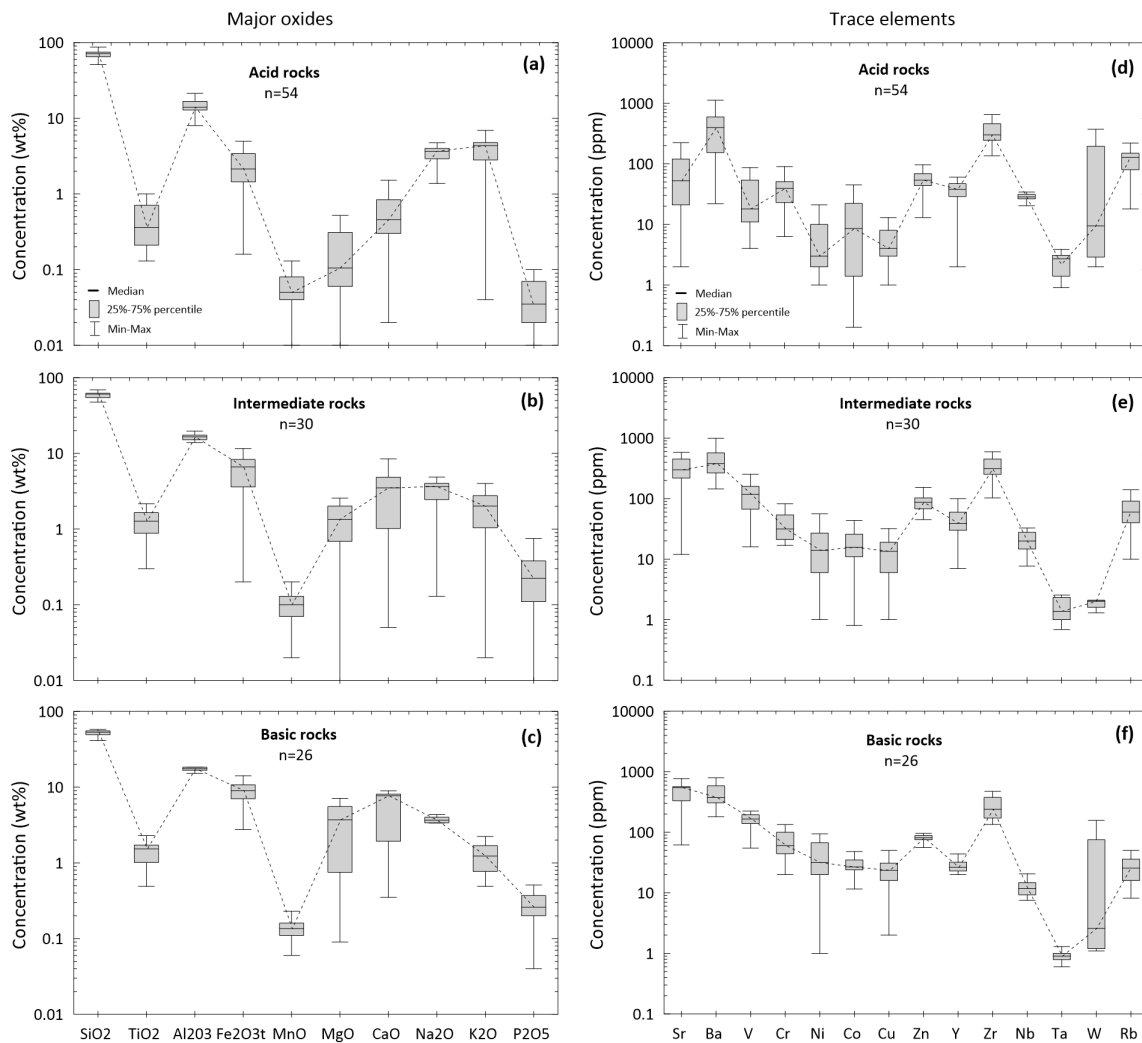


**Figure 3.6:** Statistical descriptive plot showing the concentration patterns observed for major and trace elements determined in altered and less-altered rocks of the Acoculco Geothermal System. (Santos-Raga et al., 2021).

### 3.4.2 Concentration patterns of REE and geochemical modelling

#### 3.4.2.1 Chondrite-normalized REE patterns of waters

The concentrations of REE measured in spring waters from the AGS are reported in Santos-Raga et al. (2021), see Table 3. Such concentrations were normalized with respect to chondrites using the geochemical data reported by McDonough and Sun (1995), and represented as normalized patterns in Figs. 3.7 (a-d).

Spring waters emerging from the ZIC (AP and AZ), exhibited systematic patterns of REE, which show an almost flattened distribution typified by a slight tendency to depletion from LREE (La, Ce, Pr and Nd) and MREE (Sm, Eu, Gd, Tb, Dy and Ho) to HREE (Er, Tm, Yb and Lu), and an inverse correlation with pH (i.e., higher concentrations of REE in acid waters; and a reverse behaviour for alkaline waters): Figs. 8 (a-c). Significant differences were observed in the waters emerging from the ZOC springs (JI, QTZ, and CHIG), which mostly exhibit very low concentrations of REE/chondrites (ranging from  $1 \times 10^{-5}$  to  $6 \times 10^{-3}$ ), and disordered chondrite-normalized patterns, that are consistent with their alkaline nature (see Fig. 3.7d).

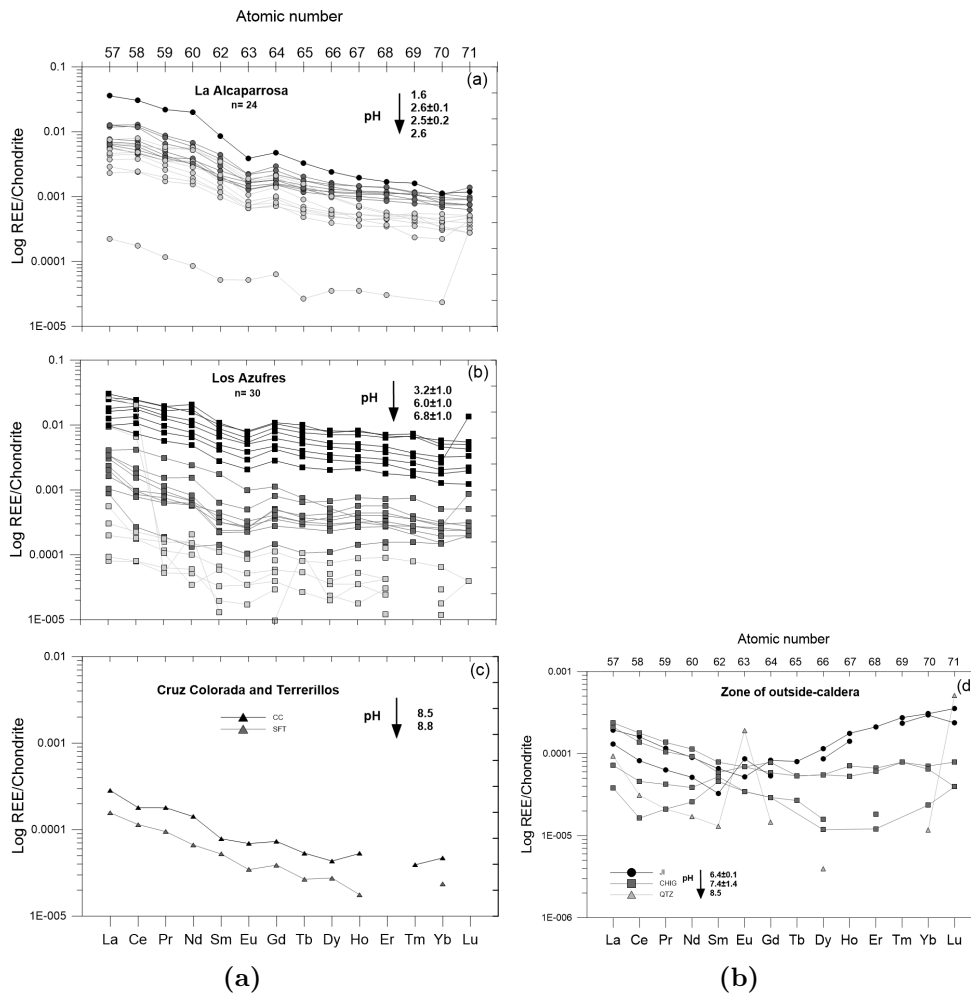


**Figure 3.7:** Chondrite-normalized patterns of REE observed in spring waters of the AGS: (a) ZIC: Alcaparrosa, AP (pH < 2.6); (b) ZIC: Los Azufres, LA (pH < 6.8), (c) ZIC: Cruz Colorada, CC and Terrerillos, SFT (pH < 8.8); and (d) ZOC: Jicolapa, JI (pH > 6.4), Chignahuapan, CHIG (pH > 7.4), and Quetzalapa, QTZ (pH > 8.5).

### 3.4.2.2 Mineral saturation state and REE speciation

The REE-mineral equilibria was calculated for different temperatures (25 °C, 50 °C, and 100 °C) using the concentrations of major elements, trace ions (Fe, Al, and F), and the REE content (in  $\mu\text{g/L}$ ) as main input data. The mineral saturation indices calculated for the cold springs from the AZ and AP sites mainly show mineral phases of S and Al: Figs. 3.8 (a-f). Significant differences in the total sum of REE ( $\Sigma\text{REE}$  in  $\mu\text{g/L}$ ) were found among the composition of the AP and AZ

### 3. Geochemical signatures of REE in spring waters and outcropping rocks from the hidden geothermal system of Acoculco

waters, where the AP exhibited lower REE values (up to 20  $\mu\text{g/L}$ ) in comparison with those estimated for the AZ (up to 50  $\mu\text{g/L}$ ).

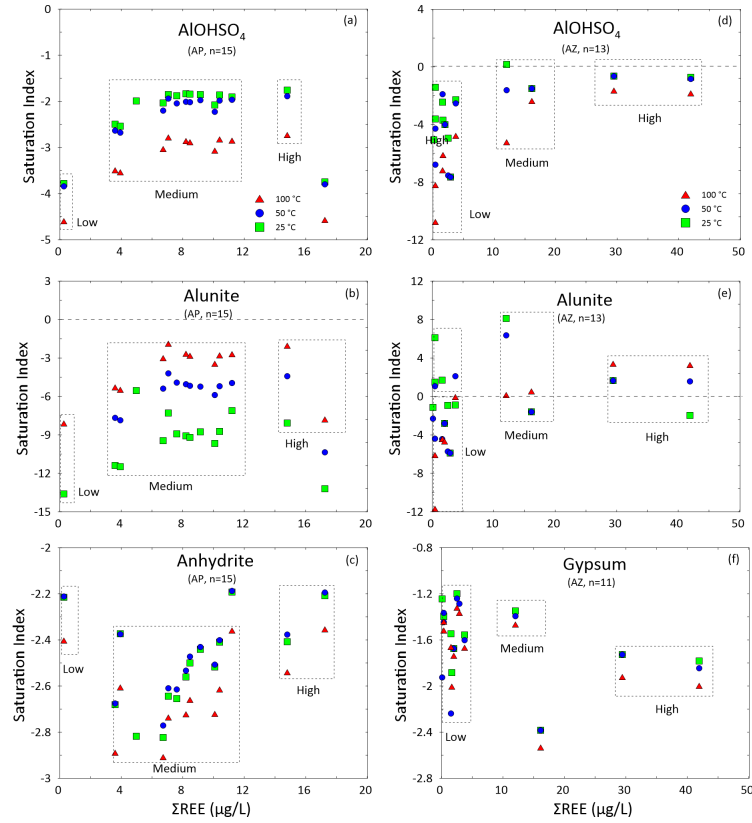


**Figure 3.8:** Saturation index of minerals for S and Al bearing minerals species versus the total sum of REE determined in spring water samples that emerge from the ZIC of the AGS (Santos-Raga et al., 2021).

The results of the REE-speciation, also calculated at 25 °C, 50 °C, and 100 °C, were presented in Figs. 3.9 (a-f) with the contribution of the main REE species ( $\text{LnSO}_4^+$ ,  $\text{Ln}^{3+}$ ,  $\text{LnF}^-$ ,  $\text{LnCl}^-$ , and  $\text{Ln}(\text{OH})^{2+}$ ) indicated as complexation percentage of the total dissolved REE concentration.

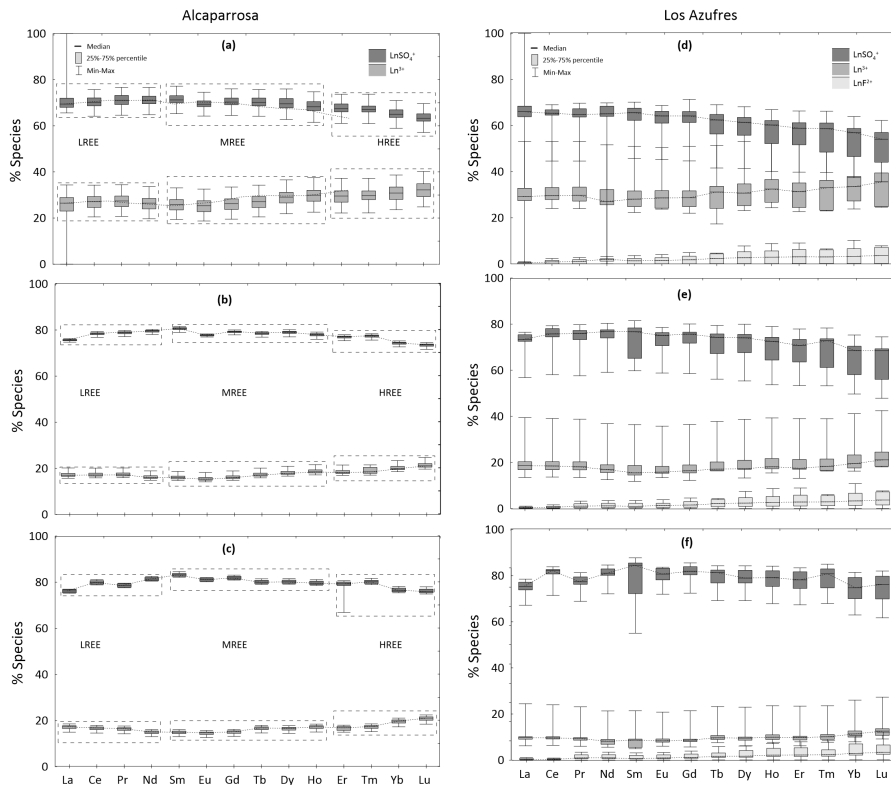


**Figure 3.9:** Aqueous speciation of REE found in cold spring waters from the AP site of the AGS at three surface temperatures (a): 25 °C, (b) 50 °C, and (c) 100 °C; and from the AZ site: (d) 25 °C, (e) 50 °C, and (f) 100 °C. The abbreviation of Ln represents any of the fourteen elements of REE (La–Lu) (Santos-Raga et al., 2021).

### 3.4.3 Rock Geochemistry

#### 3.4.3.1 Hydrothermal alteration

The rock samples under study exhibited CIA values between 46.9 to 96 (Fig. 3.10a). Acid and basic less-altered rocks were classified according to the range of CIA values proposed by Nesbitt (1979), which are 45-55 and 30-45, respectively. For intermediate rock compositions, an andesite geochemical reference material (AGV-2 with a CIA value of 45.7) was used (Pandarinath et al., 2020). This methodology was proved by using an alternative method based on the threshold estimation method proposed by Sinclair (1974), where a cumulative probability plot of LOI data was used to determine the inflexion point for an efficient discrimi-

### 3. Geochemical signatures of REE in spring waters and outcropping rocks from the hidden geothermal system of Acoculco

nation between samples with less-alteration and intensive hydrothermal alteration (Fig. 11b). After analysing both figures (Figs. 3.10a-b), the discrimination of weak and intensive hydrothermal alteration zones is in full agreement with both methodologies (CIA and LOI). In the first method (Fig. 3.10a), the discrimination boundary was found at CIA values greater than 60% which indicated an intensive hydrothermal alteration, whereas less-altered rocks exhibited CIA values below this percentage. In the second method (Fig. 3.10b), the inflexion point of the cumulative probability plot shows a logarithmic LOI value of 0.6 (or 3.82%) which represents the boundary between the intensive and weak hydrothermal alteration zones. From these methodologies, less-altered rock samples were identified from relative fresh rocks based on acid, intermediate and basic composition: AC-005 (CIA: 50.2; LOI: 0.25); AC-021 (CIA: 46.5; LOI: 1.48); and AC-016 (CIA: 43.9; LOI: 0.09), respectively.

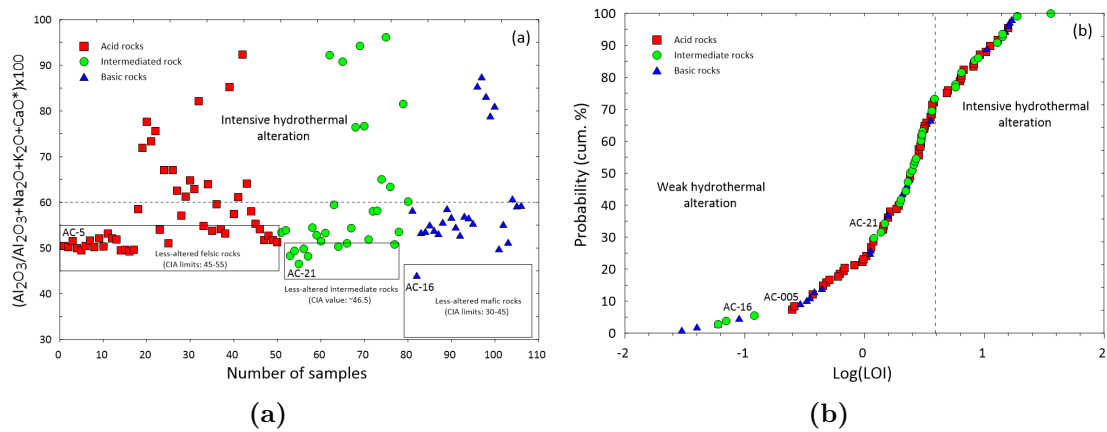


**Figure 3.10:** Classification of outcropping rocks of the AGS according to the degree of hydrothermal alteration: (a) Chemical Index of Alteration method; (b) Threshold discrimination method (Santos-Raga et al., 2021).

#### 3.4.3.2 Composition of REE in rocks

The REE concentration measured in AGS rock samples (acid, intermediate, and basic) were also plotted as chondrite-normalized patterns, respectively: Figs. 3.11(a-c). These patterns were used to evaluate the variation in the REE concentration of altered rocks with respect to less-altered rocks: Figs. 3.11(a-c). To evaluate the variability of REE concentrations, mean compositions of altered rocks (filled circles) were compared with those values corresponding to less-altered rocks: Fig. 3.11(d-f).

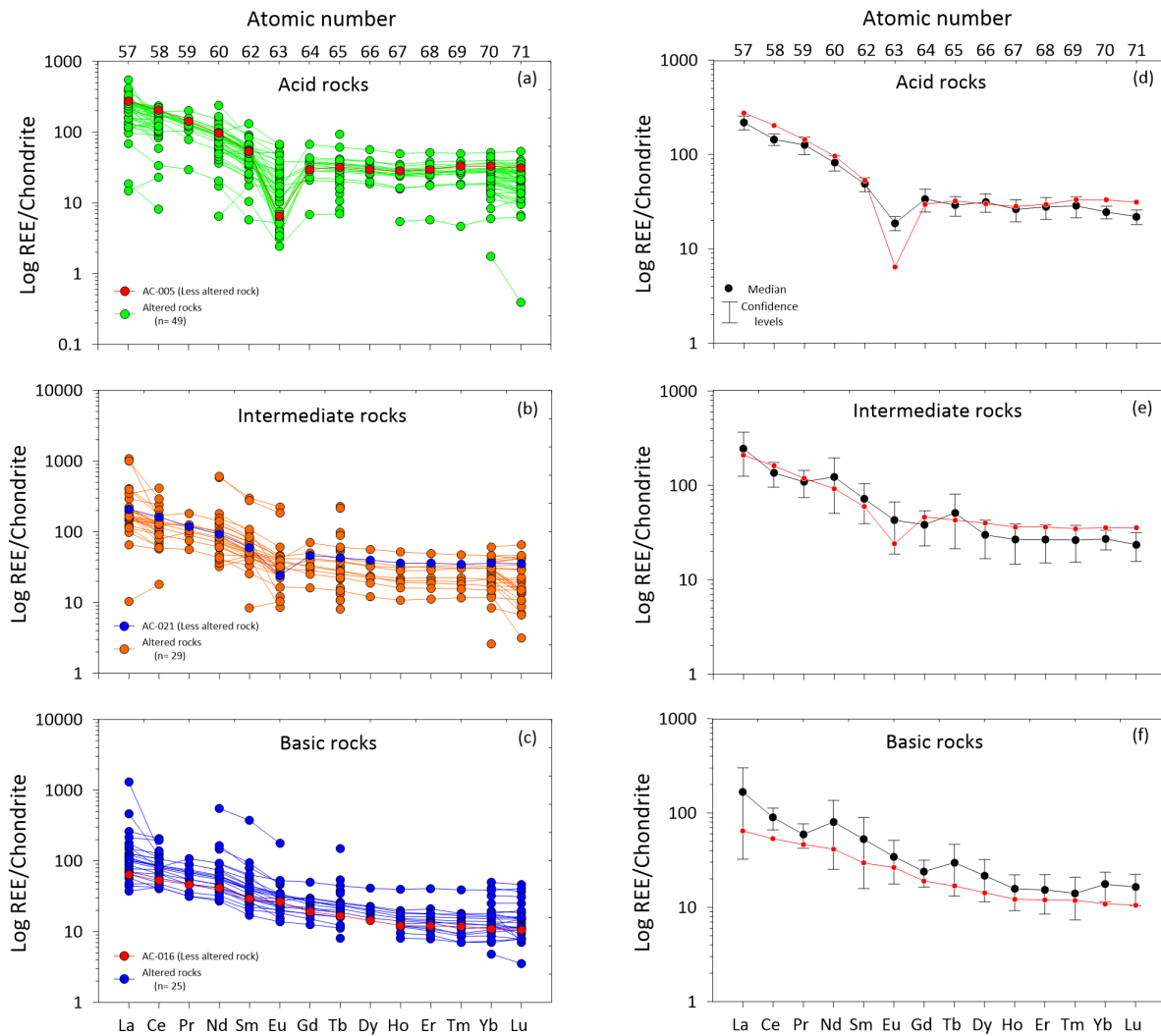


**Figure 3.11:** Chondrite-normalized patterns of REE observed in rock (acid, intermediate, and basic) samples (Santos-Raga et al., 2021).

## 3.5 Discussion

### 3.5.1 Concentration patterns of REE in water samples

The chondrite normalized REE patterns in spring waters showed that pH controls their fractionation both ZIC (AP, AZ, SFT, and CC) and ZOC (JI, QTZ, and CHIG). A clear dilution pattern in the REE concentrations of waters is proposed,

for the first time in the AGS. This geochemical signature is more evident in the spring waters of AZ, where a gradient concentration pattern was clearly observed in three groups of samples: Fig. 3.7b. The first group characterised by acidic-waters with a mean pH of  $3.2 \pm 1$  that show a systematic pattern with the highest concentrations of REE (Fig. 3.7b), almost similar to those patterns of the AP waters (Fig. 3.7a). A second group of water samples that shows a nearly systematic pattern of lower REE concentrations (probably attributed to a pH increase from 3.2 to 6.0) with some minor exceptions (Fig. 3.7b); and a third group that exhibit a more chaotic pattern as the water pH becomes more alkaline (pH of 6.8): Fig. 3.7b. Spring waters from the SFT and CC sites are characterised by alkaline pH values (from 8.5 to 8.8), which show lower REE concentration patterns with a pronounce depletion from LREE to HREE (Fig. 3.7c). In addition to these geochemical signatures, it was observed in most of the acidic-waters (AP and AZ), a systematic negative Eu anomaly in the chondrite-normalized REE patterns, which is probably associated to the AGS host rock (Göb et al., 2013). Other signatures such as the enrichment of LREE, and the positive anomaly of Gd were observed in most of the normalized REE patterns. Similar signatures of REE have been reported for andesitic-dacitic host rocks (Shakeri et al., 2015).

Significant differences were observed in the spring waters of the JI, QTZ, and CHIG, which exhibited very low concentrations of REE/chondrites (Fig. 3.7 d). Considering the calcareous host rock present in the ZOC, a strong positive Eu anomaly found in the QTZ water was the result of the preferential weathering of Eu-enriched phases as carbonates or calcic feldspars (Lewis et al., 1997). Such a strong anomaly may also due to the reduction from  $\text{Eu}^{3+}$  to  $\text{Eu}^{2+}$  which occurs in reducing environments at minimum temperatures of 250 °C (Göb et al., 2013). The REE content in acidic waters from ZIC (pH <3.5) show higher values up to three magnitude orders than those concentrations found in ZOC waters (which are characterised by slightly acid to neutral pH's, and alkaline pH's up to 9). This behaviour may help to explain the lateral fluid flow observed in the AGS with a preferential transport path of REE from the ZIC (pH < 3.5) to ZOC waters (pH >5).

## 3.5.2 Geochemical modelling of REE

### 3.5.2.1 Mineral saturation states

In relation to the mineral saturation indices calculated for the spring waters that emerge from the ZIC, it was observed that for the spring waters of AP, under-saturated states with respect to aluminium hydroxide sulphate  $[\text{Al}(\text{OH})\text{SO}_4]$ , and anhydrite  $[\text{CaSO}_4]$  minerals were observed at low-to-medium  $\Sigma\text{REE}$  values (Figs.

3.8 a-c); whereas an equilibrium state is nearly achieved with respect to alunite  $[\text{KAl}_3(\text{SO}_4)_2(\text{OH})_6]$  at  $100^\circ\text{C}$  and higher  $\Sigma\text{REE}$  values (Fig. 3.8b). Most of these patterns seem to show a tendency to reach the equilibrium with the increase of the  $\Sigma\text{REE}$ . In relation to the speciation temperatures, the  $[\text{Al}(\text{OH})\text{SO}_4]$ , and anhydrite minerals show lower IS values at higher temperatures, whereas the alunite exhibits an opposite behaviour. For the AZ cold springs, most of these waters exhibited a transient thermodynamic path from a dominant under-saturation state at low-to-medium  $\Sigma\text{REE}$  values to either the equilibrium (for the case of  $\text{Al}(\text{OH})\text{SO}_4$  minerals: Fig. 3.8d) or towards an over-saturation state at higher  $\Sigma\text{REE}$  values (for the alunite minerals: Fig. 3.8e). In both processes, the water samples seem to show an enrichment of REE given by the increase of the  $\Sigma\text{REE}$  with some preferences at low temperatures ( $25$  and  $50^\circ\text{C}$ ). Shakeri et al. (2015) pointed out that the correlation between the over-saturation of S minerals, and the increase of  $\Sigma\text{REE}$  values reveals that REE is not adsorbed on the surface of sulphate minerals. With respect to the gypsum ( $\text{CaSO}_4 \cdot 2\text{H}_2\text{O}$ ) mineral, most of the AZ waters exhibited a clear under-saturation state without showing any tendency to achieve the equilibrium with respect to the  $\Sigma\text{REE}$ . The speciation at higher temperatures seems to keep the under-saturation state. In relation to the  $\text{SiO}_2$  minerals (i.e., quartz, chalcedony, and cristobalite) observed in all areas, these are mostly oversaturated with some cases that exhibited a tendency to achieve the equilibrium state. Saturation indices with respect to some other mineral phases in association with the AGS waters were neglected.

### 3.5.2.2 Speciation of REE

With respect to the results obtained from the modelling of REE speciation in water samples from the ZIC (AP and AZ), it was found that for the spring waters of AP ( $\text{pH} < 3.5$ ), the concentration of dissolved REE at  $25^\circ\text{C}$  was dominated by sulphate complexes ( $\text{LnSO}_4^+$ ) up to  $\approx 70\%$ , and a low contribution of free-ion species ( $\text{Ln}^{3+}$ ) of about  $\approx 25\%$  (Fig. 3.9a). Other chloride ( $\text{LnCl}^-$ ), hydroxide ( $\text{Ln}(\text{OH})^{2+}$ ), and fluoride ( $\text{LnF}^-$ ) complexes exhibited a lower contribution ( $< 5\%$ ). By considering the 25% and 75% percentiles, a small variability in the complexation percentages of  $\text{LnSO}_4^+$  and  $\text{Ln}^{3+}$  were estimated for the LREE ( $\pm 1.8\%$  and  $\pm 2.5\%$ , respectively), MREE ( $\pm 1.6\%$  and  $\pm 2.3\%$ , respectively), and HREE ( $\pm 1.5\%$  and  $\pm 2.5\%$ , respectively) at  $25^\circ\text{C}$ . The small variability observed in these patterns was due to the effect of acidic waters with pH's between 2.3 to 2.8. A similar trend was observed for  $\text{LnSO}_4^+$  and  $\text{Ln}^{3+}$  complexes at  $50^\circ\text{C}$  and  $100^\circ\text{C}$  which showed a smaller variability in their percentages due to a combined effect of low pH's and higher temperatures (Figs. 3.9 b-c).

At  $50^\circ\text{C}$ , the  $\text{LnSO}_4^+$  species reach a complexation up to the  $\approx 80\%$  for LREE,

### 3. Geochemical signatures of REE in spring waters and outcropping rocks from the hidden geothermal system of Acoculco

---

$\approx 78\%$  for MREE, and  $\approx 75\%$  for HREE, whereas the free-ion species of  $\text{Ln}^{3+}$  exhibit a decrease of  $\approx 18\%$  for LREE,  $\approx 22\%$  for MREE, and  $\approx 25\%$  for HREE. A similar behaviour was obtained for the  $\text{LnSO}_4^+$  at  $100^\circ\text{C}$  with the following distribution:  $\approx 80\%$  for LREE,  $\approx 82\%$  for MREE,  $\approx 78\%$  for HREE, whereas for  $\text{Ln}^{3+}$ ,  $\approx 18\%$  was for LREE,  $\approx 15\%$  for MREE,  $\approx 20\%$  for HREE. Most of these calculations showed uncertainties of around  $\pm 1\%$ .

For the spring waters of AZ (characterized by acid to neutral pH's: 3.2-7.6), the concentration of dissolved REE at  $25^\circ\text{C}$  was dominated by sulphate complexes ( $\text{LnSO}_4^+$ ) with  $\approx 68\%$ , free-ion species ( $\text{Ln}^{3+}$ ) with  $\approx 30\%$ , and fluoride complexes with a pronounced pattern that increases with the atomic number (between  $\approx 2\%$  and  $\approx 10\%$ : Fig. 3.9d). The variability in the complexation percentages of  $\text{LnSO}_4^+$ ,  $\text{Ln}^{3+}$  and,  $\text{LnF}^-$  was estimated as  $\pm 1.8\%$ ,  $\pm 2.9\%$ , and  $\pm 0.6\%$  for LREE;  $\pm 3.4\%$ ,  $\pm 4.2\%$ , and  $\pm 2.0\%$  for MREE; and  $\pm 5.9\%$ ,  $\pm 6.1\%$ , and  $\pm 3.2\%$  for HREE, respectively. A higher variability was observed for spring waters that exhibited pH changes from slightly-acid to neutral. The increase in the complexation temperature to  $50^\circ\text{C}$  caused that the  $\text{LnSO}_4^+$  and  $\text{LnF}^-$  patterns increase their complexation percentage up to  $\approx 80\%$  ( $\pm 1.7\%$ ) and  $\approx 2\%$  ( $\pm 0.6\%$ ) for LREE;  $\approx 78\%$  ( $\pm 4.2\%$ ) and  $\approx 8\%$  ( $\pm 1.4\%$ ) for MREE; and  $\approx 75\%$  ( $\pm 2.5\%$ ),  $\approx 12\%$  ( $\pm 2.5\%$ ) for HREE; respectively (Fig. 3.9e). For free-ion species, their complexation percentages were lower,  $17\%$  ( $\pm 1.7\%$ ) for LREE;  $8\%$  ( $\pm 1.9\%$ ) for MREE; and  $12\%$  ( $\pm 2.6\%$ ) for HREE.

Finally, at a complexation temperature of  $100^\circ\text{C}$ , the  $\text{LnSO}_4^+$  reached up to  $\approx 85\%$  ( $\pm 1.4\%$ ) for LREE;  $\approx 88\%$  ( $\pm 3.3\%$ ) for MREE; and  $\approx 85\%$  ( $\pm 4.3\%$ ) for HREE; whereas the  $\text{Ln}^{3+}$  and  $\text{LnF}^-$  show much lower percentages of complexation of:  $\approx 10\%$  ( $\pm 0.6\%$ ) and  $\approx 5\%$  ( $\pm 0.5\%$ ) for LREE;  $\approx 8\%$  ( $\pm 0.9\%$ ) and  $\approx 10\%$  ( $\pm 1.1\%$ ) for MREE; and  $\approx 15\%$  ( $\pm 1.2\%$ ) and  $12\%$  ( $\pm 1.9\%$ ) for HREE; respectively (Fig. 3.9f).

The significant difference found in REE complexes between the AP and AZ cold springs was the amount of the fluoride complexes formed in the AZ waters. Regarding this geochemical signature observed in acidic waters, Gimeno-Serrano et al. (2000) pointed out that the aluminium is a more susceptible component to form fluoride complexes ( $\text{AlF}^{2+}$  and  $\text{AlF}^+$ ) in comparison with the REE. Although in fluids with pH's  $< 2$ , the  $\text{H}^+$  ion may compete for those dissolved fluoride complexes (Wood, 1990a; Shakeri et al., 2015).

With respect to the REE-chloride complexes, Shakeri et al. (2015) stated that the absence of these species in acidic waters may suggest the existence of minimum temperatures of  $200^\circ\text{C}$ , whereas Craddock et al. (2010) confirmed their presence at temperatures  $> 200^\circ\text{C}$  due to the contribution of the REE speciation in acid-sulphate waters. Both REE signatures were observed in the AGS spring waters which support the existence of a geothermal system with temperatures  $> 200^\circ\text{C}$ .

### 3.5.3 Concentration patterns of REE in outcropping rocks

The behaviour of the normalized REE concentrations show distinctive gull-wing patterns for acid and intermediate rocks, which were characterised by an enrichment of LREE, a negative Eu anomaly, and depletion of HREE with a flat tendency: Figs. 3.11 (a-b). Such a REE behaviour showed an interaction between felsic rocks and acid-sulphate waters fluids (e.g., AP and AZ). The negative Eu anomaly is usually associated with high temperatures ( $> 250^{\circ}\text{C}$ ), and extreme reducing environments (Wood and Shannon, 2003; Shakeri et al., 2015). These geochemical conditions allow the stability of  $\text{Eu}^{2+}$  in the host rock, whereas  $\text{Eu}^{3+}$  is more susceptible to be leached into the surrounding fluid (Fulignati et al., 1998). Regarding the rocks with a basic composition, these samples showed a flattened chondrite normalized REE pattern with slight depletion for HREE (Fig. 3.11c).

The REE distribution patterns of average altered-acid rocks with respect to relative-fresh rocks show a slight depletion of LREE (La and Ce), no changes in MREE (except Eu), and a decrease of Tm, Yb, and Lu in HREE (Fig. 3.11d).

On the other hand, the REE fractionation in intermediate rocks exhibited increases for La, Nd, Sm, Eu and Tb, together with a depletion of Ce, Pr, Gd, Dy, Ho, and all HREE (Fig. 3.11e). During the transport of fluids towards the surface, the temperature tends to decrease with an oxidizing state change, which enables the  $\text{Eu}^{3+}$  to be incorporated in secondary minerals by precipitation.

The increase in  $\text{Eu}^{3+}$  is observed in altered rocks with acid and intermediate composition: Figs. 3.11 (d-e). In reducing environments of high temperature ( $> 250^{\circ}\text{C}$ ), the  $\text{Eu}^{3+}$  may be also leached into the fluid. The normalized-chondrite patterns of basic rocks display an increase for all REE, more noticeable for LREE (except Pr) than in MREE (except Tb) and HREE (Fig. 3.11f). The LREE-increase result from their preferential tendency to be adsorbed on the particle surfaces, whereas the HREE have an affinity to remain dissolved in solution Yan et al. (2001).

## 3.6 Remarks of Chapter 3

A new prospection study of the promissory geothermal system of the Acoculco caldera was conducted for tracking new geochemical signatures. To face out the lack of surface geothermal manifestations (commonly evaluated in conventional hydrothermal systems), a geochemical mapping of REE and other trace elements in spring waters and outcropping rocks was successfully carried out.

A new set of geochemical signatures were identified, for the first time, in the AGS, among which stand out: (i) the bimodal frequency distribution of pH in cold

### 3. Geochemical signatures of REE in spring waters and outcropping rocks from the hidden geothermal system of Acoculco

---

and hot spring waters of the AGS with a clear dilution pattern from acid to neutral waters, and a deep preferential flow path from ZIC to ZOC; (ii) the concentration patterns of REE in waters and rocks which provide an additional evidence of the existence of a high-temperature geothermal system with pH mineral buffers and temperatures that range between 200 °C and 300 °C. Such REE patterns seem to dominate with a preferential transport path from deep heat conduction processes at the ZIC to surface geothermal manifestations at the ZOC, which is confirmed by the presence of hot spring waters with surface temperatures up to 54 °C (CHIG and JI).

All these geochemical signatures are in full agreement with the thermal state of the AGS, and the promising budget of heat stored at 2 km depth which was early evidenced from: (i) the bottomhole temperatures measured in two drilled exploratory wells (EAC-1 and EAC-2); (ii) the deep equilibrium temperatures inferred from gas geothermometry; the homogenization temperatures estimated from fluid inclusions; and (iii) the static formation temperatures extrapolated from heat conduction models.

Agregar unión de este capítulo con el siguiente, hablando de experimentos de REE

Fractionation of the rare earth elements:  
dissolution water-rock interaction  
experiments

---

4.1	Introduction . . . . .	82
4.2	Methodology . . . . .	82
4.2.1	Geochemometric treatment of experimental data . . . . .	83
4.2.2	Field work and collection of initial samples . . . . .	84
4.2.3	Sample preparation . . . . .	86
4.2.4	Experimental design . . . . .	88
4.2.5	Product sampling . . . . .	90
4.2.6	Analysis of physico-chemical parameters . . . . .	92
4.2.7	Geochemical analysis of products . . . . .	93
4.2.8	Geochemical modelling . . . . .	94
4.3	Results and discussions . . . . .	94
4.3.1	Mass balance and water-rock ratio . . . . .	94
4.3.2	Physicochemical analysis and water classification . . . . .	95
4.3.3	Distribution of major and trace elements . . . . .	97
4.3.4	Concentration patterns of REE in rock samples . . . . .	99
4.3.5	Concentration patterns of REE in water samples . . . . .	101
4.3.6	Geochemical modelling . . . . .	103
4.4	Remarks of Chapter 4 . . . . .	106

## 4.1 Introduction

Current experimental protocols, although expensive, continue to be a crucial analysis method for the practical understanding of the main water-rock interaction processes under geothermal conditions (Pérez-Zárate et al., 2015). Yáñez-Dávila et al. (2023) highlights the significance of this experiments (WRI) in addressing various challenges, including: (i) thermodynamic calibration of geothermometers for precise estimation of deep equilibrium temperatures in geothermal systems (e.g., Pérez-Zárate et al., 2015; Harvey et al., 2017); (ii) development of extraction technologies for non-toxic critical metals like lithium and REE from geothermal brines (e.g., Osvald et al., 2019; Warren, 2021); (iii) geochemical modelling of CO<sub>2</sub> capture and storage in geothermal systems (e.g., Galeczka et al., 2014; Marieni et al., 2020), and (iv) finding technical solutions to scaling and corrosion issues (e.g., Bai et al., 2012; Zhang et al., 2020). In this context, this work proposes an experimental approach to (i) the elucidation of the main mechanisms of rock-mineral dissolution and precipitation and (ii) the fractionation of major and trace elements (mainly REE) in rocks and fluids under geothermal conditions.

This chapter outlines the methodological approach involving implementing two water-rock experiments over a 6-month reaction period. The experiments involve the interaction of andesitic and trachyandesite rocks with deionized water acidified at 150C, close to conditions of a medium-temperature hydrothermal system situated on volcanic rocks. A main aspect of the experimental methodology is the application of geochemometrics, to ensure data quality and enhance result interpretation (Santoyo et al., 2007; Verma et al., 2012).

The study focuses on elucidating water-rock interaction processes, with a particular emphasis on the behaviour of REE in this environment, which has significant implications for the exploration of non-conventional geothermal systems.

## 4.2 Methodology

Figure 4.1 illustrates the methodology employed in the water-rock experiments, comprising key steps such as field sample collection, initial sample treatment, setup of experimental systems, product collection, in situ measurement of physicochemical parameters, mass balance correction, product treatment, and chemical and mineralogical analyses.

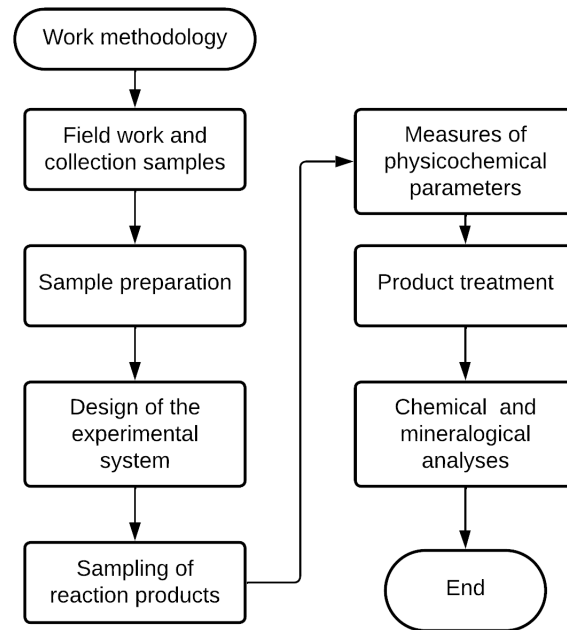


**Figure 4.1:** General methodology applied for the development of the experiments carried out at 150 °C.

The experimental parameters for these water-rock experiments were as follows (Table 4.1): the system was batch-type without agitation, volcanic rocks (basalt - trachyandesite and andesite) were utilized, uniform grain size (500-1000  $\mu\text{m}$ ) was maintained, acidified deionized water with a pH of  $3 \pm 0.1$  and resistivity of 18  $\text{M}\Omega/\text{cm}$  served as the working fluid, the initial water-rock ratio was 10:1, and the maximum reaction duration was 6 months.

**Table 4.1:** Water rock interaction experiments conditions

Batch reactor	Rock type	Fluid	Grain size ( $\mu\text{m}$ )	W/R ratio	Temperature ( $^{\circ}\text{C}$ )	Pressure (psi)	Times (months)
Polyethylene bottles	Andesite	HCl acidified water	500-1000	10	150	72.5	2, 4, 5, 6
Polyethylene bottles	Basalt - Trachyandesite	HCl acidified water	500-1000	10	150	72.5	2, 4, 5, 6

### 4.2.1 Geochemometric treatment of experimental data

Compositional data analysis involves rigorous statistical methodologies that allow better control of sources of uncertainty. Based on this, geochemometrics offers widely used techniques for the treatment of data of this nature.

Verma et al. (2012) defines Geochemistry as the science resulting from the combination of statistics, mathematics and calculus with geochemistry. The results processed in this research required prior statistical analysis. Some of the methodologies applied were as follows:

1. Mass determination as a control variable. Thirty repetitions were conducted for each mass measurement using a properly calibrated and verified analytical balance to ensure optimal accuracy and precision.
2. Identification of discordant data. Discordance tests were applied to the data using the UDASY program (Univariate Data Analysis System Verma et al., 2017) to identify potential outliers.
3. Computation of measures of central tendency and dispersion. Mean ( $\bar{x}$ ), standard deviation ( $S_x$ ), and relative standard deviation (%DER) values were calculated to assess precision control during measurements.
4. Weighted linear regression. Calculations of a linear model for steam leak during the reactor tests were carried out.

#### 4.2.2 Field work and collection of initial samples

The fieldwork was conducted at the Acoculco geothermal field from 28 to 31 March 2022, as depicted in Figure 4.5. Based on the geochemical studies of Verma (2001) and Sosa-Ceballos et al. (2018) the sampling area has undergone extensive geochemical, geochronological and lithostratigraphic studies, ensuring the acquisition of less-altered rock samples, further corroborated by field observations. The rock samples selected for the water-rock interaction experiments were andesitic lavas from Terrerillos (Tal; post-caldera stage;  $1708 \pm 54$  ka), rhyolitic dome from Lobera (Alrd; late post-caldera;  $1870 \pm 36$  ka), and basaltic - trachyandesitic lava flows from Manzanito (Mtal, early post-caldera;  $2199 \pm 24$  ka). Details of the geological setting of the Acoculco geothermal system are described in detail in section 3.2.

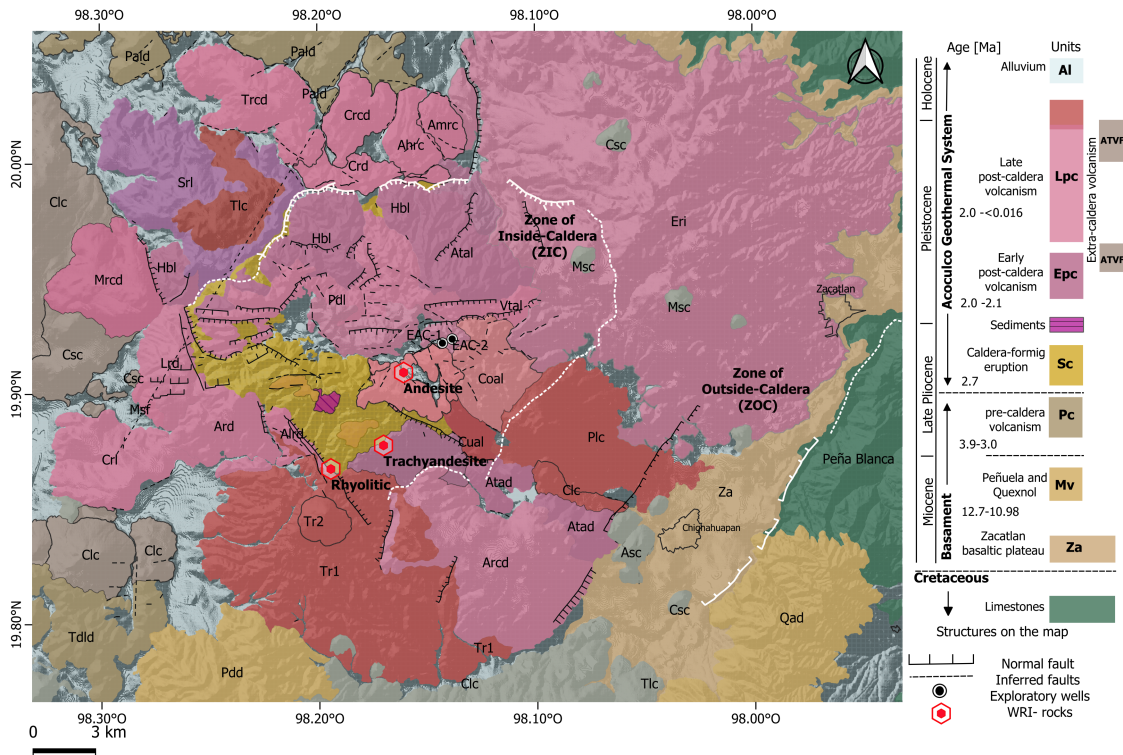


**Figure 4.2:** Geological map of the Acozulco geothermal system (modified after Avellán et al., 2020). Surface geology, faults, and hydrothermal alteration zones are also shown, including the rocks sampling for water-rock interaction experiments.

The geochemical and normative mineralogical composition of the initial rocks is presented in Table 4.2. The IgRocks program (Verma et al., 2013) was utilized for the normative mineralogical assessment of both rocks, as well as for their classification (Fig. 3.3). The basaltic rock falls within the basaltic - trachyandesite field, exhibiting a high presence of albite and ferromagnesian minerals. The andesite corresponds to a rock of intermediate composition, with a high content of plagioclase.

## 4. Fractionation of the rare earth elements: dissolution water-rock interaction experiments

**Table 4.2:** Normative chemical and mineralogical composition of the initial rocks used in the water-rock experiments. The geochemical compositions are reported with their uncertainty, the units are reported in % (w/w).

Major oxides	LOD	Normative mineralogical composition	Major oxides	LOD	Normative mineralogical composition	
<b>Andesite</b>			<b>Basalt - trachyandesite</b>			
SiO <sub>2</sub>	60.23 ± 0.44	0.01 Quartz [SiO <sub>2</sub> ]	15.63 SiO <sub>2</sub>	52.47 ± 0.63	0.01 Quartz [SiO <sub>2</sub> ]	5.43
Al <sub>2</sub> O <sub>3</sub>	14.01 ± 0.22	0.05 Orthoclase [KAlSi <sub>3</sub> O <sub>8</sub> ]	17.01 Al <sub>2</sub> O <sub>3</sub>	18.58 ± 0.33	0.05 Orthoclase [KAlSi <sub>3</sub> O <sub>8</sub> ]	7.53
Fe <sub>2</sub> O <sub>3</sub>	8.05 ± 0.19	0.05 Albite [NaAlSi <sub>3</sub> O <sub>8</sub> ]	30.77 Fe <sub>2</sub> O <sub>3</sub>	9.15 ± 0.25	0.05 Albite [NaAlSi <sub>3</sub> O <sub>8</sub> ]	32.34
MnO	0.23 ± 0.01	0.005 Anorthite [CaAl <sub>2</sub> Si <sub>2</sub> O <sub>8</sub> ]	14.89 MnO	0.15 ± 0.01	0.005 Anorthite [CaAl <sub>2</sub> Si <sub>2</sub> O <sub>8</sub> ]	26.42
MgO	2.47 ± 0.01	0.05 Corundum [Al <sub>2</sub> O <sub>3</sub> ]	— MgO	3.64 ± 0.17	0.05 Corundum [Al <sub>2</sub> O <sub>3</sub> ]	1.44
CaO	4.23 ± 0.11	0.05 Diopside [CaMgSi <sub>2</sub> O <sub>6</sub> ]	4.61 CaO	7.36 ± 0.02	0.05 Diopside [CaMgSi <sub>2</sub> O <sub>6</sub> ]	—
Na <sub>2</sub> O	3.50 ± 0.03	0.05 Hypersthene [MgOSiO <sub>2</sub> ]	11.39 Na <sub>2</sub> O	3.78 ± 0.01	0.05 Hypersthene [MgOSiO <sub>2</sub> ]	17.12
K <sub>2</sub> O	2.77 ± 0.08	0.05 Magnetite [Fe <sub>3</sub> O <sub>4</sub> ]	2.90 K <sub>2</sub> O	1.26 ± 0.05	0.05 Magnetite [Fe <sub>3</sub> O <sub>4</sub> ]	2.85
TiO <sub>2</sub>	1.17 ± 0.03	0.005 Ilmenite [FeTiO <sub>3</sub> ]	2.31 TiO <sub>2</sub>	1.64 ± 0.04	0.005 Ilmenite [FeTiO <sub>3</sub> ]	3.15
P <sub>2</sub> O <sub>5</sub>	0.20 ± 0.01	0.05 Apatite [Ca <sub>5</sub> (PO <sub>4</sub> ) <sub>3</sub> (OH,F,Cl)]	0.48 P <sub>2</sub> O <sub>5</sub>	0.37 ± 0.02	0.05 Apatite [Ca <sub>5</sub> (PO <sub>4</sub> ) <sub>3</sub> (OH,F,Cl)]	3.72
LOI	2.38		LOI	1.59		



**Figure 4.3:** Rock sample collection at the Caldera Complex Acoculco: a) rhyolitic rock, b) basaltic - trachyandesite rock, c) andesitic rock.

### 4.2.3 Sample preparation

The rocks have pre-treatment, which commences with washing using deionized water, followed by drying at 105°C for 24 hours. This process was succeeded by crushing, meshing, and ultrasonic washing. The device used for washing the rock grains was Ultrasonic Cleaner Cole Parmer 08890-11, 70 W, 42 KHz ± 6%. Subsequently, the grains were placed in the Binder<sup>®</sup> ED-115-UL oven at 105 °C for 24 hours and finally, they were transferred to a desiccator.

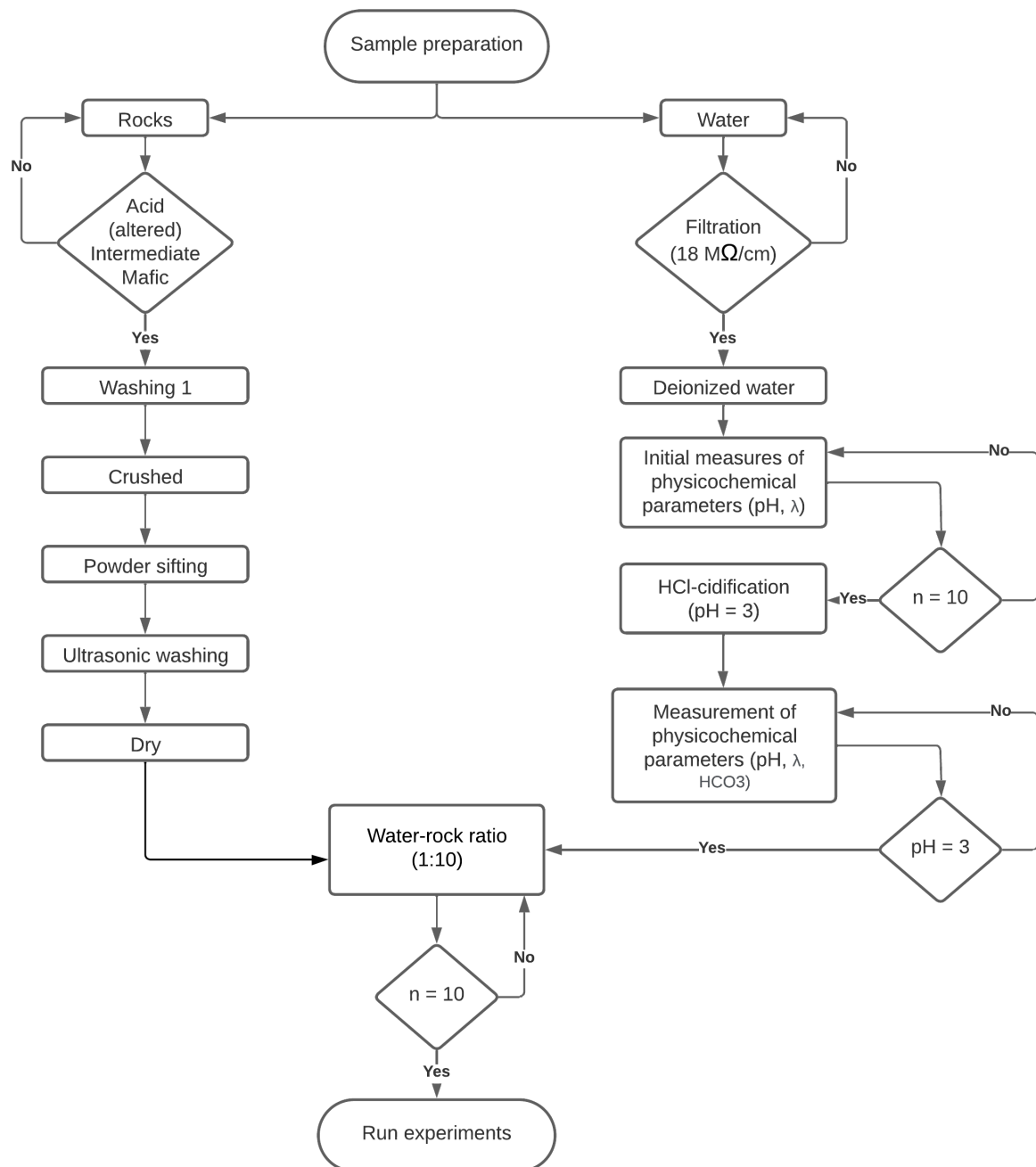


**Figure 4.4:** Sample preparation flow diagram.



**Figure 4.5:** Pre-treatment of rock samples: (a) crushed, (b) ultrasonic washing, and drying.

The fluid used in the experiments was deionised water from the chemistry laboratories of IER-UNAM. This water was processed through a Millipore<sup>®</sup> reverse osmosis distillation-deionisation system, guaranteeing a quality of 18 M $\Omega$ /cm. Subsequently, an acidification process was carried out with HCl to adjust the pH of the initial fluid to 3. The methodology for the preparation of the sample is shown in Figure 4.4.

## 4.2.4 Experimental design

### 4.2.4.1 Description of the experimental system

The experimental setup for the dissolution experiments consisted of batch reactors made of Savillex<sup>®</sup> Teflon bottles (volumen of 180 ml). Subsequently, the rock samples (trachyandesite and andesite) were placed together with deionized water inside the bottles and sealed from the atmosphere (Fig. 4.7a). Finally, they were maintained at a constant temperature of 150 °C inside a Binder<sup>®</sup> ED-115-UL digital furnace (Figs. 4.7b). Both experiments were conducted over periods of 2, 4, 5, and 6 months using a grain size between 1000-500  $\mu$ m and a water/rock ratio of 10:1. All vessels used for the preparation of the batch reactors were cleaned with an acid solution (acidify with HCl) for 24 hours, then rinsed with deionized water, and dried at room temperature.

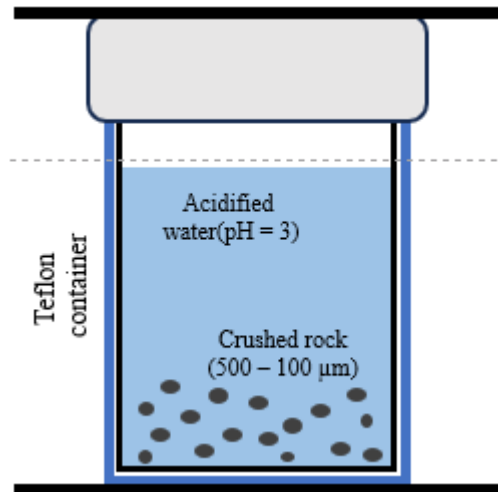


**Figure 4.6:** Conceptual model of the experimental system.



**Figure 4.7:** Experimental system: (a) teflon batch reactor, (b) Binder digital furnace, (c) metal support structure is employed to prevent steam leakage resulting from high temperature.

To reduce steam leakage and maintain a constant water-to-rock ratio in the batch reactors, a metallic liner was designed and installed (Fig. 4.7c). Afterward, vapor leakage tests were conducted by placing a batch reactor equipped with the metal liner and sealed using high-temperature silicone, maintaining a constant temperature of  $150^{\circ}\text{C}$ . The steam loss was monitored by recording the initial weight of the system both with and without fluid ( $n = 10$ ). The system remained in the furnace for a total of 40 days, with continuous weight measurements taken throughout. Based on this, a weighted linear regression analysis was employed to model the linear trend and extrapolate it to the maximum experimental duration (180 days).

## 4. Fractionation of the rare earth elements: dissolution water-rock interaction experiments

---

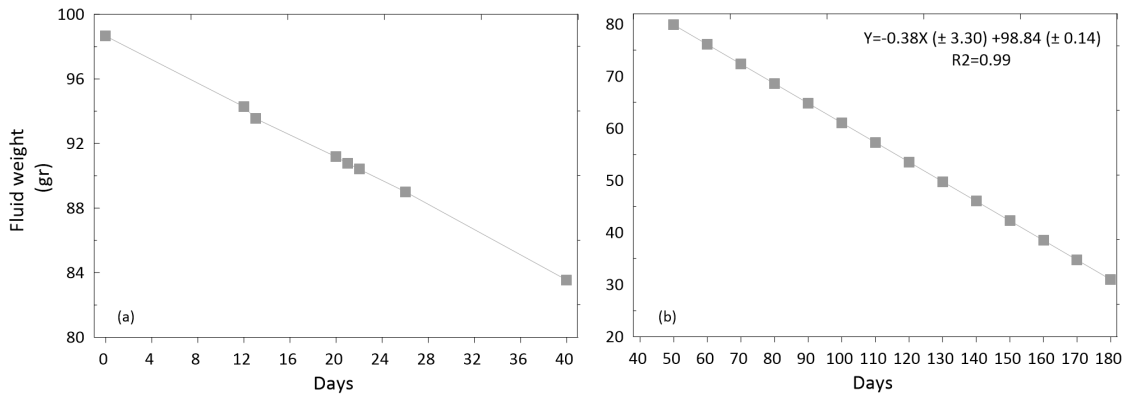


**Figure 4.8:** Experimental system: (a) Steam lake test, (b) steam leak test regression model.

### 4.2.4.2 Initial geochemical analysis

For the initial analysis of rocks, Fusion-Inductively Coupled Plasma Optical Emission Spectrometry (FUS-ICP), and Total Digestion-Inductively Coupled Plasma (TD-ICP) were used for the determination of major elements and Lost-on-Ignition (LOI), whereas the compositions of REE were measured by Instrumental Neutron Activation Analysis (INAA).

### 4.2.5 Product sampling

The general methodology for the sample collection (Figure 4.9) of the experiments at 2, 4, 5 and 6 months consisted of (i) quenching of the system, (ii) disassembly of the metallic structure, (iii) physicochemical measurements, and (iv) fluid and rock separation. Concerning the rock, the mass was measured in the wet phase and the dry phase for the mass balance calculation. Details of each stage are below:

1. Quenching of the system: The experimental systems were cooled in 4°C water for 15 minutes until reaching ambient temperature.
2. Disassembly of the metallic structure: Upon opening the systems, pH and electrical conductivity ( $\gamma$ ) readings were conducted in situ, each repeated 10 times rapidly to minimize the effect of CO<sub>2</sub>. Additionally, 25 mL aliquots of the fluid were collected in triplicate for bicarbonate determination.
3. Fluid and rock separation: The produced liquid was separated using 10 mL analytical pipettes. After separation, fluid mass measurements were taken to

estimate fluid loss during the experiment. Following liquid measurements, filtration with  $0.20\ \mu\text{m}$  micropore size filters was performed to separate possible chelates formed by Al and Fe (Bethke, 2007). Subsequently, two liquid samples were collected: (i) a sample acidified to ultra-pure nitric acid to preserve dissolved species for cationic composition and trace element determination, and (ii) a non-acidified sample for determining the anionic composition of the fluid. On the other hand, the mass of the rock was measured in wet and dry phases after undergoing a drying process to calculate total mass balance. Rock drying involved heating at  $105^\circ\text{C}$  for 24 hours (Gislason and Oelkers, 2003). Following drying, the solid phase was allowed to cool for 30 minutes, weighed using geochemometric methodology, and stored in a desiccator for subsequent chemical and mineralogical analyses.

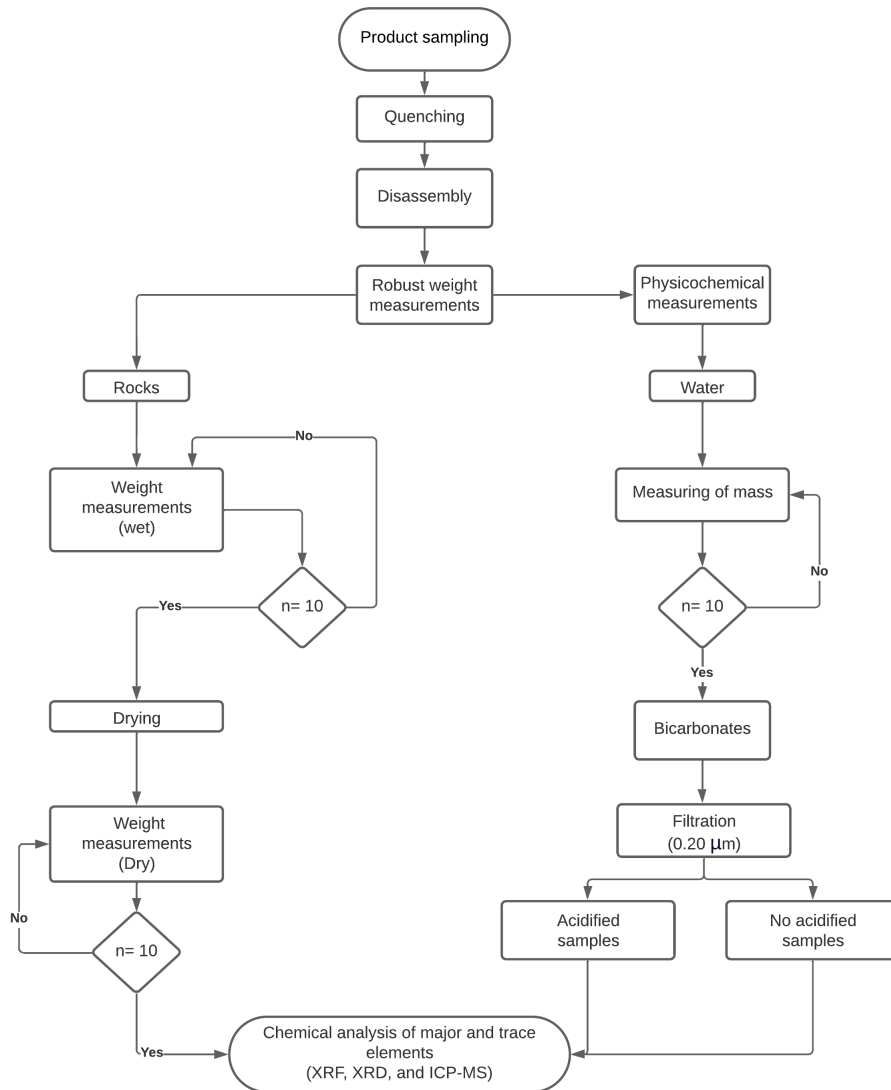


**Figure 4.9:** Flow Diagram of product sampling process.

### 4.2.6 Analysis of physico-chemical parameters

The determination of physicochemical parameters (pH and  $\gamma$ ) conductivity of the fluids were carried out applying a geochemometric methodology with a pH-con 510 meter. For pH measure, the equipment was calibrated with OAKTON<sup>®</sup> standard solutions with the following pH values:  $4.000 \pm 0.002$ ,  $7.000 \pm 0.002$ ,  $10.000 \pm 0.002$ . On the other hand, the calibration of the conductivity sensor was carried out with

the OAKTON standard with a value of 1413  $\mu\text{S}/\text{cm}$ .

## 4.2.7 Geochemical analysis of products

### 4.2.7.1 Rock geochemical analysis

For the analysis of rocks, Inductively Coupled Plasma mass spectrometry (ICP-MS), and X-ray fluorescence (XRF) were used for the determination of REE and major elements, respectively. Mineralogical analysis of the rocks was performed utilizing the Rigaku DMAX 2200<sup>®</sup> diffractometer at the Solar Materials Laboratory, Instituto de Energías Renovables-UNAM (IER-UNAM), employing the conventional  $2\theta/\theta$  method for powder analysis. The MDI Jade<sup>®</sup> program was utilized for result interpretation. Additionally, the rock grains were analyzed using scanning electron microscopy coupled with an energy-dispersed X-ray detector (SEM/EDX) to identify secondary minerals, conducted at the Nanostructures and Catalysis Laboratory from IER-UNAM.

### 4.2.7.2 Water geochemical analysis

#### *Bicarbonates*

During the volumetric titration of bicarbonates, an acid-base reaction occurs between a weak base and a strong acid, employing a visual indicator to determine the endpoint. The shape of the titration curve is influenced by the ionic strength of the acid and bases present, which in turn alters the pH of the sample. The bicarbonates quantify ( $\text{HCO}_3$ ) in the collected fluid samples was carried out with volumetric titration using the direct method (Merchand-Reyes, 2010).

#### *Major and trace elements*

Water chemical analyses for major and trace elements were conducted at commercial geochemical labs (Actlabs, Canada). The composition of REE and some cations in waters were measured by ICP-MS to achieve low detection limits, whereas the anions were analysed by ion chromatography. For the major and trace elements of water samples, the IV-STOCK-1643 certified standard was used for the instrumental calibration (Rodríguez-Espinosa et al., 2020).

The quality of water chemical analyses was assessed using the standardized charge-balance method between anions and cations. This calculation serves as a fundamental parameter for quality assurance/quality control (QA/QC) in evaluat-

ing the reliability of water chemical analyses (Nordstrom et al., 2009). According to Nicholson (1993), charge balances should ideally fall within the range of  $\pm 5\%$  to  $\pm 10\%$ , provided that both sampling and chemical analyses are conducted meticulously in the field and laboratory, respectively. However, some authors suggest that values within  $\pm 20\%$  may still be acceptable (e.g., Nordstrom et al., 2009).

### 4.2.8 Geochemical modelling

The concentrations of REE were normalized with respect to chondrites (McDonough and Sun, 1995), and plotted on a bivariate diagram for determining the fractionation processes (dissolution or precipitation), the influence of physicochemical parameters, and the identification of major geochemical signatures. Mineral saturation indexes and aqueous speciation of REE were calculated using the software TOUGHREACT in combination with the geochemical database `thd-dem_aug09t4.dat` (Pruess et al., 1999). This database considers the main aqueous species for REE complexes (carbonate, sulphate, fluoride and hydroxide ligands), and thermodynamic data of ionic strength and temperature with values up to 300 °C (Haase et al., 2013). TOUGHREACT is a numerical software developed with the introduction of reactive transport into the existing framework of a non-isothermal multi-component fluid and heat flow simulator TOUGH2 (Pruess et al., 1999). According to Xu et al. (2006), transport geochemical modelling with the TOUGHREACT simulator can be applied to many geologic systems problems, including weathering processes, geological carbon storage, geothermal systems, acid mine drainage remediation, and groundwater quality.

## 4.3 Results and discussions

### 4.3.1 Mass balance and water-rock ratio

The geochemometric methodology allowed for accurate and precise measurements throughout the experimental process. These results are reported by statistical parameters of central tendency (mean), dispersion (standard deviation), and calculation of the associated uncertainties. The WRI experiments were assembled by placing 10 g of rock (andesite, trachyandesite) with 100 g of fluid (W/R ratio = 10). The central tendency and dispersion parameters calculated with the successive mass measurements are shown in Table 4.3 for the water-andesite and water-trachyandesite systems. On the other hand, the obtained masses of rock and

**Table 4.3:** Calculation of the mean, dispersion, uncertainty and w/r ratio of the weights measured during the preparation of the experimental systems. Calculations were performed after evaluating the data for outliers.

Experimental system	Container weight (gr)			Container + rock weight			Container + rock + water			Set complete			w/r ration		
	( $\bar{x}$ )	$S_x$	U	( $\bar{x}$ )	$S_x$	U	( $\bar{x}$ )	$S_x$	U	( $\bar{x}$ )	$S_x$	U	( $\bar{x}$ )	$S_x$	U
Bk	159.9	0.007	0.003	—	—	—	256.4	0.007	0.004	1493	0.015	0.007	—	—	—
Andesite system															
AC-022	158.1	0.001	0.001	168.1	0.001	0.001	267.2	0.100	0.051	1508.4	0.006	0.003	9.90	0.009	0.005
AC-024	157.7	0.001	0.001	167.6	0.002	0.001	266.9	0.010	0.005	1508.4	0.006	0.003	9.90	0.001	0.001
AC-025	157.9	0.002	0.001	167.8	0.001	0.003	266.5	0.028	0.014	1514.6	0.008	0.004	9.90	0.004	0.002
AC-026	157.9	0.001	0.0005	167.9	0.004	0.002	266.1	0.006	0.003	1508.7	0.007	0.003	9.80	0.001	0.001
Trachyandesite system															
AC-032	157.9	0.002	0.001	169.9	7.610	3.800	267.1	0.031	0.016	1509.7	0.008	0.004	9.40	2.077	1.043
AC-034	157.8	0.001	0.002	167.7	0.350	0.170	266.7	0.010	0.005	1507.9	0.005	0.003	9.80	0.344	0.173
AC-035	158.1	0.001	0.002	167.9	0.002	0.001	267.1	0.018	0.009	1509.3	0.009	0.005	10.00	0.002	0.001
AC-036	158.2	0.001	0.002	168.1	0.001	0.0004	267.1	0.015	0.008	1514.1	0.005	0.003	10.00	0.002	0.001

fluid, as well as the calculation of the W/R ratio with its respective uncertainty, are shown in Table 4.3.

### 4.3.2 Physicochemical analysis and water classification

The pH showed a rapid increase during the initial two months of the reaction, with a maximum value of  $6.2 \pm 0.08$  for the trachyandesite rock. Subsequently, it showed a relatively constant pH value for the remaining four months (Fig. 4.10a). Bicarbonate concentration remained below 180 mg/L for both rock types.  $\text{HCO}_3$  increased rapidly in the first month of reaction, with andesite showing the highest values. As for the trachyandesite, it reached similar bicarbonate values in month five. Subsequently, its concentration decreased indicating a possible precipitation of carbonate-enriched secondary phases (Fig. 4.10b). Finally, the electrical conductivity of the fluids reached a maximum value of  $850 \pm 4 \mu\text{s}/\text{cm}$  after five months of reaction. By the end of the last month of experimentation, there was a notable decrease in this physicochemical parameter observed in both samples (Fig. 4.10c).

#### 4. Fractionation of the rare earth elements: dissolution water-rock interaction experiments

---

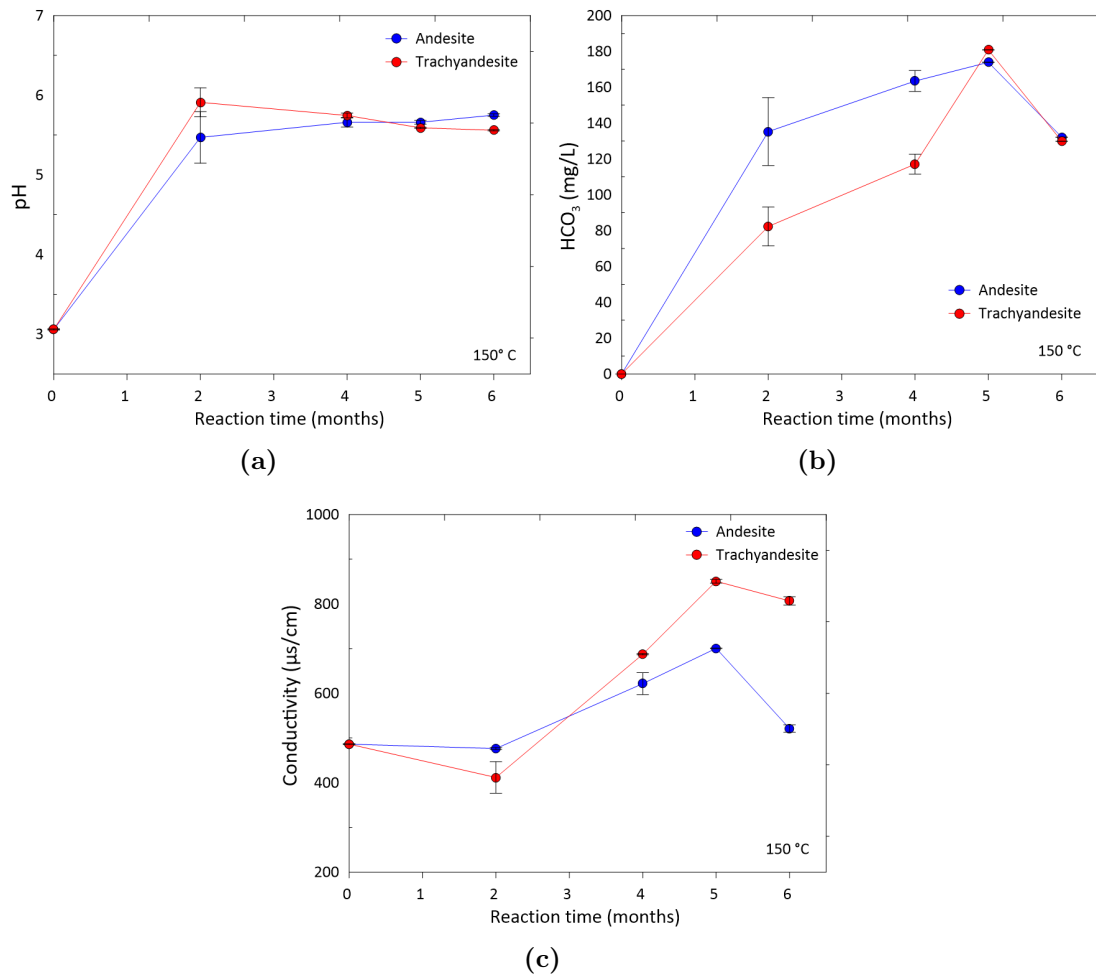


**Figure 4.10:** Time evolution of the physicochemical parameters of the experimental fluid collected at 150°C: (a) pH, (b) bicarbonate content and (c) electrical conductivity ( $\lambda$ ).

The results of the chemical analysis of major elements in the fluid of each experimental system were plotted on the Piper diagram (Fig. 4.11) to identify the chemical characterization of the solutions produced by the experiments. According to this diagram, both experiments yielded sodium-bicarbonate-type solutions. Only some samples of the fluid interacting with basalt were classified as sodium-chloride-type.

The classification of these fluids agrees with the results obtained in Fig. 4.10b, where a rapid increase in the concentration of bicarbonates is observed from the first two months. High bicarbonate values can be associated with a rapid dissolution of secondary minerals that contain carbonates in their composition. On the

other hand, this increase may be related to  $\text{CO}_2$  in the experimental systems. The presence of  $\text{CO}_2$  causes the release of  $\text{H}^+$  protons into the solution, which explains the high concentration of bicarbonate through the formation of carbonic acid.

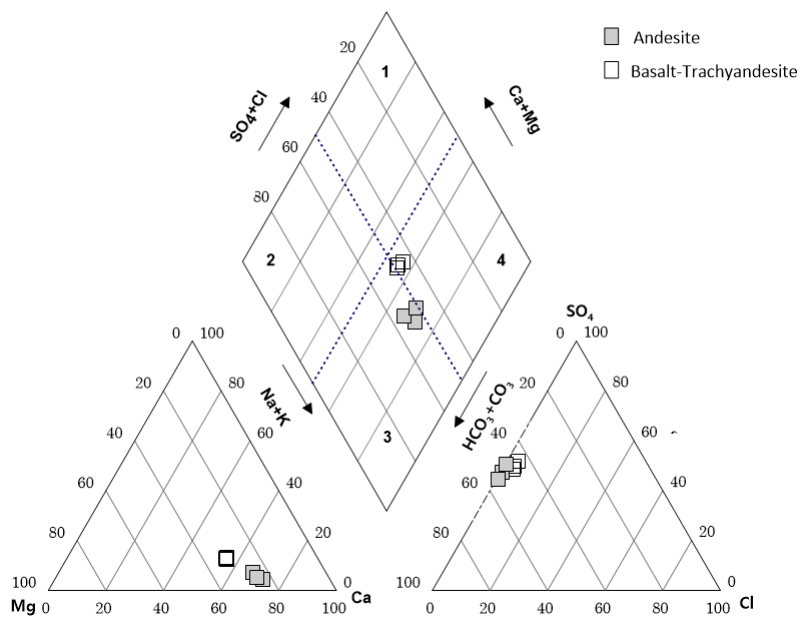


**Figure 4.11:** Piper diagram for the chemical classification of solutions produced by water-rock interaction experiments.

### 4.3.3 Distribution of major and trace elements in rocks and water samples

Extended statistical versions of the Schoeller diagram, illustrating the chemical distributions of major and trace elements in experiments, were plotted in Figs. 4.12 and 4.13 for rocks and water samples, respectively. The rock samples exhibit a similar geochemical signature to that observed in intermediate and mafic rocks (Santos-Raga et al., 2021), displaying patterns with negative anomalies of  $\text{TiO}_2$ ,  $\text{MnO}$ , and  $\text{P}_2\text{O}_5$ . Concerning to other trace elements, lower concentrations of Cr, Co, Y, Ta and W were revealed in presence of higher enrichments of Sr, Zn, Zr and Rb: Figs. 4.12c, d. Regarding the temporal geochemical evolution inherent in the dissolution experiments, the andesite and trachyandesite show minimal variation (between 25%-75% percentiles) in major oxides compared to the less-altered sample (Figs. 4.12a, b).

#### 4. Fractionation of the rare earth elements: dissolution water-rock interaction experiments

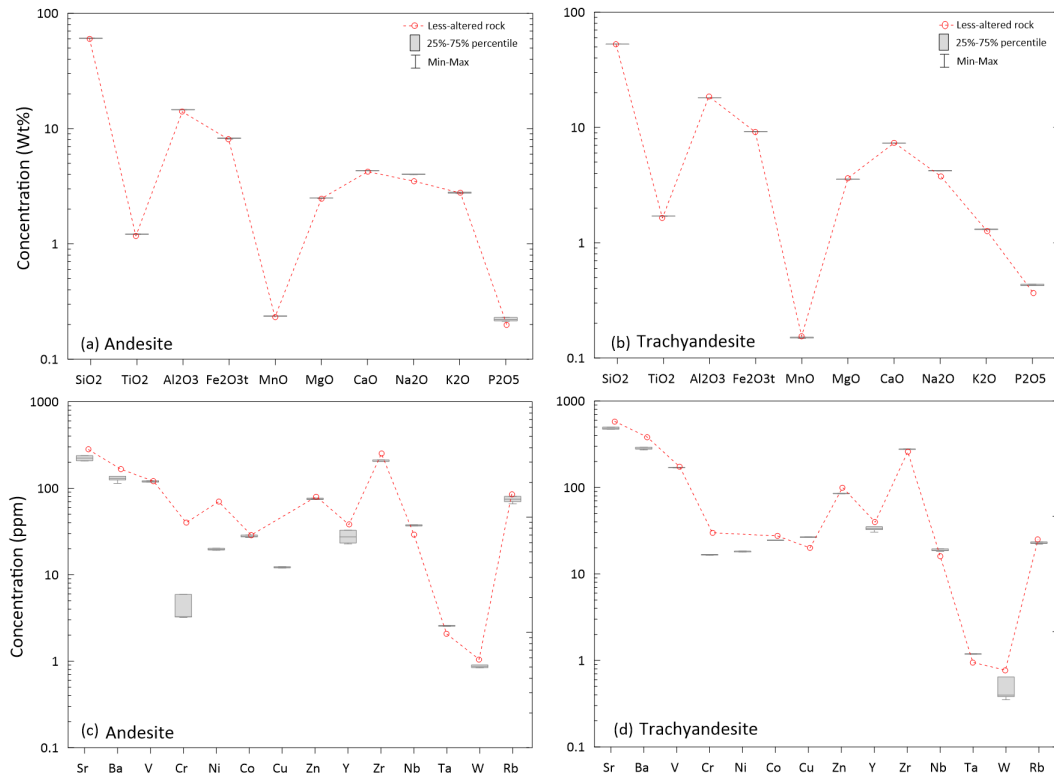


**Figure 4.12:** Statistical descriptive plot showing the main concentration patterns of major and trace elements in altered and less-altered rocks from water-rock interaction experiments.

In water samples (fig. 4.13), six major groups of elements, represented by median values and accompanied by the 25-75% percentiles, were plotted. These groups include anions, alkali metals, alkaline earth metals, metalloids, transition metals, metals, and some radioactive elements.

In both the andesite and trachyandesite waters, it was observed that Cl and  $\text{HCO}_3$  were the dominant anionic species, while Na–K and Ca–Mg were the major cations. A strong enrichment of Al, Fe, Zn, Pb, and Th was observed in the Andesite waters, while for the trachyandesite, the enrichment was pronounced in Al, Fe, Co, Ni, Cu, Zn, Ga, Pb, and Th. The enrichment signature of Al and the pH changes from acidic to alkaline play an important role in the behavior of REE in spring waters (Lewis et al., 1997, 1998; Santos-Raga et al., 2021). Negative anomalies (or depletion) in Sb were observed in the Andesite waters (see Figs. 4.13a, b). A positive correlation between Ga and high temperature systems was previously reported by Elmi et al. (2010), including the strong correlation observed for Sb (Krupp and Seward, 1987). Fall et al. (2020) highlighted that K, Th, and U often exhibit higher mobility as a result of hydrothermal alteration or weathering.

This mobility can be linked to processes such as magmatic activity, intense fluid-rock interaction, and mineralization.

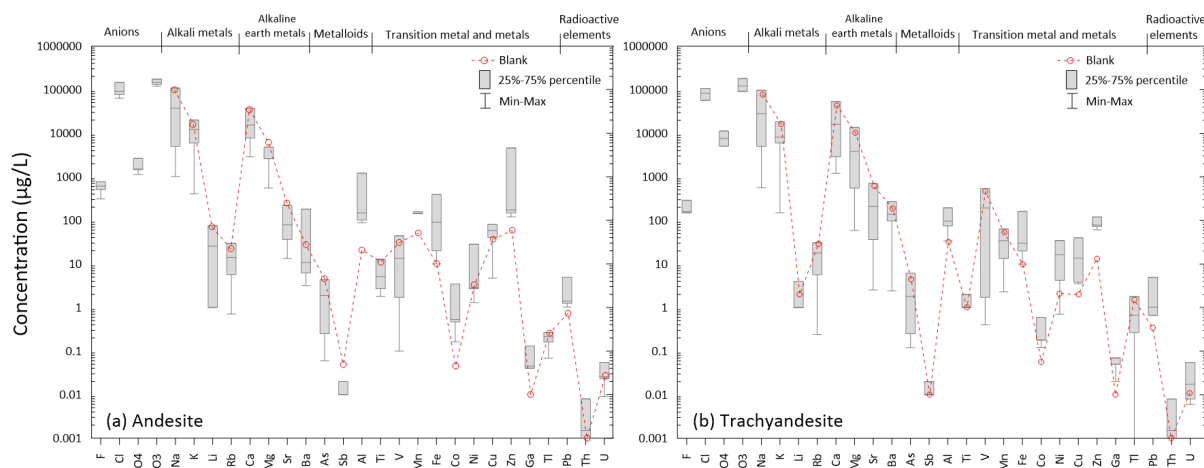


**Figure 4.13:** Statistical descriptive plot showing the main concentration patterns of major and trace elements in waters.

#### 4.3.4 Concentration patterns of REE in rock samples

The rock samples showed a decreasing trend in the concentration of all REE (Fig. 4.14). In the specific case of andesite, it can be observed that it presents an initial concentration of La, Yb, and Lu higher than that measured in trachyandesite. After 6 months of reaction, the concentration of these elements was lower than that reported for trachyandesite. Based on this evidence, a higher dissolution rate of these elements is determined in the andesite sample. On the other hand, a slight enrichment pattern of REE is identified from the fifth to the sixth month of reaction for the trachyandesite samples. Andesite shows this positive anomaly in three Middle Rare Earth Elements (MREE: Tb, Dy, and Ho) and three Heavy Rare Earth Elements (HREE: Er, Yb, Lu). This REE enrichment may be attributed to the precipitation of secondary minerals with REE in their structure.

The concentrations of REE measured in the andesite and trachyandesite rock samples were also plotted as chondrite-normalized patterns (Figs. 4.15a, b, respectively). These patterns were used to evaluate the variation of REE present in altered rocks compared to less-altered rocks, as shown in Figs. 4.15a, b. To evaluate the variability of REE concentrations, the composition of altered rocks was compared with the value of the less-altered rock.

The normalized REE concentrations exhibit distinctive gull-wing patterns for andesite rocks (Santos-Raga et al., 2021), characterized by an enrichment of LREE,

#### 4. Fractionation of the rare earth elements: dissolution water-rock interaction experiments

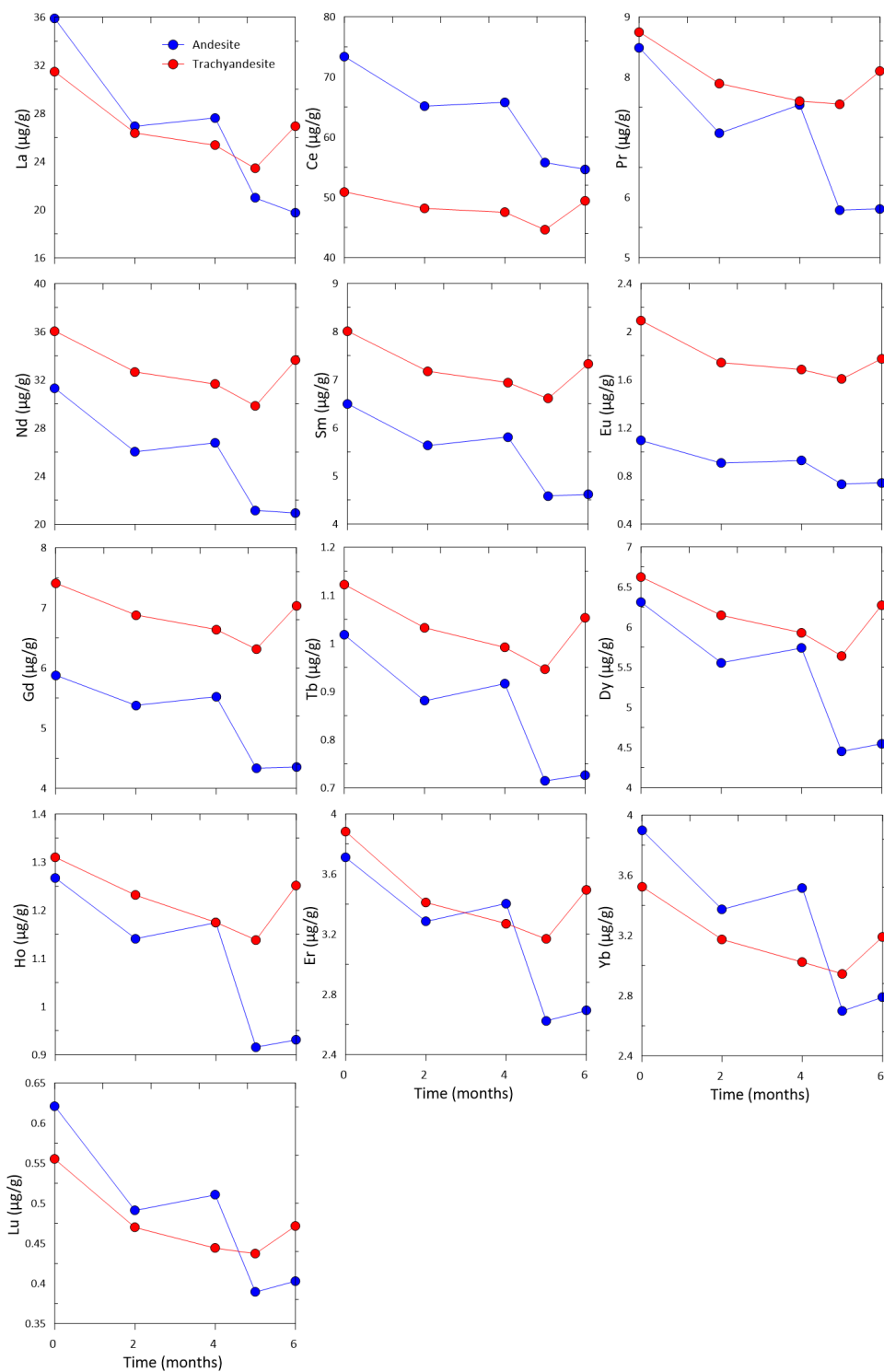


**Figure 4.14:** REE concentrations patterns (in  $\mu\text{g/g}$ ) of the experimental rocks as a function of time (months).

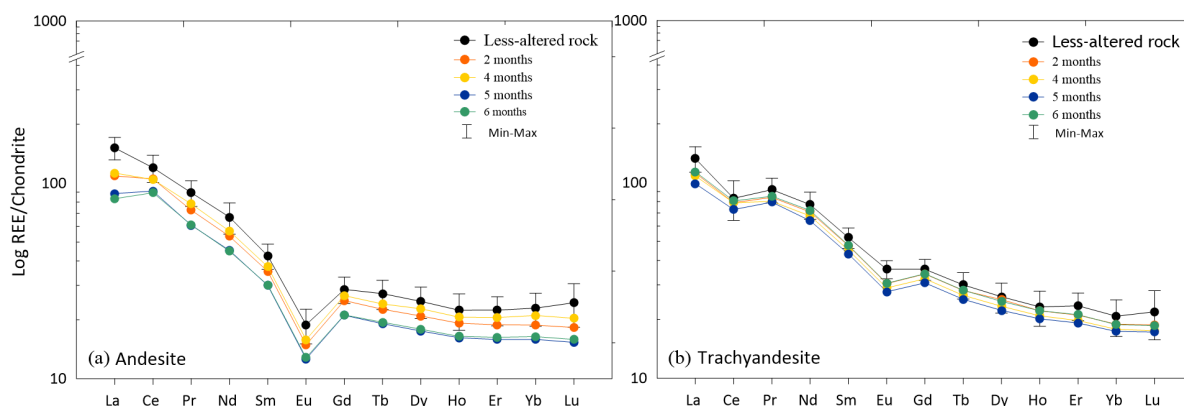


**Figure 4.15:** Chondrite-normalized patterns of REE.

a negative Eu anomaly, and depletion of HREE with a flat tendency, as depicted in Fig. 4.15a. The negative Eu anomaly is usually associated with high temperatures ( $> 250$  °C) and extreme reducing environments (Shakeri et al., 2015; Wood and Shannon, 2003).

Regarding rocks with a basic composition such as trachyandesite, they display a flattened chondrite-normalized REE pattern with slight depletion for HREE (Fig. 4.15b). The high values of LREE result from their preferential tendency to be adsorbed on particle surfaces, whereas HREE has an affinity to remain dissolved in solution (Yan et al., 2001). This REE pattern from the trachyandesite shows a slightly negative anomaly for Ce and Eu.

### 4.3.5 Concentration patterns of REE in water samples

The water samples showed an increasing trend (inverse to that observed in the rock samples) in the concentration of all REE (Fig. 4.16). Both experiments showed similar patterns of dissolved REE concentrations, with some differences in elements such as La and Lu, which exhibited higher final concentrations for trachyandesite. Conversely, elements such as Ce, Pr, Eu, Gd, Dy, Ho, Er, Tm, and Yb showed higher concentrations for andesite at the end of the sixth month of reaction.

The chondrite-normalized REE patterns of the experimental solutions showed consistent concentrations of dissolved REE in both experiments (Fig. 4.17). The andesite exhibits a flattened pattern, with a negative Eu anomaly present throughout the experimental time. On the other hand, a positive Er anomaly is shown during the first five months of the reaction. Furthermore, the sample collected after six months of reaction presents a geochemical signature much more similar

#### 4. Fractionation of the rare earth elements: dissolution water-rock interaction experiments

---

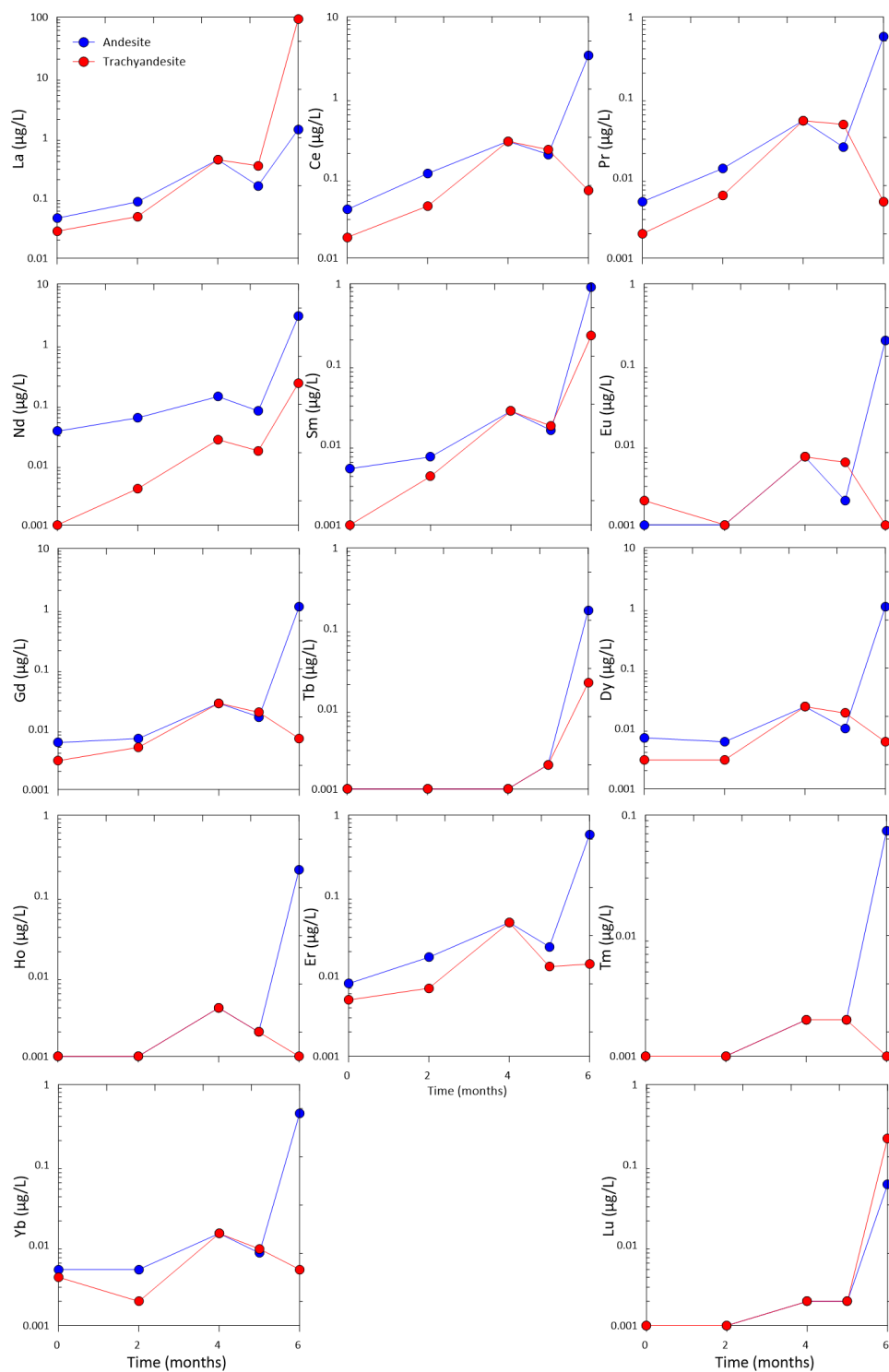


**Figure 4.16:** REE concentrations patterns (in  $\mu\text{g/L}$ ) of the experimental solutions measured using ICP-MS as a function of time (months).

to that present in the reactive rock sample. This normalization pattern (gull-wing) is characterized by a negative europium anomaly and a slight gradient of decrease from the LREE to the HREE.

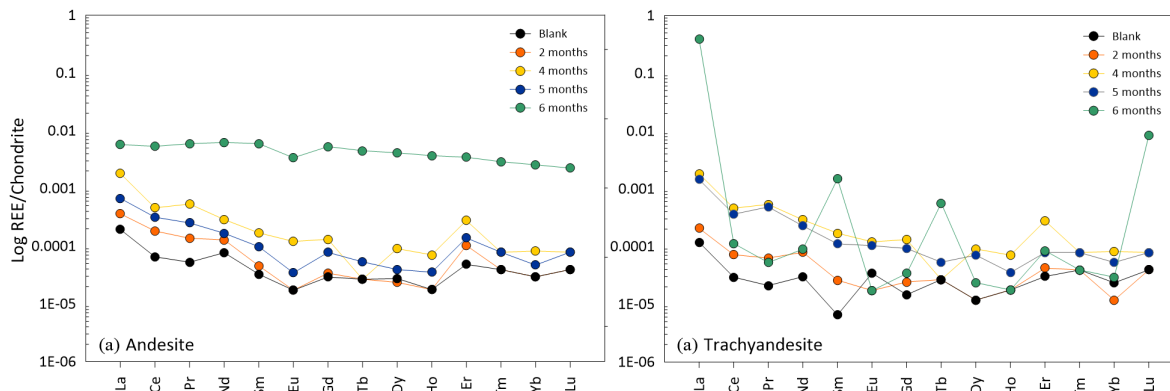


Figure 4.17: Chondrite-normalized patterns of REE.

### 4.3.6 Geochemical modelling

In this study, we present a batch numerical simulation for speciation and saturation indices calculation between volcanic rocks and fluids at hydrothermal temperatures and water saturation pressure. We simulate REE complexation in HCl-acidified water to approximate conditions typified in the Acoculco geothermal system. The simulated conditions aim to delineate the effects of pH on REE speciation between intermediate and basic volcanic rocks in reaction to acidic fluids.

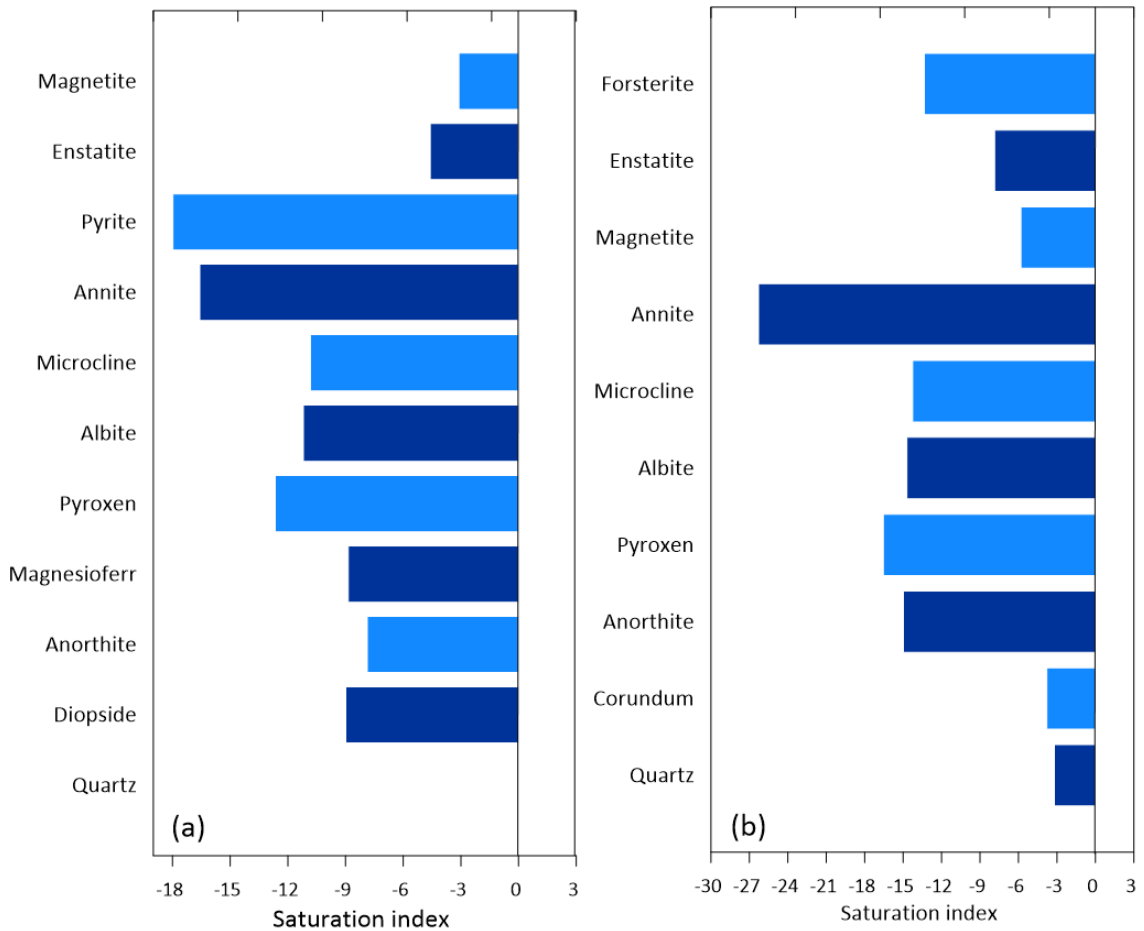
The simulation was carried out with a single mesh element, with a layer thickness of 50 m, isothermal condition ( $150^{\circ}\text{C}$ ) and a pressure of 69 psi closely replicated the experimental conditions. As a first step in the process modelling, a batch simulation is performed with the minerals listed in Table 4.2 using the initial water composition of the experiments. The simulation time is conducted for periods of 1 to 10,000 years.

Figure 4.18a shown the mineral saturation indices (SI) derived from the chemical composition of the rock and fluid samples after 6 months of reaction. It can be observed that for andesite, quartz is the only mineral that exhibits an SI greater than 0 (oversaturated). Similarly, magnetite and enstatite are the mineral phases with an SI close to zero. Among the subsaturated mineral phases, determined by a SI less than 0, the speciation revealed the presence of pyrite, annite, pyroxene, albite, microcline, magnesioferrite, diopside, and anorthite. For the basalt - trachyandesite, the mineral nearly to equilibrium state are quartz, corundum and magnetite. Other minerals such as anorthite, pyroxen, albite, microcline, annite,

#### 4. Fractionation of the rare earth elements: dissolution water-rock interaction experiments

---

and forsterite present a subsaturated state. The subsaturation state of the mineralogical composition shows that the water-rock system has not yet reached an equilibrium state, but an expected dissolution process is demonstrated during the reaction of the experiment with acidic fluid.



**Figure 4.18:** Mineral saturation indices from (a) andesite and, (b) basalt - trachyandesite

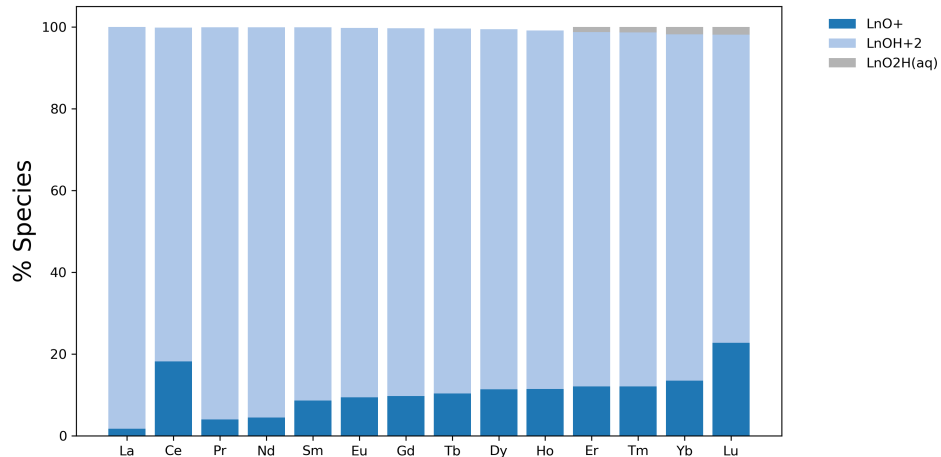
Figure Fig. 4.19 shows the contribution of the main aqueous species as a percentage of the total dissolved REE. For both samples andesite Fig. 4.19a and trachyandesite Fig. 4.19b, it's notable that  $\approx 90\%$  of the total dissolved REE is present as hydroxide complexes ( $\text{LnOH}^{+2}$ ). Another significant proportion is observed in the formation of mono-hydroxide complexes ( $\text{LnO}^{+}$ ), between 2 and 5% for LREE, except for Ce, which reaches nearly 20%. A clear trend is evident, showcasing a gradual increase in the proportion of this complex with the decrease

in the ionic radius of the REE, transitioning from LREE to HREE. Additionally, in the case of Er, Tm, Yb, and Lu, REE-dioxide complexes ( $\text{LnO}_{aq}^2$ ) formation is observed in approximately 2% of the total complexation.

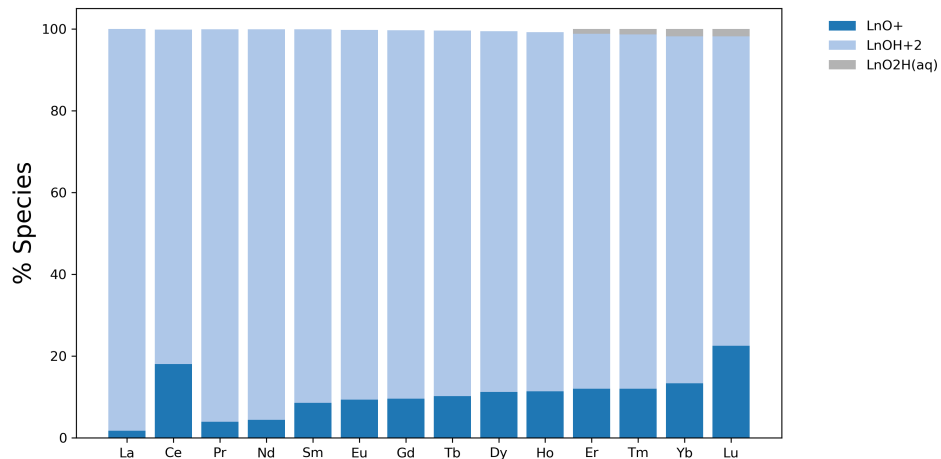
The formation of these complexes under experimental conditions with a fluid pH of 3 indicates a high concentration of hydrogen ions ( $\text{H}^+$ ) in the solution, which can lead to the protonation of chemical species present. Specifically, "LaO<sub>2</sub>H(aq)" could represent a complex where lanthanum is bound to one or more water molecules and protonated with one or more hydrogen ions. The formation of REE-hydroxide, REE-mono-hydroxide, and REE-dioxide complexes are crucial considerations in understanding the distribution and mobility of rare earth elements in aqueous environments. Other complexes of chlorides ( $\text{LnCl}^2$ ), fluorides ( $\text{LnF}^{2+}$ ) and sulfates ( $\text{LnSO}_4$ ) exhibited a minor contribution (<2%) and were depicted in the final analysis. This study agrees with some others such as (Perry and Gysi, 2020) mentions that REE hydroxyl species could function as a major carrier ligand, especially in high-temperature alkaline fluids that may be present in carbonatite systems. On the other hand, (Migdisov et al., 2016) suggest that the REE oxides hydrolyze at hydrothermal conditions to form REE hydroxides. Moreover, (Louvel et al., 2015), report spectroscopic data and solubility determinations for Yb<sub>2</sub>O<sub>3</sub> at temperatures up to 400 °C. These data suggest that the Yb oxide is stable under these conditions.

#### 4. Fractionation of the rare earth elements: dissolution water-rock interaction experiments

---



(a)



(b)

**Figure 4.19:** Aqueous speciation of REE found in the WRI experiments: (a) Andesite and (b) trachyandesite. The abbreviation of Ln represents any of the fourteen elements of REE (La–Lu).

### 4.4 Remarks of Chapter 4

A new water-rock interaction experiment was conducted to elucidate new geochemical signatures of REE.

Over the six-month experimental period, significant changes were observed in the pH, bicarbonate concentration, and electrical conductivity of the fluids. These

changes were most pronounced in the first month and showed some stability in the subsequent months, indicating a possible evolution towards chemical equilibrium.

Analysis of rock samples revealed consistent concentration patterns of major and trace elements. Negative anomalies were observed in  $\text{TiO}_2$ ,  $\text{MnO}$ , and  $\text{P}_2\text{O}_5$ , along with varying concentrations of other trace elements. The water samples also exhibited characteristic distributions of elements, with a predominance of anionic species such as  $\text{Cl}$  and  $\text{HCO}_3$ , and cations such as  $\text{Na}$ ,  $\text{K}$ ,  $\text{Ca}$ , and  $\text{Mg}$ .

Opposite trends in the concentration of rare earth elements (REE) were detected between rock and water samples during the experimental period. While rock samples showed a decrease in REE concentration, water samples showed a progressive increase. Normalized REE patterns revealed significant differences between altered and less-altered rock samples, indicating dissolution and precipitation processes of secondary phases in the water-rock system.

Numerical models of speciation and saturation index calculation revealed a complex interaction between volcanic rocks and acidic fluids. The simulation showed that certain mineral phases were in equilibrium or supersaturated under acidic conditions, suggesting a continuous dissolution process. The modelling results also highlighted the formation of REE complexes with hydroxides and monohydroxides as predominant species in solution.

These conclusions provide a detailed understanding of the geochemical dynamics in the studied water-rock interaction system, emphasizing the importance of considering various physicochemical processes in the exploration and exploitation of geothermal resources.



# Final conclusions

---

According to the main objectives of this thesis work, the results achieved have allowed to establish the following main conclusions:

- The applied bibliometric methodology has clearly outlined the evolution of REE studies and their application in the geochemical exploration of geothermal systems. Two main periods of productivity were identified, before and after 2014, characterized by exponential growth in the number of publications. This increasing research indicates a growing interest from the scientific community in REE in geothermal systems, especially in countries such as China, the United States, Mexico, Germany, and Turkey.
- State-of-the-art studies of REE in geothermal systems reveal the main challenges in this area: (i) the mobility of trace elements in geothermal systems, (ii) the study of REE fractionation during hydrothermal alteration, (iii) the determination of the major aqueous complexes of REE in hydrothermal fluids, and (iv) conduct experimental water-rock interaction studies to better understand the thermodynamic and kinetic processes of REE and its role as a natural tracer in the exploration of unconventional geothermal systems.
- Considering the review of existing literature and the need to address the absence of surface geothermal indicators, typically used in conventional hydrothermal systems, two comprehensive geochemical methodologies were developed. The first methodology was performed to investigate the main water-rock interaction processes in the Acoculco geothermal system with special emphasis on the behavior of the REE. In addition, a comprehensive analysis of experimental investigations on water-rock interaction in geothermal

environments was carried out. This led to the development of a pioneering experimental framework based on geochemometric principles. By leveraging these principles, the methodology ensures consistency and reliability of water and rock experiments over long periods.

- A new set of geochemical signatures were identified, for the first time, in the AGS, among which stand out: (i) the bimodal frequency distribution of pH in cold and hot spring waters of the AGS with a clear dilution pattern from acid to neutral waters, and a deep preferential flow path from inside caldera to outside caldera; (ii) the concentration patterns of REE in waters and rocks which provide additional evidence of the existence of a high-temperature geothermal system with pH mineral buffers and temperatures that range between 200 °C and 300 °C. Such REE patterns seem to dominate with a preferential transport path from deep heat conduction processes at the zone of the inside caldera to surface geothermal manifestations at the zone of the outside caldera, which is confirmed by the presence of hot spring waters with surface temperatures up to 54 °C (CHIG and JI).
- The interaction of volcanic rocks (andesite and basalt-trachyandesite) with deionized water at 150 °C was effectively evaluated using batch reactors, with a grain size ranging between 1000-500  $\mu\text{m}$ , a water/rock ratio of 10:1, and a maximum reaction time of 6 months. Advanced statistical methods were efficiently applied during various stages, including the collection and initial treatment of samples, preparation and assembly of experimental systems, collection of products, measurement of physicochemical parameters, and chemical and mineralogical analyses of products.
- Water-rock interaction experiments have demonstrated significant changes in the chemical composition of fluids and rocks during the experimental period. Consistent concentration patterns of major and trace elements were observed, along with opposite trends in REE concentration between rock and water samples. Numerical models of speciation and saturation index calculation have revealed a complex interaction between volcanic rocks and acidic fluids, highlighting the formation of REE complexes with hydroxides as predominant species in solution.

In summary, the results obtained from theoretical and experimental studies provide a detailed understanding of the geochemical dynamics in the studied water-rock interaction systems. These findings underscore the importance of considering various physicochemical processes in the exploration and exploitation of geothermal resources. There is a need for further research and experiments to improve our

---

understanding of REE geochemistry in geothermal environments and its potential application in the industry.



# Bibliography

---

- Allen, D. E. and Seyfried Jr, W. E. (2005). REE controls in ultramafic hosted MOR hydrothermal systems: An experimental study at elevated temperature and pressure. *Geochimica Et Cosmochimica Acta*, 69(3):675–683. 23
- Almirudis, E., Santoyo, E., Guevara, M., Paz-Moreno, F., and Portugal, E. (2018). Chemical and isotopic signatures of hot springs from east-central Sonora State, Mexico : a new prospection survey of promissory low-to-medium temperature geothermal systems. *Revista Mexicana de Ciencias Geológicas*, 35(2):116–141. 60
- Anders, E. and Grevesse, N. (1989). Abundances of the elements: Meteoritic and solar. *Geochemica et Cosmochemica Acta*, 53:197–214. 26, 27
- Andreo-Martínez, P., Ortiz-Martínez, V. M., García-Martínez, N., de los Ríos, A. P., Hernández-Fernández, F. J., and Quesada-Medina, J. (2020). Production of biodiesel under supercritical conditions: State of the art and bibliometric analysis. *Applied Energy*, 264(February):114753. 37
- Atwood, D. (2012). *The Rare Earth Elements Fundamental and Applications*. 23, 30
- Avellán, D. R., Macías, J. L., Layer, P. W., Cisneros, G., Sánchez-Núñez, J. M., Gómez-Vasconcelos, M. G., Sosa-Ceballos, G., García-Tenorio, F., Agustín, G. R., Osorio-Ocampo, S., García-Sánchez, L., Mendiola, I. F., López-Loera, H., and Benowitz, J. (2019). Geology of the late Pliocene – Pleistocene Aocolco caldera complex, eastern Trans-Mexican Volcanic. *Journal of Maps*, 15(2):8–18. 2, 58
- Avellán, D. R., Macías, J. L., Layer, P. W., Sosa-Ceballos, G., Gómez-Vasconcelos, M. G., Cisneros-Máximo, G., Sánchez-Núñez, J. M., Martí, J., García-Tenorio, F., López-Loera, H., Pola, A., and Benowitz, J. (2020). Eruptive chronology

- of the Acoculco caldera complex – A resurgent caldera in the eastern Trans-Mexican Volcanic Belt (México). *Journal of South American Earth Sciences*, 98:102412. VIII, 2, 3, 54, 56, 58, 59, 64, 85
- Bai, M., Reinicke, K. M., Teodoriu, C., and Fichter, C. (2012). Investigation on water-rock interaction under geothermal hot dry rock conditions with a novel testing method. *Journal of Petroleum Science and Engineering*, 90-91:26–30. 82
- Baker, J., Waight, T., and Ulfbeck, D. (2002). Rapid and highly reproducible analysis of rare earth elements by multiple collector inductively coupled plasma mass spectrometry. *Geochemica*, 66(20):3635–3646. 40
- Balaram, V. (1996). Recent trends in the instrumental analysis of rare earth elements in geological and industrial materials. *TrAC - Trends in Analytical Chemistry*, 15(9):475–486. 22, 40
- Balaram, V. (2019). Rare earth elements: A review of applications, occurrence, exploration, analysis, recycling, and environmental impact. *Geoscience Frontiers*, 10(4):1285–1303. 50
- Bao, S.-X., Zhou, H.-Y., Peng, X.-T., Ji, F.-W., and Yao, H.-Q. (2008). Geochemistry of REE and yttrium in hydrothermal fluids from the Endeavour segment, Juan de Fuca Ridge. *Geochemical Journal*, 42(4):359–370. 45
- Barakos, G., Mischo, H., and Gutzmer, J. (2015). *Rare Earth Underground Mining Approaches with Respect to Radioactivity Control and Monitoring Strategies*. Elsevier Inc. 50
- Barringer, J. and Johnsson, P. (1996). Theoretical considerations and a simple method for measuring alkalinity and acidity in low-pH waters by Gran titration. Technical report, U.S Geological Survey. 62
- Bau, M. (1991). Rare-earth element mobility during hydrothermal and metamorphic fluid-rock interaction and the significance of the oxidation state of europium. *Chemical Geology*, 93(3):219–230. 24
- Bethke, C. (2007). *Geochemical and biogeochemical reaction modeling*. Cambridge University Press, Cambridge. 91
- Bethke, C. M. (1996). *Geochemical Reaction Modeling: Concepts and Applications*. New York, Ny. 63
- Bogie, I. and Mackenzie, K. (1998). THE APPLICATION OF A VOLCANIC FACIES MODEL TO AN ANDESITIC STRATOVOLCANO HOSTED

- GEOHERMAL , SYSTEM AT WAYANG WINDU , JAVA , INDONESIA.  
*Geothermal Workshop*, pages 265–270. 46
- Boynton, W. V. (1984). Cosmochemistry of the Rare Earth Elements: Meteorite Studies. In *Rare Earth Element Geochemistry*, volume 2, pages 63–114. Elsevier B.V. 26, 27
- Brewer, A., Chang, E., Park, D. M., Kou, T., Li, Y., Lammers, L. N., and Jiao, Y. (2019). Recovery of Rare Earth Elements from Geothermal Fluids through Bacterial Cell Surface Adsorption. *Environmental Science and Technology*, 53(13):7714–7723. 50
- Brown, D., Duchane, D., Heiken, G., and Hriscu, V. (1966). *Mining the Earth's Heat: Hot Dry Rock Geothermal Energy*, volume 112. 8
- Calcagno, P., Evanno, G., Trumpy, E., Carlos Gutiérrez-Negrín, L., Macías, J. L., Carrasco-Núñez, G., and Liotta, D. (2018). Preliminary 3-D geological models of Los Humeros and Acoculco geothermal fields (Mexico)-H2020 GEMex Project. *Advances in Geosciences*, 45:321–333. 3, 54
- Canet, C., Arana, L., González-Partida, E., Pi, T., Prol-Ledesma, R. M., Franco, S. I., Villanueva-Estrada, R. E., Camprubí, A., Ramírez-Silva, G., and López-Hernández, A. (2010). A statistics-based method for the short-wave infrared spectral analysis of altered rocks: An example from the Acoculco caldera, Eastern Trans-Mexican Volcanic Belt. *Journal of Geochemical Exploration*, 105(1):1–10. 3, 55, 58
- Canet, C., Morton, B., Higuera, P., Hernández-Cruz, B., Flores-López, G., and Hernández-Álvarez, E. (2015a). Investigation of mercury geochemistry in the undeveloped geothermal field of Acoculco, Eastern Trans-Mexican Volcanic Belt. In *Proceedings of the International Conference on Mercury as a global pollutant*, Jeju, Korea. 3, 55
- Canet, C., Trillaud, F., Prol-Ledesma, R. M., González-Hernández, G., Peláez, B., Hernández-Cruz, B., and Sánchez-Córdova, M. M. (2015b). Thermal history of the Acoculco geothermal system, eastern Mexico: Insights from numerical modeling and radiocarbon dating. *Journal of Volcanology and Geothermal Research*, 305:56–62. 3, 55
- Cangelosi, D., Broom-Fendley, S., Banks, D., Morgan, D., and Yardley, B. (2020). Light rare earth element redistribution during hydrothermal alteration at the Okorusu carbonatite complex, Namibia. *Mineralogical Magazine*, 84(1):49–64. 31, 46

- Cao, R., Dor, J., Cai, Y. Q., Chen, X. L., Mao, X., and ren Meng, H. (2023). Geochemical and H–O–Sr–B isotope signatures of Yangyi geothermal fields: implications for the evolution of thermal fluids in fracture-controlled type geothermal system, Tibet, China. *Geothermal Energy*, 11(1). 22
- Cariaga, C. (2024). ThinkGeoEnergy’s Top 10 Geothermal Countries 2023–Power Generation Capacity(MW). 2, 9, 10, 14
- Carrión-Mero, P., Montalván-Burbano, N., Paz-Salas, N., and Morante-Carballo, F. (2020). Volcanic geomorphology: A review of worldwide research. *Geosciences (Switzerland)*, 10(9):1–17. 37
- Cetiner, Z. S. and Xiong, Y. (2008). Chemical controls on the solubility, speciation and mobility of lanthanum at near surface conditions: A geochemical modeling study. *Applied Geochemistry*, 23(8):2301–2315. 23, 45
- Chambefort, I., Lewis, B., Simpson, M. P., Bignall, G., Rae, A. J., and Ganefianto, N. (2017). Ngatamariki Geothermal System : Magmatic to Epithermal Transition in the Taupo Volcanic Zone , New Zealand. *Economic Geology*, 112:319–346. 45
- Chamorro, C. R., Mondéjar, M. E., Ramos, R., Segovia, J. J., Martín, M. C., and Villamañán, M. A. (2012). World geothermal power production status: Energy, environmental and economic study of high enthalpy technologies. *Energy*, 42(1):10–18. 9
- Chandra, S. (2019). *Geology, Chemistry and Genesis of Thermal Springs of Odisha, India*. SpringerBriefs in Earth Sciences, Odisha, India. 11
- Chen, J. R., Chao, E. C. T., Back, J. M., Minkin, J. A., Rivers, M. L., Sutton, S. R., Cygan, G. L., Grossman, J. N., and Reed, M. J. (1993). Rare earth element concentrations in geological and synthetic samples. *Nuclear Instruments North-Holland and Methods in Physics Research B75*, 75:576–581. 40
- Chudaev, O. V., Chelnokov, G. A., Bragin, I. V., Kharitonova, N. A., Rychagov, S. N., Nuzhdaev, A. A., and Nuzhdaev, I. A. (2017). Rare Earth and Major Elements Geochemistry of Geothermal Waters from Mutnovsky Volcano, Kamchatka. *Procedia Earth and Planetary Science*, 17:92–95. 22, 47, 54
- Cole, C. S., James, R. H., Connelly, D. P., and Hathorne, E. C. (2014). Rare earth elements as indicators of hydrothermal processes within the East Scotia subduction zone system. *Geochimica Et Cosmochimica Acta*, 140(0):20–38. 45, 48

- Colinet, C. (1995). The thermodynamic properties of rare earth metallic systems. *Journal of Alloys and Compounds*, 225(1-2):409–422. 24
- Craddock, P. R., Bach, W., Seewald, J. S., Rouxel, O. J., Reeves, E., and Tivey, M. K. (2010). Rare earth element abundances in hydrothermal fluids from the Manus Basin, Papua New Guinea: Indicators of sub-seafloor hydrothermal processes in back-arc basins. *Geochimica et Cosmochimica Acta*, 74(19):5494–5513. 48, 78
- Craig, H. (1961). Isotopic variations in meteoric waters. *Science*, 133(3465):1702–1703. 63
- Deb, P., Knapp, D., Marquart, G., Clauser, C., and Trumpy, E. (2020). Stochastic workflows for the evaluation of enhanced geothermal system (EGS) potential in geothermal greenfields with sparse data: the case study of Aocolco, Mexico. *Geothermics*, 88(101879):1–11. 3, 54
- DiPippo, R. (2012). Enhanced Geothermal Systems – Projects and Plants. In *Geothermal Power Plants: Principles, Applications, Case Studies and Environment Impact*, chapter 22, pages 443–481. Elsevier Ltd. 8
- DiPippo, R. and Renner, J. L. (2014). Geothermal Energy. *Future Energy*, pages 471–492. 1, 7, 8
- Dostal, J. (2016). Chapter 2 Rare Metal Deposits Associated with Alkaline/Peralkaline Igneous Rocks. *Reviews in Economic Geology*, pages 33–54. 32
- Drüppel, K., Stober, I., Grimmer, J. C., and Mertz-kraus, R. (2020). Geothermics Experimental alteration of granitic rocks : Implications for the evolution of geothermal brines in the Upper Rhine Graben , Germany. *Geothermics*, 88(June):101903. 23
- Dushyantha, N., Batapola, N., Ilankoon, I. M., Rohitha, S., Premasiri, R., Abeysinghe, B., Ratnayake, N., and Dissanayake, K. (2020). The story of rare earth elements (REEs): Occurrences, global distribution, genesis, geology, mineralogy and global production. *Ore Geology Reviews*, 122(January):103521. 22, 32
- Echchakoui, S. (2020). Why and how to merge Scopus and Web of Science during bibliometric analysis: the case of sales force literature from 1912 to 2019. *Journal of Marketing Analytics*, 8(3):165–184. 32, 35
- Elmi, S. A., Arnorsson, S., and Stefansson, A. (2010). Gallium and germanium distribution in geothermal water. In *Proceedings of the: Third East African Rift Geothermal Conference*, number November, pages 22–25. 67, 98

- Emsbo, P., Mclaughlin, P. I., Bray, E. A., Anderson, E. D., Vandenbroucke, T. R. A., and Zielinski, R. A. (2016). Rare Earth Elements in Sedimentary Phosphorite Deposits : A Global Assessment. *Rare Earth and Critical Elements in Ore Deposits*, pages 101–113. 31
- Espinoza-Ojeda, O. M., Prol-Ledesma, R. M., Iglesias, E. R., and Figueroa-Soto, A. (2017). Update and review of heat flow measurements in Mexico. *Energy*, 121:466–479. 14
- Evensen, N. M., Hamilton, P. J., and O’Nions, R. K. (1978). Rare-earth abundances in chondritic meteorites. *Geochimica et Cosmochimica Acta*, 42(8):1199–1212. 26, 27
- Fall, M., Baratoux, D., Jessell, M., Moussa, N. P., Vanderhaeghe, O., François, M. J., Baratoux, L., and Bonzi, W. M.-E. (2020). The redistribution of thorium, uranium, potassium by magmatic and hydrothermal processes versus surface processes in the Saraya Batholith (Eastern Senegal): Insights from airborne radiometrics data and topographic roughness. *Journal of Geochemical Exploration*, 219(106633):2–18. 68, 98
- Feng, J.-L., Zhao, Z.-H., Chen, F., and Hu, H.-P. (2014). Rare earth elements in sinters from the geothermal waters (hot springs) on the Tibetan Plateau, China. *Journal of Volcanology and Geothermal Research*, 287:1–11. 42, 46
- Ferrari, L., Orozco-Esquivel, T., Manea, V., and Manea, M. (2012). The dynamic history of the Trans-Mexican Volcanic Belt and the Mexico subduction zone. *Tectonophysics*, 522-523:122–149. 14, 58
- Firsching, F. H. and Brune, N. S. (1992). Solubility Products of the Trivalent Rare-Earth Phosphates. *Journal of Chemical and Engineering Data*, 36(1):93–95. 23
- Fisher, A. and Kara, D. (2016). Determination of rare earth elements in natural water samples – A review of sample separation, preconcentration and direct methodologies. *Analytica Chimica Acta*, 935:1–29. 22, 41, 54
- Fowler, A. P., Ferguson, C., Cantwell, C. A., Zierenberg, R. A., McClain, J., Spycher, N., and Dobson, P. (2018). A conceptual geochemical model of the geothermal system at Surprise Valley, CA. *Journal of Volcanology and Geothermal Research*, 353:132–148. 50
- Fowler, A. P., Zierenberg, R. A., Reed, M. H., Palandri, J., Óskarsson, F., and Gunnarsson, I. (2019a). Rare earth element systematics in boiled fluids from

- basalt-hosted geothermal systems. *Geochimica et Cosmochimica Acta*, 244:129–154. 22, 23, 45
- Fowler, A. P., Zierenberg, R. A., Reed, M. H., Palandri, J., Óskarsson, F., and Gunnarsson, I. (2019b). Rare earth element systematics in boiled fluids from basalt-hosted geothermal systems. *Geochimica et Cosmochimica Acta*, 244:129–154. 48
- Fowler, A. P. G. and Zierenberg, R. A. (2015). Rare earth element concentrations in geothermal fluids and epidote from the Reykjanes geothermal system, Iceland. In *Proceedings of the World Geothermal Congress 2015*, page 9, Melbourne, Australia. IGA. 54
- Fukuyama, M. and Chen, F. (2021). Geochemical characteristics of silica scales precipitated from the geothermal fluid at the Onuma geothermal power plant in Japan. *Journal of Mineralogical and Petrological Sciences*, 116:159–169. 43
- Fulignati, P., Gioncada, A., and Sbrana, A. (1998). Geologic model of the magmatic-hydrothermal system of Vulcano (Aeolian Islands, Italy). *Mineralogy and Petrology*, 62(3-4):195–222. 79
- Fulignati, P., Gioncada, A., and Sbrana, A. (1999). Rare-earth element (REE) behaviour in the alteration facies of the active magmatic-hydrothermal system of Vulcano (Aeolian Islands, Italy). *Journal of Volcanology and Geothermal Research*, 88(4):325–342. 46
- Galeczka, I., Oelkers, E. H., and Gislason, S. R. (2014). The chemistry and element fluxes of the July 2011 Múlakvísl and Kaldakvísl glacial floods, Iceland. *Journal of Volcanology and Geothermal Research*, 273:41–57. 82
- Gallup, D. L. (2009). Geothermics Production engineering in geothermal technology : A review. 38:326–334. 7
- Gammons, C. H., Wood, S. A., Pedrozo, F., Varekamp, J. C., Nelson, B. J., Shope, C. L., and Baffico, G. (2005). Hydrogeochemistry and rare earth element behavior in a volcanically acidified watershed in Patagonia, Argentina. *Chemical Geology*, 222(3-4):249–267. 2, 43, 45, 47, 48
- García-Palomo, A., Macías, J. L., Jiménez, A., Tolson, G., Mena, M., Sánchez-Núñez, J. M., Arce, J. L., Layer, P. W., Santoyo, M. Á., and Lermo-Samaniego, J. (2018). NW-SE Pliocene-Quaternary extension in the Apan-Acocolco region, eastern Trans-Mexican Volcanic Belt. *Journal of Volcanology and Geothermal Research*, 349:240–255. 2, 54, 56

- Gieré, R. (1993). Transport and deposition of REE in H<sub>2</sub>S-rich fluids: evidence from accessory mineral assemblages. *Chemical Geology*, 110(1):251–268. 45, 48
- Giggenbach, W. (1991). Chemical techniques in geothermal exploration, in Applications of Geochemistry in Geothermal Reservoir Development. *F.D Amore (Ed.), UNITAR .*, pages 253–273. 63
- Gilbert, C. D. and Williams-Jones, A. E. (2008). Vapour transport of rare earth elements (REE) in volcanic gas: Evidence from encrustations at Oldoinyo Lengai. *Journal of Volcanology and Geothermal Research*, 176(4):519–528. 45
- Gimeno-Serrano, M., Auqué-Sanz, L. F., and Nordstrom, D. (2000). REE speciation in low-temperature acidic waters and the competitive effects of aluminum. *Chemical Geology*, 165(3-4):167–180. 48, 78
- Gislason, S. R. and Oelkers, E. H. (2003). Mechanism, rates, and consequences of basaltic glass dissolution: II. An experimental study of the dissolution rates of basaltic glass as a function of pH and temperature. *Geochimica Et Cosmochimica Acta*, 67(20):3817–3832. 91
- Göb, S., Loges, A., Nolde, N., Bau, M., Jacob, D. E., and Markl, G. (2013). Major and trace element compositions (including REE) of mineral, thermal, mine and surface waters in SW Germany and implications for water-rock interaction. *Applied Geochemistry*, 33:127–152. 22, 76
- Gollock, A. (2022). *Handbook of Rare Earth Elements: Analytcs*. 40, 41
- Goodman (2007). Update on scopus and web of science. *The Charleston Advisor*, 8(3):15–15. 35
- Greaves, M. J., Elderfield, H., and Klinkhammer, G. P. (1989). Determination of the rare earth elements in natural waters by isotope-dilution mass spectrometry. *Analytica Chimica Acta*, 218(C):265–280. 40
- Gromet, L. P., Dymek, R. F., Haskin, L. A., and Korotev, R. L. (1984). The “North American shale composite”: Its compilation, major and trace element characteristics. *Geochemica et Cosmochemica Acta*, 48:2469–2482. 28, 29
- Gschneidner, K. A. (1990). Physical Properties of the Rare Earth Metals. *Bulletin of Alloy Phase Diagrams*, 11(3):216–224. 24
- Guerrero-Martínez, F. J., Prol-Ledesma, R. M., Carrillo-De La Cruz, J. L., Rodríguez-Díaz, A. A., and González-Romo, I. A. (2020). A three-dimensional temperature model of the Acoculco caldera complex, Puebla, Mexico, from the Curie isotherm as a boundary condition. *Geothermics*, 86:101794. 3, 54

- Gupta, H. and Roy, S. (2007). Geothermal systems and resources BT - Geothermal Energy. chapter 4, pages 49–59. Elsevier Sci., Hyderabad, India. 1, 2, 7, 8
- Gutiérrez-Negrin, L. C. (2019). Current status of geothermal-electric production in Mexico. *IOP Conference Series: Earth and Environmental Science*, 249(1). 14, 15
- Gutiérrez-Negrin, L. C. A., Félix, I. C., Romo-Jones, J. M., and Quijano-León, J. L. (2021). Geothermal energy in Mexico: update and perspectives. In *World Geothermal Congress 2020+1*, pages 1–13. 14, 15, 16, 17, 18
- Haas, J. R., Shock, E. L., and Sassani, D. C. (1995). Rare earth elements in hydrothermal systems: Estimates of standard partial molal thermodynamic properties of aqueous complexes of the rare earth elements at high pressures and temperatures. *Geochimica Et Cosmochimica Acta*, 59(21):4329–4350. 23, 24, 45, 48
- Haase, C., Dethlefsen, F., Ebert, M., and Dahmke, A. (2013). Uncertainty in geochemical modelling of CO<sub>2</sub> and calcite dissolution in NaCl solutions due to different modelling codes and thermodynamic databases. *Applied Geochemistry*, 33:306–317. 63, 94
- Hannigan, R. E. (2005). Rare earth, major, and trace element geochemistry of surface and geothermal waters from the Taupo volcanic zone, North island New Zealand . In Jonannesson, K. H., editor, *Rare earth elements in groundwater flow systems*, pages 67–88. Springer, The Netherlands. 22
- Hanson, M. C., Oze, C., and Horton, T. W. (2014). Identifying blind geothermal systems with soil CO<sub>2</sub> surveys. *Applied Geochemistry*, 50:106–114. 2
- Hari, K. R., Swarnkar, V., and Prasanth, M. P. (2018). Significance of assimilation and fractional crystallization (AFC) process in the generation of basaltic lava flows from Chhotaudepur area, Deccan Large Igneous Province, NW India. *Journal of Earth System Science*, 127(6):1–16. 31
- Harvey, M. C., Rowland, J. V., Chiodini, G., Rissmann, C. F., Bloomberg, S., Fridriksson, T., and Oladottir, A. A. (2017). ScienceDirect CO<sub>2</sub> flux geothermometer for geothermal exploration. *Geochimica et Cosmochimica Acta*, 213:1–16. 82
- Haskin, L. A., Haskin, M. A., Frey, F. A., and Wildeman, T. R. (1968). Relative and Absolute Terrestrial Abundances of the Rare Earths. In *Origin and Distribution of the Elements.*, pages 889–912. 26, 27

- Hatipo, E., Gültekin, F., and Arzu, F. (2020). Major , trace , and rare earth element geochemistry of the Ayder and İ kizdere ( Rize , NE Turkey ) geothermal waters : Constraints for water – rock interactions. *Geothermics*, 86(101810). 22
- Hatipoğlu Temizel, E., Gültekin, F., and Fırat Ersoy, A. (2020). Major, trace, and rare earth element geochemistry of the Ayder and İ kizdere (Rize, NE Turkey) geothermal waters: Constraints for water–rock interactions. *Geothermics*, 86:101810. 46, 47
- He, D.-f., Zhu, W.-g., Zhong, H., Ren, T., Bai, Z.-j., and Fan, H.-p. (2013). Journal of Asian Earth Sciences Zircon U – Pb geochronology and elemental and Sr – Nd – Hf isotopic geochemistry of the Daocheng granitic pluton from the Yidun Arc , SW China. *Journal of Asian Earth Sciences*, 67-68:1–17. 46
- Heasler, H. P. and Jaworowski, C. (2009). Geothermal systems and monitoring hydrothermal features. In Young, R. and Norby, L., editors, *Geological Monitoring: Boulder Colorado*, pages 105–140. The Geological Society of America. 1
- Henderson, P. A. U. L. (1984). GENERAL GEOCHEMICAL PROPERTIES AND ABUNDANCES OF THE RARE EARTH ELEMENTS. In P. Henderson, editor, *Developments in Geochemistry*, chapter Chapter 1, pages 1–32. volume 2 edition. 24
- Hernández, C. (1997). The Acoculco Caldera: The Highest  $3\text{He}/4\text{He}$  Values in Mexico. . 55
- Horiuchi, Y., Ohno, T., Hoshino, M., Shin, K.-C., Murakami, H., Tsunematsu, M., and Watanabe, Y. (2014). Geochemical prospecting for rare earth elements using termite mound materials. *Mineralium Deposita*, 49(8):1013–1023. 31
- Hutter, G. (2021). Geothermal power generation in the world 2015-2020 update report. In *World Geothermal Congress 2020+1*, pages 31–43. 1
- IEA (2023). World Energy Outlook 2023. Technical report. 10
- Inguaggiato, C., Burbano, V., Rouwet, D., and Garzón, G. (2017). Geochemical processes assessed by Rare Earth Elements fractionation at “Laguna Verde” acidic-sulphate crater lake (Azufra volcano, Colombia). *Applied Geochemistry*, 79:65–74. 47
- Inguaggiato, C., Pappaterra, S., Peiffer, L., Apollaro, C., Brusca, L., De Rosa, R., Rouwet, D., Caudron, C., and Suparjan (2020). Mobility of REE from a hyperacid brine to secondary minerals precipitated in a volcanic hydrothermal

- system: Kawah Ijen crater lake (Java, Indonesia). *Science of the Total Environment*, 740:140133. 47
- Inostroza, M., Moune, S., Moretti, R., Bonifacie, M., Robert, V., Burtin, A., and Chilin-Eusebe, E. (2022). Decoding water-rock interaction and volatile input at La Soufriere volcano (Guadeloupe) using time-series major and trace element analyses in gas condensates. *Journal of Volcanology and Geothermal Research*, 425(March). 22
- Izquierdo, G. M., Armenta, M. F., Montes, M. R., Manuel, G., and Figueroa, A. (2012). Estudio experimental del comportamiento de las rocas del yacimiento de Los Humeros , México , ante soluciones ácidas Experimental test on the reservoir-rocks reactions under acid solutions at Los Humeros , Mexico. *Geotermia, Rev. Mex. de Geoenergía*, 25(1):10–17. 16
- Jarvis, K. E. and Williams, J. G. (1993). Laser ablation inductively coupled plasma mass spectrometry (LA-ICP-MS): a rapid technique for the direct, quantitative determination of major, trace and rare-earth elements in geological samples. *Chemical Geology*, 106(3-4):251–262. 44
- Jensen, J. and Mackintosh, A. (1991). *Rare earth magnetism: structures and excitations*. 25
- Kaczmarczyk, M., Tomaszewska, B., and Operacz, A. (2020). Sustainable utilization of low enthalpy geothermal resources to electricity generation through a cascade system. *Energies*, 13(10). VII, 12
- Kaczor-kurzawa, D., Wysocka, I., Porowski, A., and Vassileva, E. (2022). The occurrence and distribution of rare earth elements in mineral and thermal waters in the Polish Lowlands. 237(106984). 42, 43, 45, 47
- Kikawada, Y., Ossaka, T., Oi, T., and Honda, T. (2001). Experimental studies on the mobility of lanthanides accompanying alteration of andesite by acidic hot spring water. *Chemical Geology*, 176(1-4):137–149. 23
- Köhler, S. J., Harouiya, N., Chairat, C., and Oelkers, E. H. (2005). Experimental studies of REE fractionation during water-mineral interactions: REE release rates during apatite dissolution from pH 2.8 to 9.2. *Chemical Geology*, 222(3-4):168–182. 49
- Krupp, R. and Seward, T. M. (1987). The Rotokawa geothermal system, New Zealand: An active epithermal gold-depositing environment. *Economic Geology*, 4:1109–1129. 67, 98

- Kruszewski, M., Hofmann, H., Alvarez, F. G., Bianco, C., Haro, A. J., Garduño, V. H., Liotta, D., Trumpy, E., Brogi, A., Wheeler, W., Bastesen, E., Parisio, F., and Saenger, E. H. (2021). Integrated stress field estimation and implications for enhanced geothermal system development in Acoculco, Mexico. *Geothermics*, 89(July 2020):101931. 3, 54
- Lewis, A., Komninou, A., Yardley, B. W. D., and Palmer, M. R. (1998). Rare earth element speciation in geothermal fluids from Yellowstone National Park, Wyoming, USA. *Geochimica et Cosmochimica Acta*, 62(4):657–663. 23, 45, 54, 63, 98
- Lewis, A., Palmer, M. R., and Kemp, A. J. (1994). Variations of the rare earth elements abundances in hydrothermal waters from the Yellowstone hydrothermal system, Wyoming, USA. *Mineralogical Magazine*, 58A:525–526. 45
- Lewis, A., Palmer, M. R., Sturchio, N. C., and Kemp, A. J. (1997). The rare earth element geochemistry of acid-sulphate and acid-sulphate-chloride geothermal systems from Yellowstone National Park, Wyoming, USA. *Geochimica et Cosmochimica Acta*, 61(4):695–706. 24, 42, 43, 45, 46, 47, 63, 76, 98
- Leybourne, M. I., Goodfellow, W. D., Boyle, D. R., and Hall, G. M. (2000). Rapid development of negative Ce anomalies in surface waters and contrasting REE patterns in groundwaters associated with Zn-Pb massive sulphide deposits. *Applied Geochemistry*, 15(6):695–723. 45
- Li, B., Kong, Q., Wang, G., Liu, F., Guo, L., Liu, C., Liao, F., and Shi, Z. (2022). Controls on the behaviors of rare earth elements in acidic and alkaline thermal springs. *Applied Geochemistry*, 143(March). 43, 45, 46, 47
- Li, Y., Dor, J., Zhang, C., Wang, G., and Zhang, B. (2021). Genesis of the Xifeng Low-Temperature Geothermal Field, Guizhou, SW China: Constraints From Geology, Element Geochemistry, and D-O Isotopes. *Frontiers in Earth Science*, 9(December):1–17. 47
- Liang, P., Liu, Y., and Guo, L. (2005). Determination of trace rare earth elements by inductively coupled plasma atomic emission spectrometry after preconcentration with multiwalled carbon nanotubes. *Spectrochimica Acta Part B: Atomic Spectroscopy*, 60(1):125–129. 22
- Libbey, R. and Williams-Jones, A. (2016). Lithochemical approaches in geothermal system characterization: An application to the Reykjanes geothermal field, Iceland. *Geothermics*, 64:61–80. 45

- Líndal, B. (1992). Review of industrial applications of geothermal energy and future considerations. *Geothermics*, 21(5-6):591–604. 11
- ling Wang, G., Zhang, W., Ma, F., jing Lin, W., yun Liang, J., and Zhu, X. (2018). Overview on hydrothermal and hot dry rock researches in China. *China Geology*, 1(2):273–285. 1
- Lintjewas, L. and Setiawan, I. (2018). Mobility of rare earth element in hydrothermal process and weathering product: A review. *IOP Conference Series: Earth and Environmental Science*, 118(1). 45
- Liotta, D., Brogi, A., Wheeler, W. H., Bastensen, E., Hugo, V., Sosa-ceballos, G., Pola, A., Bianco, C., Olvera-garcía, E., Fidel, G., Israde-alcantara, I., Jim, A., Piccardi, L., and Zucchi, M. (2023). Tectonic-magmatic-hydrothermal interactions in a hot dry rock geothermal system : The role of the transfer and normal faults in the Acoculco caldera ( Mexico ) ´ n Avell a. *Journal of Volcanology and Geothermal Research*, 444(107963). 2
- Liu, Y., Xue, D., Li, W., and Li, C. (2020). The determination of ultra-trace rare-earth elements in iron minerals via HR-ICP-MS following chemical purification by polyurethane foam †. *J. Anal. At. Spectrom.*, 35:2156–2164. 44
- López Hernández, A. (2009). *Evolución Volcánica del Complejo Tulancingo-Acoculco y su Sistema Hidrotermal, Estados de Hidalgo y Puebla, México*. Doctorado, Universidad Nacional Autónoma de México, México. 3, 54, 55, 58, 66
- López-Hernández, A., García-Estrada, G., Aguirre-Díaz, G., González-Partida, E., Palma-Guzmán, H., and Quijano-León, J. L. (2009). Hydrothermal activity in the Tulancingo–Acoculco Caldera Complex, central Mexico: Exploratory studies. *Geothermics*, 38(3):279–293. 2, 54
- Lorenzo-Pulido, C., Flores-Armenta, M., and Ramírez-Silva, G. (2010). Characterization of the Acoculco geothermal zone as a HDR system. *Geothermal Resources Council Transactions*, 34:369–372. 54
- Louvel, M., Bordage, A., Testemale, D., Zhou, L., and Mavrogenes, J. (2015). Hydrothermal controls on the genesis of REE deposits: Insights from an in situ XAS study of Yb solubility and speciation in high temperature fluids (T < 400 Å°C). *Chemical Geology*, 417:228–237. 45, 105
- Lü, T., Gao, X.-w., Wang, X.-d., and Zhao, Y. (2009). The geothermal power and main technical problems. In *International Conference on Sustainable Power Generation and Supply, 2009. SUPERGEN '09.*, pages 1–4, Naijing, China. IEEE. 8

## BIBLIOGRAPHY

---

- Lund, J. W. and Boyd, T. L. (2016). Direct utilization of geothermal energy 2015 worldwide review. *Geothermics*, 60:66–93. 12
- Lund, J. W., Freeston, D. H., and Boyd, T. L. (2011). Direct utilization of geothermal energy 2010 worldwide review. *Geothermics*, 40(3):159–180. 8
- Marieni, C., Matter, J. M., and Teagle, D. A. H. (2020). ScienceDirect Experimental study on mafic rock dissolution rates within CO<sub>2</sub>-seawater-rock systems. *Geochimica et Cosmochimica Acta*, 272:259–275. 82
- Marín-Camacho, P., Velasco-Tapia, F., Bernard-Romero, R., Weber, B., and González-Guzmán, R. (2022). New geochemical evidence constraining the water-rock-gas interaction on geothermal fluids of the Querétaro Graben, northern Trans-Mexican Volcanic Belt. *Journal of South American Earth Sciences*, 114(103702). 22, 42, 45, 47
- Marini, L. (2000). Geochemical techniques for the exploration and exploitation of geothermal energy. 1
- Marks, M. A. and Markl, G. (2017). A global review on agpaitic rocks. *Earth-Science Reviews*, 173(June):229–258. 31
- Masuda, A. (1987). Lanthanide two mutually tetrad opposite effects types , in nature :. 21:119–124. 45
- McDonough, W. F. and Sun, S. s. (1995). The composition of the Earth. *Chemical Geology*, 120(3-4):223–253. 26, 27, 28, 63, 64, 70, 94
- Mcguire, T. (1972). Magnetism of Rare-Earth Elements, Alloys, and Compounds. *IEEE Transactions on Magnetism*, 8(1):105–130. 25
- McLennan, S. M. (1989). *Chapter 7 S. M. McLennan RARE EARTH ELEMENTS IN SEDIMENTARY ROCKS: INFLUENCE OF PROVENANCE AND SEDIMENTARY PROCESSES*. 29, 30
- McLennan, S. M. (1993). Weathering and global denudation. *The journal of Geology*, 101(Kronberg 1985):295–303. 64
- McLennan, S. M. and Taylor, S. R. (2012). Geology, Geochemistry and Natural Abundances. *Encyclopedia of Inorganic and Bioinorganic Chemistry*. 25, 26, 30
- Merchand-Reyes, G. (2010). *IMPLEMENTACIÓN DE UNA METODOLOGÍA PARA EL ESTUDIO QUÍMICO DE CATIONES Y BICARBONATOS EN MANANTIALES DE BAHÍA CONCEPCIÓN (BAJA CALIFORNIA SUR, MÉXICO)*. PhD thesis. 93

- Michard, A. (1989). Rare earth element systematics in hydrothermal fluids. *Geochimica et Cosmochimica Acta*, 53(3):745–750. 23, 45, 53
- Michard, A. and Albarède, F. (1986). The REE content of some hydrothermal fluids. *Chemical Geology*, 55(1-2):51–60. 45, 53
- Michard, G. and Roekens, E. (1983). Modelling of the chemical composition of alkaline hot waters. *Geothermics*, 12(2-3):161–169. 53
- Middleton, A. W., Förster, H.-J., Uysal, I. T., Golding, S. D., and Rhede, D. (2013). Accessory phases from the Soultz monzogranite, Soultz-sous-Forêts, France: Implications for titanite destabilisation and differential REE, Y and Th mobility in hydrothermal systems. *Chemical Geology*, 335(0):105–117. 45, 46
- Migaszewski, Z. M. and Gałuszka, A. (2015a). The Characteristics , Occurrence , and Geochemical Behavior of Rare Earth Elements in the Environment : A Review and Geochemical Behavior of Rare Earth Elements in the Environment : A Review. *Critical Reviews in Environmental Science and Technology*, 45:429–471. 41
- Migaszewski, Z. M. and Gałuszka, A. (2015b). The Characteristics, Occurrence, and Geochemical Behavior of Rare Earth Elements in the Environment: A Review. *Critical Reviews in Environmental Science and Technology*, 45(5):429–471. 25
- Migdisov, A., Williams-Jones, A. E., Brugger, J., and Caporuscio, F. A. (2016). Hydrothermal transport, deposition, and fractionation of the REE: Experimental data and thermodynamic calculations. *Chemical Geology*, 439:13–42. 23, 45, 48, 49, 54, 105
- Migdisov, A. A. and Williams-Jones, A. E. (2006). A spectrophotometric study of erbium (III) speciation in chloride solutions at elevated temperatures. *Chemical Geology*, 234(1-2):17–27. 49, 54
- Migdisov, A. A., Williams-Jones, A. E., and Wagner, T. (2009). An experimental study of the solubility and speciation of the Rare Earth Elements (III) in fluoride- and chloride-bearing aqueous solutions at temperatures up to 300 Å°C. *Geochimica Et Cosmochimica Acta*, 73(23):7087–7109. 23, 49
- Moeller, T. (1962). THE L A N T H A N I D E S. volume 60. 25
- Möller, P. (2002). Rare earth elements and yttrium in geothermal fluids. pages 1–31. 45

- Möller, P., Dulski, P., and Ózgür, N. (2008). Partitioning of rare earths and some major elements in the Kizildere geothermal field, Turkey. *Geothermics*, 37(2):132–156. 22
- Möller, P., Morteani, G., Dulski, P., and Preinfalk, C. (2009). Vapour/liquid fractionation of rare earths, Y<sup>3+</sup>, Na<sup>+</sup>, K<sup>+</sup>, NH<sub>4</sub><sup>+</sup>, Cl<sup>-</sup>, HCO<sub>3</sub><sup>-</sup>, SO<sub>4</sub><sup>2-</sup> and borate in fluids from the Piancastagnaio geothermal field, Italy. *Geothermics*, 38(4):360–369. 45
- Monecke, T., Kempe, U., Monecke, J., Sala, M., and Wolf, D. (2002). Tetrad effect in rare earth element distribution patterns: a method of quantification with . . . . *Geochimica et Cosmochimica Acta*, 66(7):1185–1196. 45, 46
- Monecke, T., Kempe, U., Trinkler, M., Thomas, R., Dulski, P., and Wagner, T. (2011). Unusual rare earth element fractionation in a tin-bearing magmatic hydrothermal system. *Geological Society of America*, 39(4):295–298. 24, 53
- Monecke, T., Monecke, J., Mönch, W., and Kempe, U. (2000). Mathematical analysis of rare earth element patterns of fluorites from the Ehrenfriedersdorf tin deposit, Germany: evidence for a hydrothermal mixing process of lanthanides from two different sources. *Mineralogy and Petrology*, 70(3-4):235–256. 30
- Mourad Mahdy, N., Hany Mahmoud, S., Mohamed Helmy, H., Farage Osman, A., El Sawey, E. S. H., and Korany Abu Zeid, E. (2013). Trace and REE element geochemistry of fluorite and its relation to uranium mineralizations, Gabal Gattar Area, Northern Eastern Desert, Egypt. *Arabian Journal of Geosciences*, 7(7):2573–2589. 45
- Navrotsky, A., Lee, W., Mielewczyk-Gryn, A., Ushakov, S. V., Anderko, A., Wu, H., and Riman, R. E. (2015). Thermodynamics of solid phases containing rare earth oxides. *Journal of Chemical Thermodynamics*, 88:126–141. 23, 24
- Nesbitt, H. W. (1979). Mobility and fractionation of rare earth elements during weathering of a granodiorite. *Nature*, 279(5710):206–210. 23, 64, 73
- Neupane, G. and Wendt, D. S. (2017). Assessment of Mineral Resources in Geothermal Brines in the US Enhanced Geothermal Systems View project Rare Earth Elements View project Assessment of Mineral Resources in Geothermal Brines in the US. *42nd Workshop on Geothermal Reservoir Engineering, Stanford University*, (February). 50
- Nicholson, K. (1993). Gas Chemistry. In *Geothermal Fluids: Chemistry and Exploration Techniques*, pages 87–115. Springer Berlin Heidelberg, Berlin, Heidelberg. 61, 65, 94

- Nordstrom, D., Blaine McCleskey, R., and Ball, J. W. (2009). Sulfur geochemistry of hydrothermal waters in Yellowstone National Park: IV Acid–sulfate waters. *Applied Geochemistry*, 24(2):191–207. 61, 62, 66, 94
- Oddone, M., Meloni, S., and Genova, N. (1984). Neutron activation analysis: A powerful tool for assay of rare-earth elements in terrestrial materials. *Inorganica Chimica Acta*, 94(6):283–290. 40
- Ohannesson, K. E. H. J., Arnham, I. R. M. F., Uo, C. A. G., and Tetzenbach, K. L. J. S. (1999). Rare earth element fractionation and concentration variations along a groundwater flow path within a shallow , basin-fill aquifer , southern Nevada , USA. *Geochemica et Cosmochemica Acta*, 63(18):2697–2708. 45
- Opare, E. O., Struhs, E., and Mirkouei, A. (2021). A comparative state-of-technology review and future directions for rare earth element separation. *Renewable and Sustainable Energy Reviews*, 143(February):110917. 22, 50
- Osvald, M., Kilpatrick, A. D., Rochelle, C. A., Szanyi, J., and Kóbor, B. (2019). Batch and flow-through leaching of different metallic rocks under geothermal reservoir circumstances. In *European Geothermal Congress*, number June, pages 11–14. 82
- Ottolini, L. P., Raffone, N., Fridleifsson, G. Ó., Tonarini, S., Orazio, M. D., and Gianelli, G. (2012). A geochemical investigation of trace elements in well RN-17 at Reykjanes geothermal system , SW- Iceland A geochemical investigation of trace elements in well RN-17 at Reykjanes geothermal system , SW-Iceland. *Materials Science and Engineering*, 32(01). 46
- Öztürk, H., Hanilçi, N., Altuncu, S., and Kasapçi, C. (2019). Rare earth element (REE) resources of Turkey: An overview of their characteristics and origin. *Bulletin of the Mineral Research and Exploration*, 159:129–143. 31
- Palacios, A., Koon-Koon, R., Miranda-Flores, G., Lewis, S., Castro-Olivera, P. M., Cordova-Lizama, A., and Hernandez-Garcia, A. I. (2024). A Monte Carlo-based approach for the evaluation of Mexico’s geothermal potential. *Renewable Energy*, 223(November 2023):120006. 2
- Palme, H., Schultz, L., Spettel, B., Weber, H. W., Wänke, H., Michel-Levy, M. C., and Lorin, J. C. (1981). The Acapulco meteorite: Chemistry, mineralogy and irradiation effects. *Geochimica et Cosmochimica Acta*, 45(5). 26, 27
- Pan, C., Chávez, O., Romero, C. E., Levy, E. K., Aguilar Corona, A., and Rubio-Maya, C. (2016). Heat mining assessment for geothermal reservoirs in Mexico using supercritical CO<sub>2</sub> injection. *Energy*, 102:148–160. 14

- Pandarínath, K., Dulski, P., Torres-Alvarado, I. S., and Verma, S. P. (2008). Element mobility during the hydrothermal alteration of rhyolitic rocks of the Los Azufres geothermal field, Mexico. *Geothermics*, 37(1):53–72. 22, 46, 54
- Pandarínath, K., García-Soto, A. Y., Santoyo, E., Guevara, M., and Gonzalez-Partida, E. (2020). Mineralogical and geochemical changes due to hydrothermal alteration of the volcanic rocks at Acoculco geothermal system, Mexico. *Geological Journal*, (March):1–19. 22, 54, 57, 73
- Pappaterra, S., Inguaggiato, C., Rouwet, D., Mora-Amador, R., Ramírez-Umaña, C., González, G., Brusca, L., Peiffer, L., Levresse, G., and Bellomo, S. (2022). Rare Earth Elements Variations in a Hyperacid Crater Lake and Their Relations With Changes in Phreatic Activity, Physico-Chemical Parameters, and Chemical Composition: The Case of Poás Volcano (Costa Rica). *Frontiers in Earth Science*, 9(January):1–22. 22
- Pardo, M. and Suárez, G. (1995). Shape of the subducted Rivera and Cocos plates in southern Mexico : Seismic and tectonic implications. *Journal of Geophysical Research*, 100(B7):357–373. 58
- Parkhurst, D. L. and Appelo, C. (2013). Description of Input and Examples for PHREEQC Version 3 - A Computer Program for Speciation, Batch-Reaction, One-Dimensional Transport, and Inverse Geochemical Calculations. In *U.S. Geological Survey Techniques and Methods*, chapter 43, page 497. 62
- Peiffer, L., Bernard-Romero, R., Mazot, A., Taran, Y. A., Guevara, M., and Santoyo, E. (2014). Fluid geochemistry and soil gas fluxes (CO<sub>2</sub>-CH<sub>4</sub>-H<sub>2</sub>S) at a promissory Hot Dry Rock Geothermal System: The Acoculco caldera, Mexico. *Journal of Volcanology and Geothermal Research*, 284:122–137. 3, 55, 66
- Peiffer, L., Taran, Y. A., Lounejeva, E., Solís-Pichardo, G., Rouwet, D., and Bernard-Romero, R. A. (2011). Tracing thermal aquifers of El Chichón volcano-hydrothermal system (México) with <sup>87</sup>Sr/<sup>86</sup>Sr, Ca/Sr and REE. *Journal of Volcanology and Geothermal Research*, 205:55–66. 54, 55
- Pereira, H. A., Mironuk Frescura, L., de Menezes, B. B., Duarte, R., Villetti, M. A., Hilgemann, M., and da Rosa, M. B. (2019). A multivariate approach at the thermodynamic properties of rare earth elements. *Thermochimica Acta*, 678(June):178315. 23, 24
- Pérez-Orozco, J. D., Sosa-Ceballos, G., and Macías, J. L. (2021). Tectonic and magmatic controls on the evolution of post-collapse volcanism. Insights from the Acoculco caldera complex, Puebla, México. *Lithos*, (105878):380–381. 2, 54

- Pérez-Zárate, D. (2014). *Desarrollo de experimentos de interacción agua-roca y modelación geoquímica para el estudio de la disolución de feldespatos alcalinos y sus implicaciones en la calibración del geotermómetro Na/K a baja y mediana temperatura*. PhD thesis, Universidad Nacional Autónoma de México. 8
- Pérez-Zárate, D., Santoyo, E., Guevara, M., Torres-Alvarado, I., Peiffer, L., and Martínez-Frías, J. (2015). Geochemometric modeling and geothermal experiments of Water/Rock Interaction for the study of alkali-feldspars dissolution. *Applied Thermal Engineering*, 75:1244–1261. 82
- Pérez-Zárate, D., Santoyo, E., Jacome-Paz, M., Guevara, M., Guerrero, F., Yáñez-Dávila, D., and Santos-Raga, G. (2024). Geochemistry Soil CO<sub>2</sub> fluxes measured in the Acochulco Geothermal System, Mexico: Baseline emissions from a long-term prospecting programme. *Chemie der Erde - Geochemistry*, (March). 3
- Perry, E. and Gysi, A. P. (2020). Hydrothermal calcite-fluid REE partitioning experiments at 200 °C and saturated water vapor pressure. *Geochimica et Cosmochimica Acta*. 23, 30, 105
- Petrosino, P., Sadeghi, M., Albanese, S., Andersson, M., Lima, A., and De Vivo, B. (2013). REE contents in solid sample media and stream water from different geological contexts: Comparison between Italy and Sweden. *Journal of Geochemical Exploration*, 133:176–201. 31
- Pinto, F. G., Junior, R. E., and Saint’Pierre, T. D. (2012). Sample Preparation for Determination of Rare Earth Elements in Geological Samples by ICP-MS: A Critical Review. *Analytical Letters*, 45(12):1537–1556. 42, 45
- Pirajno, F. (2009). *Hydrothermal Processes and Mineral Systems*. Springer, Netherlands. 45, 64
- Polak, B. G., Prasolov, E. M., Kononov, V. I., Verkhovskiy, A. V., González, A., Templos, L. A., Espíndola, J. M., Arellano, J. M., and Mañón, A. (1982). Isotopic composition and concentration of inert gases in Mexican hydrothermal systems (Genetic and applied aspects). *Geofísica Internacional*, 21(3):193–227. 3, 55
- Pourmand, A., Dauphas, N., and Ireland, T. J. (2012). A novel extraction chromatography and MC-ICP-MS technique for rapid analysis of REE, Sc and Y: Revising CI-chondrite and Post-Archean Australian Shale (PAAS) abundances. *Chemical Geology*, 291:38–54. 28, 29, 40, 44

## BIBLIOGRAPHY

---

- Price, D. (1963). *Little Science, Big Science*. Columbia University Press, New York. 37, 38
- Pruess, K., Oldenburg, C. M., and Moridis, G. J. (1999). TOUGH2 User's Guide, Version 2.0. Technical report. 94
- Pulido, C. L., Armenta, M. F., and Silva, G. R. (2011). Caracterización de un yacimiento de roca seca caliente en la zona geotérmica de Acoculco, Pue. *Geotermia*, 24:59. 2
- Quinto, A., Santoyo, E., Torres, V., González, E., and Castillo, D. (1995). Estudio geoquímico-ambiental de los efluentes naturales producidos en la zona geotérmica de Acoculco, Puebla. *Ingeniería Hidráulica en México*, 10(3):21–27. 3, 55, 66
- Ramanaiah, G. V. (1998). Determination of yttrium, scandium and other rare earth elements in uranium-rich geological materials by ICP-AES. *Talanta*, 46(4):533–540. 44
- Ramasamy, R., Subramanian, S. P., and Sundaravadivelu, R. (2013). Carbonates and REE bearing barite from Carbonatite complex of Tiruppattur, Tamil Nadu, India. *International Journal of Engineering and Technical Research*, 1(7). 31, 45
- Rillard, J., Pourret, O., Censi, P., Inguaggiato, C., Zuddas, P., Toulhoat, P., Gombert, P., and Brusca, L. (2019). Behavior of rare earth elements in an aquifer perturbed by CO<sub>2</sub> injection: Environmental implications. *Science of the Total Environment*, 687:978–990. 45, 54
- Rodriguez-Espinosa, P. F., Sabarathinam, C., Ochoa-Guerrero, K. M., Martínez-Tavera, E., and Panda, B. (2020). Geochemical evolution and Boron sources of the groundwater affected by urban and volcanic activities of Puebla Valley, south central Mexico. *Journal of Hydrology*, 584(January):124613. 93
- Roelandts, I. (1981). Determination of Light Rare Earth Elements in Apatite by X-ray Fluorescence Spectrometry after Anion Exchange Extraction. *Analytical Chemistry*, 53(4):676–680. 40
- Rudnick, R. L. and Gao, S. (2003). Composition of the Continental Crust. *Treatise On Geochemistry*, 3:1–64. 28, 29
- Rybach, L. (2022). Global Status, Development and Prospects of Shallow and Deep Geothermal Energy. *International Journal of Terrestrial Heat Flow and Applications*, 5(1):20–25. 1

- Sallet, R., Moritz, R., and Fontignie, D. (2005). The use of vein fluorite as probe for paleofluid REE and Sr-Nd isotope geochemistry: The Santa Catarina Fluorite District, Southern Brazil. *Chemical Geology*, 223(4):227–248. 31
- Sanada, T., Takamatsu, N., and Yoshiike, Y. (2006). Geochemical interpretation of long-term variations in rare earth element concentrations in acidic hot spring waters from the Tamagawa geothermal area, Japan. *Geothermics*, 35(2):141–155. 49, 54
- Sánchez-Córdova, M. M., Canet, C., Rodríguez-Díaz, A., González-Partida, E., and Linares-López, C. (2020). Water-rock interactions in the Acoculco geothermal system, eastern Mexico: Insights from paragenesis and elemental mass-balance. *Chemie der Erde*, 80(1):125527. 2, 22, 54, 55
- Sanematsu, K. and Watanabe, Y. (2019). Characteristics and Genesis of Ion Adsorption-Type Rare Earth Element Deposits. *Rare Earth and Critical Elements in Ore Deposits*, 2010:55–79. 31
- Santos-Raga, G., Santoyo, E., Almirudis, E., Guevara, M., and Yáñez-Dávila, D. (2020). Study of the Water-Rock-Interaction Processes in the Hidden Geothermal System of Acoculco Puebla ( México ) by using a Geochemometric Modeling. In *Proceedings of the World Geothermal Congress*, number 2019, pages 1–8. 55
- Santos-Raga, G., Santoyo, E., Guevara, M., Almirudis, E., Pérez-Zárate, D., and Yáñez-Dávila, D. (2021). Tracking geochemical signatures of rare earth and trace elements in spring waters and outcropping rocks from the hidden geothermal system of Acoculco , Puebla ( Mexico ). *Journal of Geochemical Exploration*, 227(106798). VII, VIII, 2, 3, 40, 41, 42, 43, 45, 46, 47, 48, 58, 60, 61, 65, 66, 68, 69, 70, 72, 73, 74, 75, 97, 98, 99
- Santoyo, E., Almirudis, E., Pérez-Zárate, D., Guevara, M., Portugal, E., García, E., and Santos-Raga, G. (2020). The origin of radon anomalies along geological structures and degassing pathways of the geothermal system of Acoculco, Puebla (Mexico). In *Proceedings of the World Geothermal Congress 2020*, page 10, Reykjavik, Iceland. 3, 55
- Santoyo, E., Canet, C., Díaz-González, L., García-Mandujano, E., González-Partida, E., Guevara, M., Hernández-Cruz, G., Jones, D., Pandarinath, K., Portugal Marín, E., and Shankar, R. (2019). Development and application of new advanced methods in fluid geochemistry and hydrothermal alteration for the exploration of geothermal systems. 60
- Santoyo, E., García, R., Galicia-Alanis, K. A., Verma, S. P., Aparicio, A., and Santoyo-Castelazo, A. (2007). Separation and quantification of lanthanides in

- synthetic standards by capillary electrophoresis: A new experimental evidence of the systematic "odd-even" pattern observed in sensitivities and detection limits. *Journal of Chromatography A*, 1149(1):12–19. 22, 41, 43, 54, 82
- Santoyo, E. and Verma, S. P. (2003). Determination of lanthanides in synthetic standards by reversed-phase high-performance liquid chromatography with the aid of a weighted least-squares regression model Estimation of method sensitivities and detection limits. 997:171–182. 43
- Sanyal, S. K. (2005). Classification of geothermal system - a possible scheme. In *Thirtieth Workshop on Geothermal Reservoir Engineering*, number 1, page 176, Stanford, California. 22, 53
- Sarapaa, O., Al Ani, T., Lahti, S. I., Lauri, L. S., Sarala, P., Torppa, A., and Kontinen, A. (2013). Rare earth exploration potential in Finland. *Journal of Geochemical Exploration*, 133:25–41. 31
- Sasmaz, A., Zuddas, P., Cangemi, M., Piazzese, D., Ozek, G., Venturi, M., and Censi, P. (2021). Zirconium and hafnium fractionation and distribution of Rare Earth Elements in neutral-alkaline waters: Case study of Lake Van hydrothermal system, Turkey. *Journal of Geochemical Exploration*, 226(March):106784. 47
- Schmidt, C., Rickers, K., Bilderback, D. H., and Huang, R. (2007a). In situ synchrotron-radiation XRF study of REE phosphate dissolution in aqueous fluids to 800°C. *Lithos*, 95(1-2):87–102. 45
- Schmidt, K., Garbe-Schönberg, D., Bau, M., and Koschinsky, A. (2010). Rare earth element distribution in >400°C hot hydrothermal fluids from 5°S, MAR: The role of anhydrite in controlling highly variable distribution patterns. *Geochimica Et Cosmochimica Acta*, 74(14):4058–4077. 42
- Schmidt, K., Koschinsky, A., and Garbe-schönberg, D. (2007b). Geochemistry of hydrothermal fluids from the ultramafic-hosted Logatchev hydrothermal field , 15 ° N on the Mid-Atlantic Ridge : Temporal and spatial investigation. *Chemical Geology*, 242:1–21. 42
- Schmidt, R. B., Bucher, K., Drüppel, K., and Stober, I. (2017). Experimental interaction of hydrothermal Na-Cl solution with fracture surfaces of geothermal reservoir sandstone of the Upper Rhine Graben. *Applied Geochemistry*, 81:36–52. 47
- Schramm, R. (2016). Use of X-ray fluorescence analysis for the determination of rare earth elements. *Physical Sciences Reviews*, 1(9):1–17. 40

- Seitz, M., Oliver, A. G., and Raymond, K. N. (2007). The Lanthanide Contraction Revisited of incomplete series including solid-state materials , 4 as well as. *J. AM. CHEM. SOC*, 1460(36):11153–11160. 24
- SENER (2019). Programa de Desarrollo del Sistema Eléctrico Nacional. Technical report. 47
- SENER (2022). Balance Nacional de Energía. *Secretaría de Energía, Subsecretaría de Planeación y Transición Energética.*, page 15. 17
- Sengupta, D. and Gosen, B. S. V. (2019). Placer-Type Rare Earth Element Deposits. *Rare Earth and Critical Elements in Ore Deposits*, pages 81–100. 31
- Shakeri, A., Ghoreyshinia, S., Mehrabi, B., and Delavari, M. (2015). Rare earth elements geochemistry in springs from Taftan geothermal area SE Iran. *Journal of Volcanology and Geothermal Research*, 304:49–61. 46, 48, 54, 76, 77, 78, 79, 101
- Shimada, Y., Yonezu, K., Okaue, Y., Watanabe, K., Iwanaga, T., and Yokoyama, T. (2010). Rare Earth Elements in the silica scales from geothermal water. *J. Geotherm. Res. Soc. Japan*, 32(2):77–86. 43
- Shock, E. L., Sassani, D. C., Willis, M., and Sverjensky, D. A. (1997). Inorganic species in geologic fluids: Correlations among standard molal thermodynamic properties of aqueous ions and hydroxide complexes. *Geochimica Et Cosmochimica Acta*, 61(5):907–950. 23
- Shoedarto, R. M., Tada, Y., Kashiwaya, K., Koike, K., and Iskandar, I. (2022). Advanced characterization of hydrothermal flows within recharge and discharge areas using rare earth elements, proved through a case study of two-phase reservoir geothermal field, in Southern Bandung, West Java, Indonesia. *Geothermics*, 105(105):102507. 22, 42, 43, 45, 47
- Silva-Romo, G. and Mendoza-Rosales, C. (2011). *Manual para el Trabajo Geológico de Campo*. Universidad Nacional Autónoma de México, Facultad de Ingeniería, Ciudad de México, 1st ed edition. 61
- Sinclair, A. J. (1974). Selection of threshold values in geochemical data using probability graphs. *Journal of Geochemical Exploration*, 3(2):129–149. 37, 64, 73
- Skinner, B. (2022). Mineral deposit. 30

- Smith, M. P., Henderson, P., and Campbell, L. S. (2000). Fractionation of the REE during hydrothermal processes: constraints from the Bayan Obo Fe-REE-Nb deposit, Inner Mongolia, China. *Geochimica Et Cosmochimica Acta*, 64(18):3141–3160. 24, 45
- Smith, Y. R., Kumar, P., and McLennan, J. D. (2017). On the Extraction of Rare Earth Elements from Geothermal Brines. *Resources*, 6(3):1–16. 50
- Sosa-Ceballos, G., Macías, J., Avellán, D., Salazar-Hermenegildo, N., Boijseauneau-López, M., and Pérez-Orozco, J. (2018). The Acoculco caldera complex magmas: Genesis, evolution and relation with the Acoculco geothermal system. *Journal of Volcanology and Geothermal Research*, 358:288–306. 2, 42, 46, 54, 84
- Stead, C. V., Tomlinson, E. L., Kamber, B. S., Babechuk, M. G., and McKenna, C. A. (2017). Rare Earth Element Determination in Olivine by Laser Ablation-Quadrupole-ICP-MS: An Analytical Strategy and Applications. *Geostandards and Geoanalytical Research*, 41(2):197–212. 44
- Stober, I. and Bucher, K. (2012). History of Geothermal Energy Use. In *Geothermal Energy From Theoretical Models to Exploration and Development*, pages 15–21. Londres. 1, 8
- Stringfellow, W. and Dobson, P. (2020). Retrospective on Recent DOE-Funded Studies Concerning the Extraction of Rare Earth Elements & Lithium from Geothermal Brines. Technical report, Lawrence Berkeley National Laboratory. 50
- Sun, S., McDonough, W. F., and Coe, K. (1989). Chemical and isotopic systematics of oceanic basalts: Implications for mantle composition and processes. In Saunders, A. D. and Norry, M. J., editors, *Magmatism in the Ocean Basins*, volume Geological, pages 313–345. Published for The Geological Society by Blackwell Scientific Publications, Oxford. 26, 27, 28
- Taran, Y., Rouwet, D., Inguaggiato, S., and Aiuppa, A. (2008). Major and trace element geochemistry of neutral and acidic thermal springs at El Chichón volcano, Mexico: Implications for monitoring of the volcanic activity. *Journal of Volcanology and Geothermal Research*, 178(2):224–236. 54
- Taylor, S. . R. ., McLennan, S. . M. ., Armstrong, R. . L. ., and Tarney, J. . (1981). The Composition and Evolution of the Continental Crust : Rare Earth Element Evidence from Sedimentary Rocks [ and Discussion ]. *Philosophical Transaction Royal Society*, 301(1461):381–399. 28

- Taylor, S. R. and McLennan, S. M. (1985). *The continental crust: Its composition and evolution*. 28, 29
- Taylor, S. R. and McLennan, S. M. (1995). The geochemical the continental evolution crust. *Reviews of Geophysics*, 33(2):241–265. 28
- Tello-Hinojosa, E. (1994). Química de los fluidos hidrotermales de la zona geotérmica de la caldera de Acoculco, Puebla. *CFE-GPG internal report*, page 14. 66
- Temizel, E. H. and Gültekin, F. (2018). Hydrochemical, isotopic, and reservoir characterization of the Pasinler (Erzurum) geothermal field, eastern Turkey. *Arabian Journal of Geosciences*, 11(1). 46
- Tenzer, H. (2001). Development of Hot Dry Rock Technology. In IGA, editor, *International workshop on hot dry rock technology*, chapter 3.1, page 14. IGA. 1
- Terakado, Y., Fujitani, T., and Takada, J. (1993). Experimental study on the sorption of rare-earth elements and other trace elements during rhyolite-hydrothermal water interactions. *Chemical Geology*, 106(3-4):317–330. 23, 49
- Thair, A. and Sarapaa, O. (2014). REE-Minerals in Carbonatite, Alkaline and Hydrothermal Rocks, Northern and Central Finland. *1st European Rare Earth Resources Conference*. 45
- Tian, J., Pang, Z., Wang, Y., and Guo, Q. (2019). Fluid geochemistry of the Cuopu high temperature geothermal system in the eastern Himalayan syntaxis with implication on its genesis. *Applied Geochemistry*, 110:104422. 43, 47
- Tomarov, G. V. and Shipkov, A. A. (2023). Brief Review of the Current Status and Trends in the Development of Geothermal Energy. *Thermal Engineering*, 70(2):108–116. 8, 9, 10, 11
- Torres-Alvarado, I. S. (2002). Chemical Equilibrium in Hydrothermal Systems: The Case of Los Azufres Geothermal Field, Mexico. *International Geology Review*, 44(7):639–652. 15
- Torres-Alvarado, I. S., Pandarinath, K., Verma, S. P., and Dulski, P. (2007). Mineralogical and geochemical effects due to hydrothermal alteration in the Los Azufres geothermal field, Mexico. *Revista Mexicana de Ciencias Geológicas*, 24:15–24. 22, 46, 54
- Toth, A., Bobok, E., Toth, A., and Bobok, E. (2017). What Is Geothermal Energy? *Flow and Heat Transfer in Geothermal Systems*, pages 1–19. 7

- Treiman, A. and Essene, E. (1985). The Oka carbonatite complex, Quebec: geology and evidence for silicate-carbonate liquid immiscibility. *American Mineralogist*, 20:1101–1113. 30
- Trofanenko, J., Williams-Jones, A. E., Simandl, G. J., and Migdisov, A. A. (2016). The nature and origin of the REE mineralization in the Wicheeda Carbonatite, British Columbia, Canada. *Economic Geology*, 111(1):199–223. 30, 31
- U.S. Geological Survey (2023). Mineral commodity summaries 2023. Technical report, Reston, VA. 50
- Van Gosen, B., Verplanck, P., Seal, R., Long, K., and Gambogi, J. (2017). Rare-earth elements. In *Critical mineral resources of the United States— Economic and environmental geology and prospects for future supply*, chapter Chapter 0. U.S. Geological Survey Professional Paper. 25, 30
- Van Schmus, W. R. and Wood, J. A. (1967). A chemical-petrologic classification for the chondritic meteorites. *Geochimica et Cosmochimica Acta*, 31(5). 26
- Vasyukova, O. and Williams-Jones, A. (2020). Partial melting, fractional crystallisation, liquid immiscibility and hydrothermal mobilisation – A ‘recipe’ for the formation of economic A-type granite-hosted HFSE deposits. *Lithos*, 356-357. 30, 31
- Vasyukova, O. and Williams-Jones, A. E. (2014). Fluoride-silicate melt immiscibility and its role in REE ore formation: Evidence from the Strange Lake rare metal deposit, Québec-Labrador, Canada. *Geochimica et Cosmochimica Acta*, 139:110–130. 30
- Veksler, I. V., Dorfman, A. M., Kamenetsky, M., Dulski, P., and Dingwell, D. B. (2005). Partitioning of lanthanides and Y between immiscible silicate and fluoride melts, fluorite and cryolite and the origin of the lanthanide tetrad effect in igneous rocks. *Geochimica et Cosmochimica Acta*, 69(11):2847–2860. 30
- Vera-Baceta, M. A., Thelwall, M., and Kousha, K. (2019). Web of Science and Scopus language coverage. 35
- Verma, S. P. (2001). Geochemical evidence for a lithospheric source for magmas from Acoculco caldera, eastern Mexican Volcanic Belt. *International Geology Review*, 43(1):31–51. 46, 84
- Verma, S. P. (2020). *Road from Geochemistry to Geochemometrics*. Springer Nature Singapore Pte Ltd, Singapore. 43, 61

- Verma, S. P., Arredondo-Parra, U. C., Andaverde, J., Gómez-Arias, E., and Guerrero-Martínez, F. J. (2012). Three-dimensional temperature field simulation of a cooling of a magma chamber, La Primavera caldera, Jalisco, Mexico. *International Geology Review*, 54(7):833–843. 82, 83
- Verma, S. P., Pandarinath, K., Bhutani, R., and Dash, J. K. (2018). Mineralogical, chemical, and Sr-Nd isotopic effects of hydrothermal alteration of near-surface rhyolite in the Los Azufres geothermal field, Mexico. *Lithos*, 322:347–361. 22, 42, 46, 54
- Verma, S. P., Pandarinath, K., Santoyo, E., González-Partida, E., Torres-Alvarado, I. S., and Tello-Hinojosa, E. (2006). Fluid chemistry and temperatures prior to exploitation at the Las Tres Vírgenes geothermal field, Mexico. *Geothermics*, 35(2):156–180. 15
- Verma, S. P., Rosales-Rivera, M., Díaz-González, L., and Quiroz-Ruiz, A. (2017). Improved composition of hawaiian basalt BHVO-1 from the application of two new and three conventional recursive discordancy tests. *Turkish Journal of Earth Sciences*, 26(5):331–353. 84
- Verma, S. P. and Santoyo, E. (2007). High-performance liquid and ion chromatography: Separation and quantification analytical techniques for rare earth elements. *Geostandards and Geoanalytical Research*, 31(3):161–184. 24
- Verma, S. P., Santoyo, E., and Velasco-Tapia, F. (2002). Statistical evaluation of analytical methods for the determination of rare-earth elements in geological materials and implications for detection limits. *International Geology Review*, 44(4):287–335. 22, 40, 43, 54
- Verma, S. P., Torres-Alvarado, I. S., Satir, M., and Dobson, P. F. (2005). Hydrothermal alteration effects in geochemistry and Sr, Nd, Pb, and O isotopes of magmas from the Los Azufres geothermal field (Mexico): A statistical approach. *Geochemical Journal*, 39:141–163. 64
- Verplanck, P. L., Antweiler, R. C., Nordstrom, D. K., and Taylor, H. E. (2001). Standard reference water samples for rare earth element determinations. *Applied Geochemistry*, 16(2):231–244. 54
- Verplanck, P. L., Mariano, A. N., and Mariano, A. (2016). Rare Earth Element Ore Geology of Carbonatites. *Rare Earth and Critical Elements in Ore Deposits*, pages 5–32. 31, 32
- Viggiano-Guerra, J. C., Flores Armenta, M., and Ramírez Silva, G. (2009). Evolución del sistema geotérmico de Acoculco, Pue., México: un estudio con

- base en estudios petrográficos del pozo EAC-2 y en otras consideraciones. In *Memorias del XVII Congreso Anual Asociación Geotérmica Mexicana*, page 13 p., Morelia, Michoacán, Mexico. 2
- Voncken, J. (2016). *The rare earth elements: an introduction*. 30, 31, 32
- Wakita, H., Rey, P., and Schmitt, R. (1971). Abundances of the 14 rare-earth elements and 12 other trace elements in Apollo 12 samples: five igneous and one breccia rocks and four soils. In *Proceedings of the Second Lunar Science Conference*, pages 1319–1329. 26, 27
- Wall, F. (2021). Rare Earth Elements. *Encyclopedia of Geology*, pages 680–693. 22, 24, 25
- wan Wei, C., Xu, C., lei Song, W., Chen, W., Shi, A., Li, Z., and Fan, C. (2023). Heavy rare earth element and crustal-derived silicon enrichment in Huayangchuan carbonatites, Qinling orogenic belt. *Lithos*, 436-437(December 2022):106987. 30, 31
- Wang, M., Zhou, X., Liu, Y., Xu, H., Wu, Y., and Zhuo, L. (2020). Major , trace and rare earth elements geochemistry of geothermal waters from the Rehai high-temperature geothermal field in Tengchong of China. *Applied Geochemistry*, 119(January):104639. 32, 45, 46, 47
- Wang, W., Jiang, S. Y., and Xiao, Y. (2023). Fluid-rock interaction effects on Li isotope behavior in continental geothermal systems. *Chemical Geology*, 631(January):121525. 22
- Wang, X., Zeng, Z., Chen, S., Yin, X., and Chen, C.-T. (2013). Rare earth elements in hydrothermal fluids from Kueishantao, off northeastern Taiwan: Indicators of shallow-water, sub-seafloor hydrothermal processes. *Chinese Science Bulletin*, 58(32):4012–4020. 32
- Warren, I. (2021). Techno-Economic Analysis of Lithium Extraction from Geothermal Brines. Technical report. 82
- Wasson, J. T. and Chou, C.-l. (1974). FRACTIONATION OF MODERATELY VOLATILE ELEMENTS IN ORDINARY CHONDRITES. *Meteoritics*, 9(1). 26
- Wedepohl, K. H. (1995). The composition of the continental crust \*. *Geochemica et Cosmochemica Acta*, 59(7):1217–1232. 28, 29

- Wei, S., Liu, F., Zhang, W., Zhang, H., Yuan, R., Liao, Y., and Yan, X. (2022a). Geochemical Characteristics of Rare Earth Elements in the Chaluo Hot Springs in Western Sichuan Province, China. *Frontiers in Earth Science*, 10(March):1–16. 22, 45
- Wei, S., Liu, F., Zhang, W., Zhang, H., Zhao, J., Liao, Y., and Yan, X. (2022b). Typical geothermal waters in the Ganzi–Litang fault, western Sichuan, China: hydrochemical processes and the geochemical characteristics of rare-earth elements. *Environmental Earth Sciences*, 81(23):1–23. 22, 46, 47
- Weydt, L., Ramírez-Guzmán, Á. A., Pola, A., Lepillier, B., Kummerow, J., Mandrone, G., Comina, C., Deb, P., Norini, G., Gonzalez-Partida, E., Avellán, D. R., Macías, J. L., Bär, K., and Sass, I. (2020). Petrophysical and mechanical rock property database of the Los Humeros and Acoculco geothermal fields (Mexico). *Earth System Science Data Discussions*, (July):1–39. 3, 54
- Woitischek, J., Dietzel, M., Inguaggiato, C., Böttcher, M. E., Leis, A., Cruz, J. V., and Gehre, M. (2017). Characterisation and origin of hydrothermal waters at São Miguel (Azores) inferred by chemical and isotopic composition. *Journal of Volcanology and Geothermal Research*, 346:104–117. 54
- Wood, S. A. (1990a). The aqueous geochemistry of the rare-earth elements and yttrium: 1. Review of available low-temperature data for inorganic complexes and the inorganic REE speciation of natural waters. *Chemical Geology*, 82(0):159–186. 24, 48, 78
- Wood, S. A. (1990b). The aqueous geochemistry of the rare-earth elements and yttrium: 2. Theoretical predictions of speciation in hydrothermal solutions to 350°C at saturation water vapor pressure. *Chemical Geology*, 88(1-2):99–125. 48
- Wood, S. A. (2006). Rare earth element systematics of acidic geothermal waters from the Taupo Volcanic Zone, New Zealand. *Journal of Geochemical Exploration*, 89(1-3):424–427. 22, 53, 54
- Wood, S. A. and Shannon, W. M. (2003). Rare-earth elements in geothermal waters from Oregon, Nevada, and California. *Journal of Solid State Chemistry*, 171(1-2):246–253. 45, 54, 79, 101
- Wood, S. A. and Williams-Jones, A. E. (1994). The aqueous geochemistry of the rare-earth elements and yttrium 4. Monazite solubility and REE mobility in exhalative massive sulfide-depositing environments. *Chemical Geology*, 115(1-2):47–60. 45

- Xiao, Y. W., Zhi, G. Z., Shuai, C., XueBo, Y., and Chen-Tung, A. C. (2013). Rare earth elements in hydrothermal fluids from Kueishantao, off northeastern Taiwan: Indicators of shallow-water, sub-seafloor hydrothermal processes . *Chinese Science Bulletin*, 58(32):4012–4020. 22
- Xiong, Y. (2011). Organic species of lanthanum in natural environments: Implications to mobility of rare earth elements in low temperature environments. *Applied Geochemistry*, 26(7):1130–1137. 23
- Xu, T., Sonnenthal, E., Spycher, N., and Pruess, K. (2006). TOUGHREACT - A simulation program for non-isothermal multiphase reactive geochemical transport in variably saturated geologic media: Applications to geothermal injectivity and CO<sub>2</sub> geological sequestration. *Computers and Geosciences*, 32(2):145–165. 94
- Yan, Q., Wang, A., Wang, G., Yu, W., and Chen, Q. (2010). Resource evaluation of global geothermal energy and the development obstacles. In *2010 International Conference on Advances in Energy Engineering*, pages 115–119, Beijing, China. IEEE. 1
- Yan, X. P., Kerrich, R., and Hendry, M. J. (2001). Distribution of the rare earth elements in porewaters from a clay-rich aquitard sequence, saskatchewan, Canada. *Chemical Geology*, 176(1-4):151–172. 79, 101
- Yáñez-Dávila, D., Santoyo, E., and Santos-Raga, G. (2023). Worldwide research progress and trends on geothermal water–rock interaction experiments: a comprehensive bibliometric analysis. *Earth Science Informatics*, 16(1):1–24. 32, 33, 34, 38, 82
- Yang, J., Bai, J., Liu, M., Chen, Y., Wang, S., and Yang, Q. (2018). Determination of phosphorus in soil by ICP-OES using an improved standard addition method. *Journal of Analytical Methods in Chemistry*, 2018. 44
- Yolcan, O. O. (2023). World energy outlook and state of renewable energy: 10-Year evaluation. *Innovation and Green Development*, 2(4):100070. 9
- Yongliang, X. and Yusheng, Z. (1991). The mobility of rare-earth elements during hydrothermal activity: A review. *Chinese Journal of Geochemistry*, 10(4):295–306. 22, 45, 49, 54
- Zapp, P., Schreiber, A., Marx, J., and Kuckshinrichs, W. (2022). Environmental impacts of rare earth production. *MRS Bulletin*, 47(3):267–275. 50

- Zawisza, B., Pytlakowska, K., Feist, B., Polowniak, M., Kita, A., and Sitko, R. (2011). Determination of rare earth elements by spectroscopic techniques : a review. *J. Anal. At. Spectrom.*, 26:2373–2390. 43, 44
- Zeng, Y.-C., Su, Z., and Wu, N.-Y. (2013). Numerical simulation of heat production potential from hot dry rock by water circulating through two horizontal wells at Desert Peak geothermal field. *Energy*, 56:92–107. 23
- Zhang, F., Li, Y., Zhou, X., Huang, T., Tian, J., Cheng, Y., and Zhao, Y. (2023). Geochemical behaviors of rare earth elements in granite-hosted geothermal systems in SE China. *Geothermics*, 115(September):102826. 22
- Zhang, W., Du, J., Zhou, X., and Wang, F. (2016a). Mantle volatiles in spring gases in the Basin and Range Province on the west of Beijing, China: Constraints from helium and carbon isotopes. *Journal of Volcanology and Geothermal Research*, 309:45–52. 47
- Zhang, Y., Liu, J., and Meng, F. (2012). Geochemistry of Cenozoic volcanic rocks in Tengchong, SW China: Relationship with the uplift of the Tibetan Plateau. *Island Arc*, 21(4):255–269. 42, 46
- Zhang, Y., Tan, H., Zhang, W., Wei, H., and Dong, T. (2016b). Geochemical constraint on origin and evolution of solutes in geothermal springs in western Yunnan, China. *Chemie der Erde*, 76(1):63–75. 43
- Zhang, Y., Zhou, X., Liu, H., and Fang, B. (2020). Geochemistry of rare earth elements in the hot springs in the Simao Basin in southwestern China. *Environmental Earth Sciences*, 79(6):1–10. 47, 82
- Zierenberg, R. A., Schiffman, P., Barfod, G. H., Leshner, C. E., Marks, N. E., Lowenstern, J. B., Mortensen, A. K., Pope, E. C., Elders, W. A., Bird, D. K., and Reed, M. H. (2013). Composition and origin of rhyolite melt intersected by drilling in the Krafla geothermal field , Iceland. *Contributions to Mineralogy and Petrology*, 165:327–347. 50
- Zupic, I. and Čater, T. (2015). Bibliometric Methods in Management and Organization. *Organizational Research Methods*, 18(3):429–472. 36

